CHEMOSELECTIVE LIPOSOME FUSION FOR CELL-SURFACE AND TISSUE ENGINEERING APPLICATIONS

Debjit Dutta

A dissertation submitted to the faculty of the University of North Carolina at Chapel Hill in partial fulfillment of the requirements for the degree of Doctor of Philosophy in the Department of Chemistry

Chapel Hill
2011

Approved by

Advisor: Prof. Muhammad N. Yousaf

Chair: Prof. Gary Pielak

Prof. Matthew R. Redinbo

Prof. Christopher Fecko

Prof. Brian Hogan

ABSTRACT

DEBJIT DUTTA: CHEMOSELECTIVE LIPOSOME FUSION FOR CELL-SURFACE AND TISSUE ENGINEERING APPLICATIONS
(Under the direction of Dr. Muhammad Yousaf)

Proper cell-cell communication through physical contact is crucial for a range of fundamental biological processes including, cell proliferation, migration, differentiation, and apoptosis and for the correct function of organs and other multi-cellular tissues. The spatial and temporal arrangements of these cellular interactions *in vivo* are dynamic and lead to higher-order function that is extremely difficult to recapitulate *in vitro*. The development of 3-dimensional (3D), *in vitro* model systems to investigate these complex, *in vivo* interconnectivities would generate novel methods to study the biochemical signaling of these processes, as well as provide platforms for tissue engineering technologies. Herein, we develop and employ a strategy to induce specific and stable cell-cell contacts in 3D through chemoselective cell-surface engineering based on liposome delivery and fusion to display bio-orthogonal functional groups from cell membranes. This strategy uses liposome fusion for the delivery of ketone or oxyamine groups to different populations of cells for subsequent cell assembly via oxime ligation. We demonstrate how this method can be used for several applications including, the delivery of reagents to cells for fluorescent labeling, the formation of small, 3D spheroid cell assemblies, and the generation of large and dense, 3D multi-layered tissue-like structures. We were also able to create dynamic and switchable cell tissue assemblies through chemoselective conjugation and release chemistry. Cell membranes are

decorated with a range of molecules that can be released *in vitro* for subsequent rounds of molecular conjugation and release. Each step to modify the cell surface: activation, conjugation, release, and regeneration can be monitored and modulated by non-invasive, label-free analytical techniques. Additionally, we also develop and demonstrate a novel liposome fusion based delivery strategy to incorporate a unique bio-orthogonal lipid that has the dual ability to serve as a receptor for chemoselective cell surface tailoring and as a reporter to track cell behavior.

ACKNOWLEDGEMENT

This work is dedicated to my parents and brother for their continuous support and to all my friends and family for their encouragement. Many thanks to my advisor Dr. Muhammad N. Yousaf and colleagues for their support and advice: Dr. Diana Hoover, Dr. Devin Barret, Dr. Weil Luo, Dr. Brian Lamb, Dr. Sungjin Park and Dr. Weil Luo. Special thanks goes to Abby Pulsipher and Dr. Nathan Westcott for sharing many useful insights and collaborating in major projects.

TABLE OF CONTENTS

LIST OF FIGURES

LIST OF SCHEMES AND TABLES

LIST OF SYMBOLS AND ABBREVIATIONS

μm	micrometer
nm	nanometer
μM	micromolar
mM	millimolar
d	days
h	hours
^{1}HNMR	proton nuclear magnetic resonance
ECM	extracellular matrix
EG	ethylene glycol
$EG_4C_{11}SH$	tetra (ethylene glycol) undecane thiol
HQ	hydroquinone
Q	quinone
OA	oxyamine
PEG	poly (ethylene) glycol
PDMS	poly (dimethoxy) silane

RGD	arginine-glycine-aspartic acid
SAM	self-assembled monolayer
SEM	scanning electron microscopy
TEM	transmission electron microscopy
DLS	dynamic light scattering
ITC	isothermal titration calorimetry
FRET	Fourier resonance energy transfer
FRAP	fluorescence recovery after photobleaching
MALDI-MS	matrix-assisted laser/desorption ionization spectroscopy
μFl	microfluidic lithography
FACS	fluorescence activated cell sorting
POPC	1-palmitoyl-2-oleoyl- sn-glycero-3-phosphocholine
POPG	1-palmitoyl-2-oleoyl- sn-glycero-3-phosphoglycerol
DOTAP	1,2-dioleoyl-3-trimethylammonium-propane
3D	three dimension
PBS	phosphate buffer saline

fb	fibroblast
hMSC	human mesenchymal stem cell
SPR	surface plasmon resonance
UV	ultraviolet
TRITC	tetramethyl rhodamine isothiocyanate
Rhod-ONH_2	rhodamine-oxyamine
Rhod-PE	egg 1,2-dipalmitoyl-sn-glycero-3-phosphoethanolamine-N-(lissamine rhodamine B sulfonyl) (ammonium salt)

CHAPTER 1

Literature Review on Cell-Surface Engineering and it's Applications

1.1 Introduction

Cell surfaces are fertile grounds for scientists to manipulate cell phenotypes and biological fates. These manipulations not only help to answer basic biological questions, but also serve roles in diagnostic and therapeutic applications. A number of synergistic approaches combining chemistry, material science and biology have been applied for direct engineering and manipulation of living cells. Desirable chemical functionalities and materials can be introduced onto the cell surface by covalent and noncovalent chemistry, as well as through specific biological recognition events, including antibody/antigen and ligand/receptor interactions. These strategies have been used in various applications that include designing biomaterial scaffolds[1,2] to control cell fate, labeling cells with molecular and nanoparticle probes to image and visualize cellular processes and molecular pathways[3-5], delivering diverse species into cells[6,7], and patterning cells for drug discovery[8-10]. To date, cell-surface engineering has been primarily been achieved through the use of molecular biology and genetic engineering. However, perturbations of cellular physiology that are inherent to such strategies may interfere with significant cellular functions. Thus, there is a need of developing tools that will provide simple alternatives to genetic and biosynthetic pathways.

Cell-surface modifications have been generally achieved using three methods: (1) covalent conjugation of surface protein amino groups, (2) incorporation of amphiphilic

	Modification sites	Treatment	Cell	Introduced functional groups or polymers
Covalent bond	Amino groups of membrane protein Membrane protein	Chemical reaction Metabolic reaction	Red blood cells, islets, peripheral blood mononuclear cells, murine splenocytes. Jurkat cells, HeLa cells, CHO cells	PEG-NHS Biotin-NHS PEG-cyanuric chloride, Phosphine by Staudinger ligation Azide, biotin and ketone groups
Electrostatic interaction	Negatively charged cell surface	Non-covalent reaction	Islets, human fibroblasts, MCF-7 breast cancer cells, Mouse MSC	Poly(diallyl dimethyl ammonium chlrode), Poly-L-lysine (PLL), Poly(ethyleneimine)
Hydrophobic interaction	Lipid bilayer membrane	Non-covalent reaction	Islets, HEK293, CCRF-CEM	PEG-lipid PVA-alkyl

Table 1. Cell-Surface Modification techniques

polymers into the lipid bilayer membrane of cells by hydrophobic interactions, and (3) electrostatic interactions between cationic polymers and a negatively charged surface.

Attempts have been made with various types of synthetic and natural polymers for the surface modifications of cells and biomaterials. Such methods are summarized in table 1.

1.2 Covalent bond method

For the covalent conjugation of polymers, surface modifications of living cells have been achieved through chemical or enzymatic treatment or by metabolic introduction.[10-19] N-hydroxyl-succinimidyl (NHS) ester groups and cyanuric chloride are frequently used to chemically form covalent bonds to membrane protein amino groups. However, potential toxic effects may be exerted on membrane proteins.[15-19] Enzymatic treatment and metabolic introduction have also been employed to add various functional groups, such as biotin, azido, and ketone groups to living cell surfaces.[10-11] However, these technologies are limited to the introduction of specified small molecules to cells and may perturb cell physiology.[12,13] Although covalent immobilization is expected to resist chemical degradation and be stable for long time periods, because of the covalent bond is formed with membrane proteins, the introduced polymer and functional groups disappear from the cell surface over time.[14,16,22]

1.3 Hdrophobic interactions and cell-surface modification

Amphiphilic polymers, such as PEG-conjugated phospholipids (PEG-lipid) and poly(vinyl alcohol) bearing hydrophobic alkyl side chains (PVA-alkyl), have been used in cell-surface modification.[12,13,20-26] In these methods, the hydrophobic alkyl chains of amphiphilic polymers are spontaneously anchored into the lipid bilayer membranes through hydrophobic interactions. These spontaneous insertions can be monitored by a surface plasmon resonance (SPR) when a PEG lipid solution is applied to supported lipid membranes that are formed on a SPR sensor. The spontaneous incorporation is greatly affected by the length of phospholipid alkyl chains, that is, their hydrophobicity.

1.4 Electrostatic interactions

Several groups have explored the possibility of constructing thin polymer membranes on the surface of cells through electrostatic interactions between negatively charged cell surfaces and cationic polymers and then further modified them using a layer-by-layer technique of anionic and cationic polymers.[27-31] The ionic polymers that have been employed are poly(allylamine hydrochloride), poly(styrene sulfate), poly-L-lysine and poly(ethyleneimine). A layer-by-layer method is a simple and attractive technique to modify cell surfaces.[32] The outermost layer of the polymer controls the surface properties. The thickness of the layer is also controllable by the number of polymer solution applications. Unfortunately, most polycations, such as PLL and PEI, were found to be extremely cytotoxic and severely damaged the treated cells. PEI, which interacts with cells, were not degraded and not excluded from the cell because PEI immediately destroyed the cell membrane after interaction with the cell surface.

1.5 Bioactive substances immobilized through an intermediary molecule

Bioactive substances have been immobilized on cell surfaces. Two classifications of this method exist. The first strategy includes the immobilization of substances through an intermediary molecule, which is covalently bound to membrane proteins on the surface via amide bonding with hetero- or homo-bifunctional crosslinkers. In one example, biotin molecules were covalently bound to the amino groups of the proteins through crosslinkers. The surface was then sequentially treated with avidin and heparin solutions. Heparin was immobilized to the surface through an electrostatic interaction with avidin (isoelectric point of avidin, pI = 10). Phosphine molecules have also been covalently conjugated to amino groups of membrane proteins and then thrombomodulin was

immobilized using Staudinger ligation. The immobilization of serum albumin has been performed using PEG that was functionalized with NHS groups at both ends; was used for anchoring to the membrane protein amino groups and for the immobilization of serum albumin. These covalent modification methods have been reported to exert minor toxic effects on cell viability and cell functions.[33]

The other method is formation of an intermediary polymer layer through hydrophobic interactions using amphiphilic polymers, such as PEG-lipid and PVA-alkyl, which bear various functional groups. The functional groups that are introduced on the cell surfaces through the amphiphilic polymers can be used for the immobilization of bioactive substances. In one example, PVA-alkyl presenting SH groups were used for the immobilization of bioactive substances displaying maleimide groups. By the same means, PEG-lipids presenting maleimide at the end of the PEG chain was also used for the immobilization of bioactive substances tethering SH groups without cytotoxicity.

1.6 Dynamic surfaces for cell studies

Surface chemistry provides a useful approach to prepare customized model substrates.[34,35] By using self-assembled monolayers (SAMs), it is possible to design model substrates[36] with sufficient control over surface properties to potentially mimic cell-extracellular matrix (ECM) interactions.[37-39] Introducing a dynamic aspect (i.e. the ability to modify the surface with an external stimulus) enables many further opportunities in designing surfaces for cell culture and the reversible control over surface properties.

Dynamic control over SAMs for cell adhesion might provide an additional handle to direct and study the attachment of cells to surfaces. For example, SAMs would enable the

study of cell spreading from a predetermined pattern to screen the cytotoxicity of drug candidates.[40] However, how to reversibly control the adhesion of cells to a dynamic substrates is not well understood.

1.7 SAMs for cell adhesion

SAMs are spontaneously organized assemblies of molecules, formed by adsorption from the solution or the gas phase onto the surface of the solids.[41-43] The molecules bear a terminus that has a specific affinity for a substrate, which is sufficient to displace preadsorbed materials. An extensive variety of functional groups that bind to specific metals, metal oxides, SiO_2, and semiconductors are available.

In vivo, most cells adhere to the ECM;[44] conversely, *in vitro*, SAMs present a method to generate and study model substrates presenting specific ligands via which cells can adhere.[45] The most important benefit of using SAMs for these studies, compared to methods that involve polymer films or adsorbed proteins, is the level of control over the exact composition of the substrate achievable via a predetermined approach. These are key aspects that are necessary for conducting mechanistic studies of cell immobilization and investigating intracellular signaling upon binding.

1.8 Bioinert SAMs

Surfaces that are able to resist the nonspecific (physical) adsorption of biomolecules and cells are generally referred to as 'bio-inert' surfaces. Self-assembling compounds terminated with oligo- or poly(ethylene glycol) (OEG or PEG) units are used extensively to render surfaces inert to cell adhesion.[46-50] However, the specific essential structural requirements to resist the adsorption of proteins and cells remain unclear.[51] Nevertheless, there are several classes of SAMs that inhibit the adhesion of proteins and cells

effectively, including SAMs terminated with oligosarcosines, oligosulfoxides, perfluoroalkyls, or oligo(phosphorylcholine) groups.[51-54]

Dynamic surfaces for immobilizing cells on-demand present new possibilities for studying the mechanistic pathways involved in responses to alterations in the cells' immediate environment. Dynamic changes in the ECM affect cell behavior in several critical stages. Among these are the migration and differentiation of cells during the growth and spread of cancer. Our understanding of the dynamic processes, which occur in the ECM is limited due to their complexity, and hence, studying dynamic substrates that allow for explicit control over changes in the cell-adhesion properties may lead to improved understanding of the ECM as well as cell adhesion to surfaces.

1.9 Cell-surface engineering: Applications and recent developments

1.9.1 *Cell Targeting:* Delivery of systemically infused cells, particularly stem/progenitor cells, into damaged or diseased tissue holds enormous promise for treatment of a variety of disease worldwide.[57] For instance, hematopoietic stem cell (HSC) transplantation (i.e. bone marrow transplantation), which has been used in clinic for several decades to treat blood diseases and cancer, requires systemically infused HSCs to home to the bone marrow from the blood. Mesenchymal stem cells (MSCs) are similarly believed to be home to various sites of inflammation and injury in the body after being systemically infused. MSCs are capable of differentiating into connective tissue cells types that can produce bone, cartilage, and fat, and produce immunomodulatory cytokines and are currently being tested in clinical trials for treatment of various diseases, including graft versus host disease, myocardial infarction, multiple sclerosis, and skeletal tissue repair. Unfortunately systemically administered therapeutic cells that are home to the target sites

at low efficiencies (typically < 1%), due to, at least in part, the lack of expression (or loss during culture expansion) of key homing receptors.[58] Therefore, efforts have been made to introduce cell homing ligands onto cell membranes. Cell homing ligands (on the homing cell) and receptors (on the endothelium) allow homing cells to tether, roll, adhere, and then transmigrate on endothelium as part of the cell homing cascade. Methods include genetic[59-61] and enzymatic engineering[62] treatment with cytokines[63] and chemical approaches.[64,65] The Karp lab has recently developed a simple technology to chemically attach cell adhesion molecules to MSC surface to improve the homing efficiency of inflamed tissues. Their chemical approach involves the stepwise process listed below.

1) Treat the cell amine groups with sulfonated biotinyl-NHS to introduce biotin groups on the cell surface;
2) Add streptavidin, which binds to the biotin on the cell surface and presents unoccupied binding sites, and
3) attach biotinylated homing ligands.

In this model system, biotinylated sialyl Lewis X (SLeX), is a ligand that binds to P and E selectins, which are expressed on the inflamed endothelium and allows cells to roll on the endothelial layer. This ligand was conjugated on the MSC surface. The SLeX modified MSCs demonstrated a robust rolling response on a P-selectin coated substrate under shear stress conditions *in vitro* and on inflamed endothelium *in vivo*. In addition, homing ligands can be introduced onto the cell membrane using non-covalent chemical modification.[66] In a recent work from Dennis and co-workers, MSCs were treated with palmitated protein G where the palmitate chain was incorporated into lipid bilayer

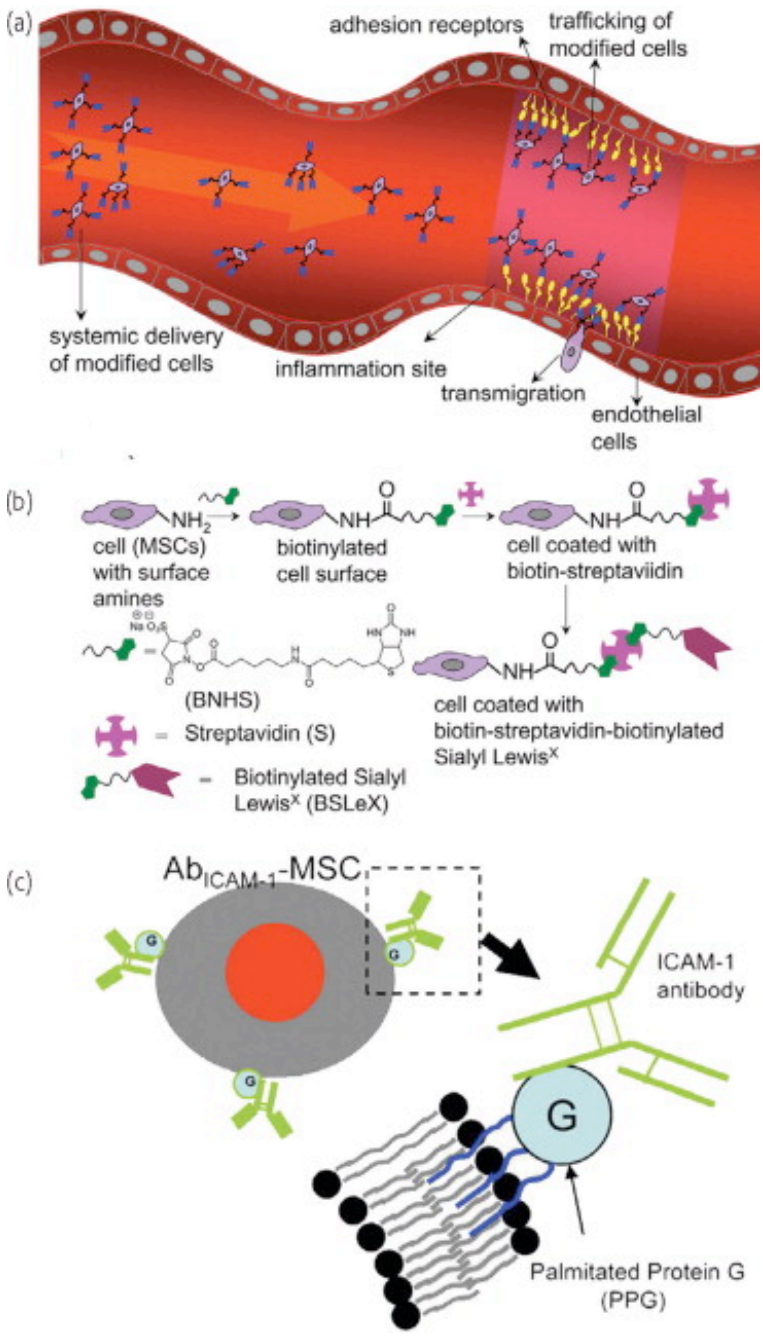

Figure 1.1 a) Schematic showing the targeting of cells from blood to inflamed endothelium expressing receptors that bind to ligands engineered on the cell surface. Two methods of engineering the homing ligand onto the cell surfaces, using covalent and noncovalent chemistry are shown in b) and c), respectively. b) A stepwise process of attaching SLeX to MSCs using biotin-streptavidin linkers and, c) incorporation of palmitated protein G into the cell membrane and subsequent conjugation with an ICAM-1 antibody.

via hydrophobic interactions and protein G provides generic binding sites for antibodies. In a proof-of-concept work, intercellular cell adhesion molecule-1 (ICAM-1) was conjugated onto MSCs, which enabled the cells to bind to ICAM-1, a critical adhesion molecule expressed on activated endothelium. These chemical approaches to modify cell surfaces and immobilize required ligands are not limited to MSCs and the above-mentioned ligands and should have broad implications on cell therapies that utilize systemic administration and require targeting of cells to specific tissues. Presumably, if we know which receptors are present on the endothelium in a targeted anatomical site, we could deliver cells specifically to that site by engineering the complementary ligands to the cell surface.

1.9.2 *Programmed cell-substrate and cell-cell assembly:* The precise 3D arrangements and orientation of cells and their substrate (e.g., extracellular matrix) are key criterion in cell-based assays and microfluidic devices, as well as tissue engineering where one goal is to mimic the 3D complexity of native tissues.[67] Towards this end, chemists and material scientists have begun to engineer cells with biorecognition moieties that are not possessed by native cells to control cell-cell and cell-substrate interactions.[68,69] Francis and colleagues demonstrated the use of single-stranded DNA (ssDNA) to mediate cell adhesion on a substrate.[70] In their work, ssDNA was attached onto cells via a Staudinger ligation reaction between azido (delivered to cell surface glycans via a metabolism process)[71] and phosphine groups modified on ssDNA or by a simple NHS ester (on DNA) and NH_2 (on cell surface).[72] The ssDNAs attached on cells directed the assembly of cells on complementary DNA-attached substrate via DNA hybridization. Such DNA-modified

cells can also be assembled on single cell level on microfabricated patterned sensor devices that may be used for single cell analyses, such as measuring cellular electrical and metabolic activation. In a more recent work from Mathies and co-workers,[73] iridium oxide pH microelectrode arrays were patterned using lithography. The array was enclosed within a microfluidic channel on which ssDNA was attached using silane chemistry. Such devices could then capture complementary DNA-modified cells and measure the single cell metabolism using pH as an indicator. They demonstrated that such devices are able to discriminate between healthy primary T cells and cancerous jurkat T cells that have a higher metabolism.

The DNA-based approach can also be used for the programmable assembly of 3-D cell structure, which may find applications in synthesizing artificial tissues.[74,75] Recently, Gartner and Bertozzi demonstrated the assembly of DNA-modified cells into microtissues in a well defined manner (i.e., structures were controlled by varying the DNA site density on the cell surface, cell concentration and DNA sequence). Briefly, by adjusting the stoichiometry (i.e., 1:50) of two Jurkat cell population that were modified with complementary DNA strands, single cell clusters were produced where the limiting cell type was surrounded by cells added in excess. Interestingly, using fluorescently labeled DNA, they showed that DNA strands are clustered at the cell-cell interface, confirming their specific role in cell-cell assembly. Significantly, such assembled cell clusters could be isolated and purified using flow cytometry and subsequently used as the core for further iterative cell assembly (i.e., adding another layer of DNA-modified cells). More importantly, the authors demonstrated that cells within the assembled microtissues communicate via a paracrine mechanism, which is a prerequisite for the development of

the therapeutically functional tissues. Specifically, in a proof-of-concept model, a CHO cell line engineered to express growth factor interleukin-3 (IL-3) was used as a first building block and the second was an untransformed hematopoietic progenitor cell line (FL5.12) whose survival and replication depends on the presence of IL-3. Cell composites were assembled using the above-mentioned and DNA and then embedded

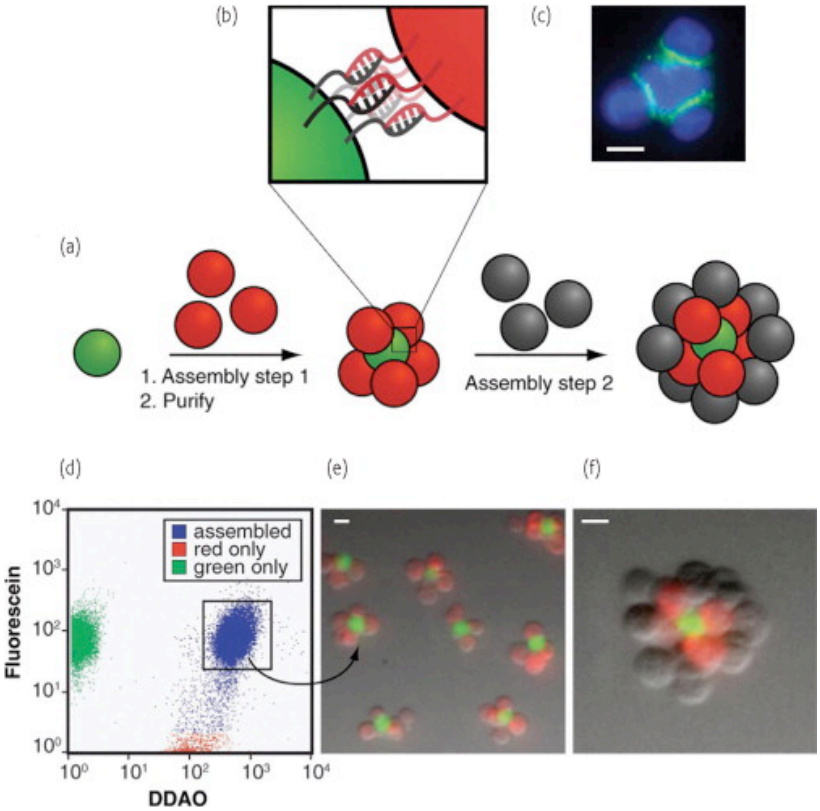

Figure 1.2 a) General schematic of multilayered cell assembly using DNA hybridization. b) Schematic of DNA hybridization between two cells (shown in red and green). c) Fluorescence image of a cluster of assembled cells (blue) with intercellular DNA linkages (green). Clustering of DNA crosslinkers cellular interfaces can be observed. d) Gating of assembled cells in fluorescence activated flow cytometry. e) Fluorescence image showing assembled cells isolated by flow cytometry. f) Fluorescence image of an assembled cell cluster from which (e) a second assembly step occurred to acquire another layer of cells.

within a 3-dimensional agarose matrix. After 16 h, the cell structures underwent accelerated growth due to the presence of IL-3. By contrast, when CHO cells lacking the

gene coding in IL-3 were used in the microtissue, FL5.12 cells showed no growth and instead underwent a morphological change corresponding to the absence of IL-3 induced apoptosis. Finally, other advantages of using DNA assembly in such systems include their reversibility and versatility with respect to engineering multiple orthogonal cell-cell interactions. In addition to ssDNA, self-assembled cargo-carrying DNA arrays can also be attached to cell surfaces. Reiche and colleagues attached hexagonal DNA arrays on cells using streptavidin and antibody as bridges.[76] In their study, it was observed that one or two DNA array patches often attached to one cell, and that single DNA arrays often bridged cells. Occasionally, micron-sized DNA arrays seemed capable of binding to and enveloping multiple cells into larger cellular structures. These larger structures may have the potential to form the foundation for the construction of tissues or organs for transplantation in tissue engineering.

Engineered cell-cell interactions in a bottom-up tissue engineering approach can also be achieved by attaching cell-adhesive polyelectrolyte patches on the cell surface. Swiston et al. recently used a photolithographic-patterning technique to engineer multilayer polymer patches containing a payload component (i.e., super-paramagnetic nanoparticles) onto T cell surfaces.[77] The magnetic nanoparticles allowed cells to be spatially manipulated using an external magnetic field. Importantly, patch-functionalized cells could be programmed to assemble into sheets, rings, or cluster structures. Patches that are cell-adhesive may allow the polymerization of cellular species, with individual cells being the monomers and the patches serving as bifunctional linkages, for construction of macroscopic, functional tissues.

1.9.3 *Bioimaging and Sensing:* One particularly important application of cell-surface engineering is to introduce sensing and imaging probes to visualize cellular and molecular events both in cells and living organisms. The Bertozzi group has pioneered the use of chemical reporters for such purposes with a focus on those that can be incorporated through metabolic pathways.[78]

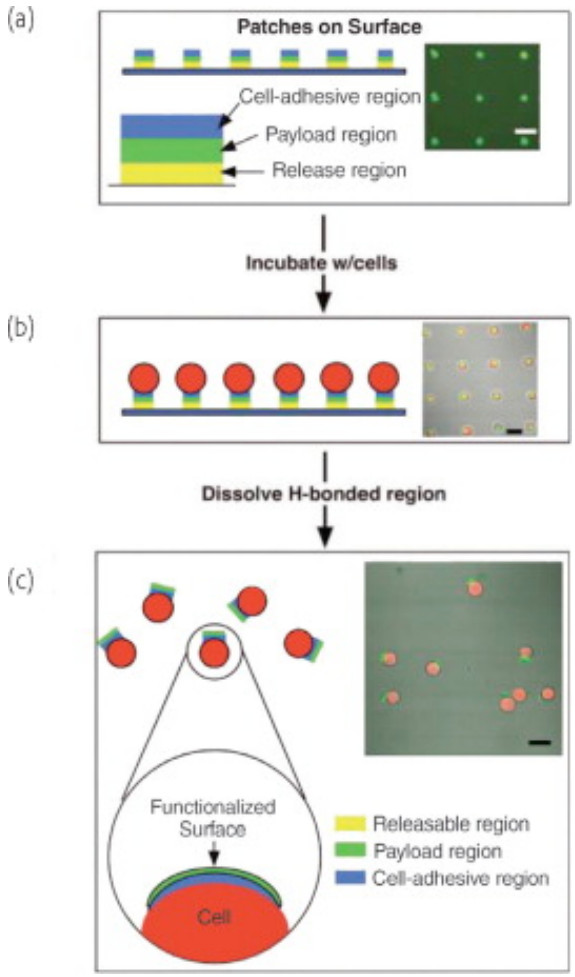

Figure 1.3 Overview of a cell functionalization scheme, using cell adhesive polyelectrolyte patches. In this particular example, cell adhesive region, payload region and release region are chitosan-hyaluronic acid, FITC-poly(allylamine hydrochloride), poly(methacrylic acid)-poly(N-isopropylacrylamide) respectively. a) A regular array of surface-bound patches spaced 50 μm apart. Payload regions are labeled green. After cell incubation and attachment, (b) a majority of the surface bound patches are occupied. Cell cytoplasm is labeled red. (c) After the temperature is reduced to 4 °C for 30 min, the patches are released from the surface while remaining attached to the cell membrane. Scale bars represent 25 μm.

An example of their technology is the engineering of chromatic polydiacetylene (PDA) polymer patches onto cell surfaces for imaging structural perturbations of the membrane bilayer.[79] Specifically, vesicles comprising of diacetylene and lipid molecules including 1,2-dimyristoyl-sn-glycero-phosphoethanolamine and 1,2-dimyristoyl-sn-glycero-3-[phospho-rac-(1-glycerol)] were first formed in solution. These lipid vesicles were then fused with cell membrane and PDA was formed *in situ* upon UV-mediated polymerization. The conjugated PDA nanopatches on cells exhibited an intense blue color and underwent a blue-to-red color change upon structural perturbations of the cell membrane due to conformational transitions in the conjugated (ene-yne) polymer backbone. During this blue-to-red color transition, the initial non-fluorescent PDA also emitted fluorescence at 560 nm and 640 nm. The PDA nanopatches can therefore be used to visualize the cell bilayer perturbations induced by, for example, lidocaine, polymyxin-B, cholesterol, and oleic acid and to screen toxic pesticides and other environmentally toxic small molecules.[80]

1.9.4 *Manipulating cell biological fate:* One ultimate goal of engineering the cell surface is to use externally applied chemical moieties and materials to control cell biology. As an initial effort, Ingber and co-workers demonstrated the use of magnetic nanoparticles on cell membrane to regulate cellular signaling pathways.[81] Specifically, mast cells express membrane FcεRI receptors that can bind t the Fc region of IgE molecules. Multivalent antigens (dinitrophenyl DNP) that bind to IgE can then induce FcεRI receptor oligomerization on cell membrane whereas monovalent antigens do not. The FcεRI receptor clustering quickly triggers an intracellular signaling response characterized by a rapid rise of cytosolic Ca^{2+}, which in turn leads to the local inflammatory response of

mast cells. Instead of using antigen ligand to induce such signaling pathway, Ingber and colleagues immobilized DNP-attached magnetic nanoparticles on IgE-tethered mast cells.[82] The authors ensured that only one DNP molecule was attached on each particle so that receptor clustering did not occur. When an external magnetic field is applied, magnetic nanoparticles clustered on the cell membrane, which caused the oligomerization of FcεRI receptors, a process that could be visualized by the local Ca^{2+} concentration change. Significantly, such magnetic nanoparticles mediated cellular signaling is reversible, switching on and off the magnetic field directly corresponds to a local Ca^{2+} concentration oscillation.

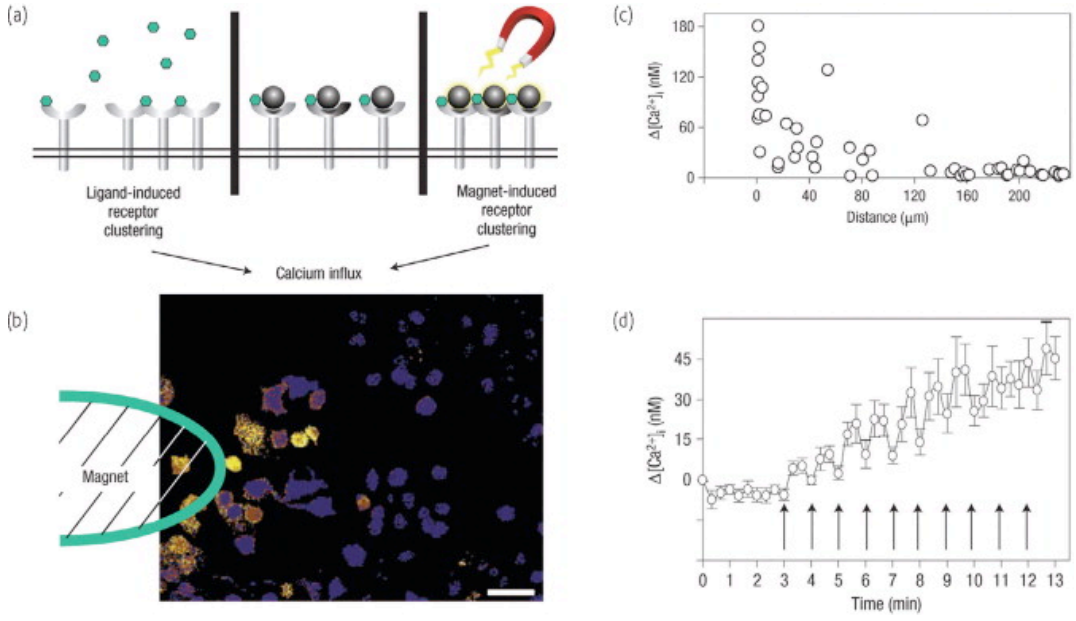

Figure 1.4 Nanomagnetic control of receptor signal transduction. a) The biochemical mechanism that stimulates downstream signaling (left) involves the binding of multi-valent ligands (represented by green hexagons) that induce oligomerization of individual IgE/FcεRI receptor complexes. In the magnetic switch, monovalent ligand-coated magnetic nanobeads (dark grey circles), similar in size to individual FcεRI receptors bind individual IgE/FcεRI receptor complexes without inducing receptor clustering (centre). However, applying a magnetic field that magnetizes the beads and pulls them into tight clusters (right) rapidly switches on receptor oligomerization and calcium signaling. b)

The pseudocolored microfluorimetric image shows the local induction of calcium signaling (yellow) in cells near the tip of the electromagnet within 20 s of the field being applied. Scale bar represents 50 μm. c) Quantification of peak changes in intracellular calcium relative to time 0 measured within individual cells during a 1-min pulse of applied magnetic force as a function of the distance of the tip from the cell surface. d) Effect of a rapid cyclical magnetic stimulation regimen (40 s on, 20 s off) on intracellular calcium signaling.

1.10 Membrane Fusion

Membrane fusion, one of the most fundamental processes of life, occurs when two separate lipid membranes merge into a single continuous bilayer. Experimental and theoretical studies[83,84] concur that membrane fusion proceeds at least through two steps: membrane docking and actual fusion, resulting in the mixing of membrane lipids and membrane-bound contents. Fusion may occur upon close (1-2 nm^2) docking of target membranes, driven by the binding of surface groups. Docking 'strains' the surfaces, allowing the lipids from the two membranes to mix and ultimately form a fusion pore that connects the two compartments. Insertion of a hydrophobic anchor into the lipid matrix can frustrate efficient lipid packing and activate the membrane toward noncovalent reactions, such as lysis and fusion. These reactions are essentially lipidic[85] and are precisely controlled in nature by molecular recognition events. Much of our experimental data on selective membrane fusion has been gathered in studies of synaptic[86] vesicle fusion machinery, as well as in viral membrane fusion machinery.[87-89] Physical membrane deformation or insertion of a hydrophobic fusion peptide enables the formation of a high-energy intermediate nonbilayer lipid surface[90] that fuses with its target membrane when drawn into apposition by surface binding. Native membrane recognition elements are proteins and in class I viral fusion and synaptic vesicle fusion are coiled-coils. Helical bundle formation draws the membranes into apposition; this binding is thought to locally

dehydrate and mechanically deform the membrane, lowering the activation energy for lipid mixing and fusion. Notably, enveloped viruses such as HIV and influenza similarly employ coiled-coil recognition to guide fusion with the host membrane. While considerable advances have furthered our understanding of membrane fusion, fusion has proven difficult to study in living systems. Thus, the mechanism of vesicle fusion remains largely unknown. As a result, efforts have been made to interrogate whether recognition strategies between small molecules would also be fusion competent.[91,92] Such a minimal fusogenic molecular system would be useful for determining the fundamental requirements for membrane fusion catalysis. A simple synthetic model system of specific fusion via molecular recognition would allow physical organic methods to be applied to rigorously probe the scope and limitations of controlled lipid membrane fusion. In my work lipid vesicles, functionalized with ketone and oxyamine molecules, display complementary chemistry and undergo recognition, docking, and subsequent fusion upon covalent oxime bond formation. Liposome fusion was characterized by several techniques including, matrix-assissted laser-desorption/ionization mass spectrometry (MALDI-MS), light scattering, Fourier resonance energy transfer (FRET), isothermal calorimetry (ITC), and transmission electron microscopy (TEM). When cultured with cells, ketone- and oxyamine-containing liposomes undergo spontaneous membrane fusion to present the respective molecules from cell surfaces. The synthetic ketone and oxyamine molecules fused on the cell membrane serve as cell-surface receptors, providing tools for the attachment of other functional materials, biomolecules, and probes on cell surfaces.

1.11 Conclusions

Phospholipid vesicles (liposomes) are widely used for applications in cell tracking, nonviral gene transfer (transfection), and drug delivery. On the basis of their compositions, liposomes are more bioavailable than synthetic polymer capsules or quantum dots. Their cellular uptake has been intensely investigated and shows a strong preference for endocytotic cellular uptake over fusion or lipid-mediated poration. As discussed earlier, a continuous effort has been extended toward replacing genetic and molecular biology tools with simple chemical methods to modify cell surfaces with various probes, furthering applications in tissue engineering. Our liposome fusion strategy to engineer cell surfaces was inspired by the work of Wilson et al. and Csiszar et al. who reported a noncovalent cell-surface engineering strategy via cationic graft copolymer adsorption and a fluorescent cell labeling technique via cationic and aromatic lipid fusion, respectively. These methods are general and do not perturb the cellular machinery of the cells. Liposome fusion can serve as a very important tool among many other techniques that have been previously described to modify and tailor cell surfaces with biologically relevant molecules, significantly contributing to tissue engineering fields in generating 3D tissue constructs.

1.12 Dissertation Organization

This dissertation is organized into seven chapters. Chapter I provides a general discussion of cell-surface engineering techniques and their biomedical applications. Chapter II describes the development of a chemoselective and electroactive fluid lipid bilayer system, which serves as a platform for studying ligand-receptor interactions. Chapter III reports the development of a chemoselective synthetic cell receptor system

based on a liposome delivery and fusion strategy. Chapter IV focuses on the application of the liposome delivery and fusion strategy to generate 3D spheroid cellular assemblies with controlled interconnectivity and patterned multi-layered tissue-like structures. Chapter V describes the development of a novel general and straightforward liposome fusion-based methodology to deliver dynamic and switchable bio-orthogonal chemistries to tailor cell membranes and direct the formation of 3D co-culture tissue structures. Chapter VI discusses the development and demonstration of a novel liposome fusion based delivery strategy to incorporate a unique bio-orthogonal lipid that has the dual ability to serve as a receptor for chemoselective cell-surface tailoring and as a reporter to track cell behavior. Chapter VII describes the general conclusions and future research projects.

1.13 References

1. Huebsch, N.; Mooney, D. J. *Nature*, **2009**, *462*, 426.

2. Zhao, W.; Karp, J. M. *ChemBioChem*, **2009**, *10*, 2308.

3. Anker, J. N.; *Nat. Mater.* **2008**, *7*, 442.

4. Zhao, W.; Karp, J. M. *Nat. Mater.* **2009**, *8*, 453.

5. Glepmans, B. N. G.; *Science*, **2006**, *312*, 217.

6. Schimdt, U. *FASEB J.* **2001**, *15*, 1646.

7. Akin, D. *Nature Nanotech.* **2007**, *2*, 441.

8. Chen, S.; Smith, L. M. *Langmuir*, **2009**, *25*, 12275.

9. Kang, L. *Biomedical Mater. Res Part A*, **2009**

10. Falconnet, D. *Biomaterials*, **2006**, *27*, 3044.

11. Saxon, E.; Bertozzi, C. R. *Science*, **2000**, *287*, 2007.

12. Prescher, J. A.; Dube, D. H.; Bertozzi, C. R. *Nature*, **2004**, *430*, 873.

13. Rabuka, D.; Forstner, M. B.; Groves, J. T.; Bertozzi, C. R.; *J. Am. Chem. Soc.* **2008**, *130*, 5947.

14. Paulick, M. G.; Forstner, M. B.; Groves, J. T.; Bertozzi, C. R. *Proc. Natl. Acad. Sci. U.S.A.* **2007**, *104*, 20332.

15. Lee, D. Y.; Nam, J. H.; Byun, Y. *Biomaterials*, **2007**, *28*, 1957.

16. Lee, D. Y.; Lee, S.; Nam, J. H.; Byun, Y. *Am. J. Transplant.* **2006**, *6*, 1820.

17. Cabric, S.; Sanchez, J.; Lundgren, T.; Foss, A.; Felldin, M.; Kallen, R.; Salmela, K.; Tibell, A.; Tufveson, G.; Larsson, R.; Korsgren, O.; Nilsson, B. *Diabetes*, **2007**, *56*, 2008.

18. Stabler, C. L.; Sun, X. L.; Cui, W.; Wilson, J. T.; Haller, C. A.; Chaikoff, C. A. *Bioconjugate Chem.* **2007**, *18*, 1713.

19. Contreras, J. L.; Xie, D.; Mays, J.; Smyth, C. A.; Eckstein, C.; Rahemtulla, F. G.; Young, C. J.; Anthony, J. T.; Bilbao, G.; Curiel, D. T.; Eckhoff, D. T. *Surgery*, **2004**, *136*, 537.

20. Teramura, Y.; Kaneda, Y.; Iwata, H. *Biomaterials*, **2007**, *28*, 4818.

21. Miura, S.; Teramura, Y.; Iwata, H. *Biomaterials*, **2006**, *27*, 5828.

22. Teramura, Y.; Kaneda, Y.; Totani, T.; Iwata, H. *Biomaterials*, **2008**, *29*, 1345.

23. Teramura, Y.; Iwata, H. *Bioconjugate Chem.* **2008**, *19*, 1389.

24. Totani, T.; Teramura, Y.; Iwata, H. *Biomaterials*, **2008**, *29*, 2878.

25. Teramura, Y.; Iwata, H. *Biomaterials*, **2009**, *30*, 2270.

26. Teramura, Y.; Iwata, H. *Transplantation*, **2009**, *88*, 624.

27. Krol, S.; Guerrera, S.; Grupillo, M.; Diaspro, A.; Gliozzi, A.; Marchetti, P. *Nano Lett.* **2006**, *6*, 1933.

28. Elbert, D. L.; Herbert, C. B.; Hubbell, J. A. *Langmuir*, **1999**, *15*, 5355.

29. Chanana, M.; Gliozzi, A.; Diaspro, A.; Chodnevskaja, I.; Huewel, S.; Moskalenko, V.; Ulrichs, K.; Galla, H. J.; Krol, S. *Nano Lett.* **2005**, *5*, 2605.

30. Germain, M.; Balaguer, P.; Nicolas, J. C.; Lopez, F.; Esteve, J. P.; Sukhorukov, G. V.; Winterhalter, M.; Richard-Foy, H. *Biosens. Bioelectron*, **2006**, *21*, 1566.

31. Veerabadran, N. G.; Goli, P. L.; Stewart-Clark, S. S.; Lvov, Y. M.; Mills, D. K. *Macromol. Biosci.* **2007**, *7*, 877.

32. Decher, G. *Science*, **1997**, *277*, 1232.

33. Ozmen, L.; Ekdahl, K. N.; Elgue, G.; Larsson, R.; Korsgren, O.; Nilsson, B. *Diabetes*, **2002**, *51*, 1779.

34. Mendes, P. M. *Chem. Soc. Rev.* **2008**, *37*, 2512.

35. Guo, Y.; Li, M. Y.; Mylonakis, A.; Han, J. J.; MacDiarmid, A. G.; Chen, X. S.; Lelkes, P. I.; Wei, Y. *Biomacromolecules*, **2007**, *8*, 3025.

36. Mrksich, M. A*cta Biomater.* **2009**, *5*, 832.

37. Mrksich, M.; Whitesides, G. M. *Annu. Rev. Biophys. Biomol. Struct.* **1996**, *25*, 55.

38. Mrksich, M. *Chem. Soc. Rev.* **2000**, *29*, 267.

39. Love, J. C.; Estroff, L. A.; Kriebel, J. K.; Nuzzo, R. G.; Whitesides, G. M. *Chem. Rev.* **2005**, *105*, 1103.

40. Jiang, X.; Bruzewicz, D. A.; Wong, A. P.; Piel, M.; Whitesides, G. M. *Proc. Natl. Acad. Sci. U. S. A.* **2005**, *102*, 975.

41. Love, J. C.; Wolfe, D. B.; Haasch, R.; Chabinye, M. L.; Paul, K. E.; Whitesides, G.

M.; Nuzzo, R. G. *J. Am. Chem. Soc.* **2003**, *125*, 25897.

42. Schreiber, F. *Prog. Surf. Sci.* **2000**, *65*, 151.

43. Onclin, S.; Ravoo, B. J.; Reinhoudt, D. N. *Angew. Chem. Intd. Ed.* **2005**, *44*, 6282.

44. Alberts, B.; Johnson, A.; Lewis, J.; Raff, M.; Roberts, K.; Walter, P. *Molecular Biology of the Cell*, Garland Science, London, 2002.

45. Ostuni, E.; Yan, L.; Whitesides, G. M. *Colloids Surf. B.* **1999**, *15*, 3.

46. Mirksich, M.; *Curr. Opin. Colloid Interface Sci.* **1997**, *2*, 83.

47. Mora, M. *J. Biomater. Sci. Polym. Ed.* ***2000****, 11*, 547.

48. Genzer, J.; Efimenko, K. *Biofouling,* **2006***, 22*, 339.

49. Aldred, N.; Clare, A.S. *Biofouling,* **2008***, 24*, 351.

50. Schuler, M.; Trentin, D.; Textor, M.;Tosatti, S. G. P. *Nanomedicine,* **2006***, 1*, 449.

51. Veiseh, M.; Zhang, M. Q. *J. Am. Chem. Soc.* **1996***, 118*, 5136.

52. Deng, L.; Mrksich, M.; Whitesides, G. W. *J. A. Chem. Soc.* **1996***, 118*, 5136.

53. Luk, Y.-Y.; Kato, M.; Mirksich, M. *Langmuir,* **2000***, 16*, 9604.

54. Kane, R. S.; Deschatelets, P.; Whitesides, G. W. *Langmuir,* **2003***, 19*, 2388.

55. Caffrey, M.; Wang, J. *Annu. Rev. Biophys. Biomol. Strtuct.* **1995***, 24*, 351.

56. Chen, S. F.; Lui, L. Y.; Jiang, S. Y. *Langmuir,* ***2006****, 22*, 2418.

57. Karp, J. M.; Teo, G. S. L. *Cell Stem Cell,* **2009***, 4*, 206.

58. Rombouts, W. J. C.; Ploemacher, R. E. *Leukemia,* **2003***, 17*, 160.

59. Kumar, S.; Selim, M. G.; Caplan, L. R. Gene Ther. 2010, 17, 105.

60. Brenner, S.; Whitting-Theobald, N.; Kawai, T.; Linton, G. F.; Rudikoff, A. G.; Choi, U.; Ryser, M. F.; Murphy, P. M.; Sechler, J. M. G.; Malech, H. L. *Stem Cells,* **2004***,*

7, 1128.
61. Zhang, D.; Fan, G-C.; Zhou, X.; Zhao, T.; Pasha, Z.; Xu, M.; Zhu, Y.; Ashraf, M.; Wang, Y. *J. Mol. Cell. Cardiol.* **2008***, 44*, 281.

62. Sackstein, R.; Merzaban, J. S.; Cain, D. W.; Dagia, N. M; Spencer, J. A.; Lin, C. P.; Wohlgemuth, R. *Nat. Med. 2008, 14*, 181.

63. Chavakis, E.; Urbich, C.; Dimmelar, S. *J. Mol. Cell. Cardiol.* **2008***, 4*, 514.

64. Sarkar, D.; Vemula, P. K.; Teo, G. S. L.; Spelke, D.; Karnik, R.; Wee, L. Y.; Karp, J. M. *Bioconjugate Chem.* **2008***, 19*, 2105.

65. Ko, I. K.; Kean, T. J.; Dennis, J. E. *Biomaterials,* **2009***, 22*, 3702.

66. Rabuka, D.; Forstner, M. B.; Groves, J. T.; Bertozzi, C. R. *J. Am. Chem. Soc.* **2008***, 130*, 5947.

67. Khademhosseini, A.; Vacanti, J. P.; Langer, R. *Scientific American,* **2009***, 300*, 64.

68. Borisenko, G. G.; Zaltseva, M. A.; Chuvlin, A. N.; Pozmogova, G. E. Nucleic Acids Res. 2009, 37, e 28.

69. Kamitani, R.; Niikura, K.; Okajima, T.; Matsuo, Y.; Ijiro, K. ChemBioChem, 2009, 2, 230.

70. Chandra, R. A.; Douglas, E. S.; Mathies, R. A.; Bertozzi, C. R.; Francis, M. B. *Angew. Chem. Intd. Ed.* **2006***, 6*, 896.

71. Prescher, J. A.; Dube, D. H.; Bertozzi, C. R. *Nature,* **2004***, 430*, 873.

72. Hsiao, S. C.; Shum, B. J.; Onoe, H.; Douglas, E. S.; Gartner, Z. J.; Mathies, R. A.; Bertozzi, C. R.; Francis, M. B. *Langmuir,* **2009***, 25*, 6985.

73. Douglas, E. S.; Hsiao, S. C.; Onoe, H.; Bertozzi, C. R.; Francis, M. B.; Mathies, R. A. *Lab Chip,* **2009***, 9*, 2010.

74. Paul, A. D. B. Biotechnol. Bioeng. 2007, 97, 1617.

75. Gartner, Z. J.; Bertozzi, C. R. Proc. Natl. Acad. Sci. U. S. A. 2009, 106, 4606.

76. Koyfman, A. Y.; Braun, G. B.; Reich, N. O. J. *Am. Chem. Soc.* **2009***, 131*, 14237.

77. Swiston, A. J.; Cheng, C.; Um, S. H.; Irvine, D. J.; Cohen, R. E.; Rubner, M. F. *Nano Lett.* **2008***, 8*, 4446.

78. Prescher, J. A.; Bertozzi, C. R. *Nat. Chem. Biol.* **2005***, 1*, 13.

79. Orynbayeva, Z.; Kolusheva, S.; Livneh, E.; Lichtenshtein, A.; Nathan, I.; Jelinek, R. *Angew. Chem. Intd. Ed.* **2005***, 7*, 1092.

80. Mech, A.; Orynbayeva, Z.; Irgebayev, K.; Kolusheva, S.; Jelinek, R. *Chem. Res. Toxicol.* **2009***, 22*, 90.

81. Mannix, R. J.; Kumar, S.; Cassiola, F.; Montoya-Zavala, M.; Feinstein, E.; Prentiss, M.; Ingber, D. E. *Nat. Nanotech.* **2008***, 3*, 36.

82. Yung, C. W.; Fiering, J.; Mueller, A. J.; Ingber, D. E. *Lab Chip* **2009***, 9*, 1171.

83. Jahn, R.; Lang, T.; Sudhoff, T. C. *Cell* **2003***, 112*, 519.

84. Blumenthal, R.; CLague, M. J.; Durell, S. R.; Epand, R. M. *Chem. Rev.* **2003***, 103*, 53.

85. Lentz, B.; Malinin, V.; Haque, M. E.; Evans, K. *Curr. Opi. Struct. Biol.* **2000***, 10*, 607.

86. Lin, R. C.; Scheller, R. H. *Annu. Rev. Cell Dev. Biol.* **2000***, 16*, 19.

87. Sollner, T. H. *Curr. Opin. Cell Biol.* **2004***, 16*, 429.

88. Chan, D. C.; Kim, P. S. *Cell* **1998***, 93*, 681.

89. Carr, C. M.; Chaudhry, C.; Kim, P. S. *Proc. Natl. Acad. Sci. U. S. A.* **1997***, 94*, 14306.

90. Yang, L.; Ding, L.; Huang, H. W. *Biochemistry* **2003***, 42*, 6631.

91. Gong, Y.; Ma, M.; Luo, Y.; Bong, D. *J. Am. Chem. Soc.* **2008***, 130*, 6196.

92. Gong, Y.; Luo, Y.; Bong, D. *J. Am. Chem. Soc.* **2006***, 128*, 14430.

CHAPTER 2

Selective Tethering of Ligands and Proteins to a Microfluidically Patterned Electroactive Fluid Lipid Bilayer Array

2.1 Introduction:

The formation of supported fluid lipid bilayers on surfaces has generated tremendous research interest due to their ability to model the natural cell plasma and organelle membranes. As a result, these platforms have been used for a range of application from the design of biosensor technologies, the investigation of fundamental biomembrane properties[1], intermembrane interactions[2] to cell adhesion and migration. To characterize lipid raft clustering and ligand-binding interactions at supported membranes several analytical tools have been employed, including atomic force microscopy (AFM),[3] surface plasmon resonance (SPR),[4] and microfabricated microfluidic cassettes. To form patterns and arrays of bilayers on surfaces several strategies have been developed ranging from microcontact printing[5], microfluidics[6], nanoshaving[7], mechanical scratching[8], photolithography[9] to photopolymerization[10]. Formation of these patterns and arrays serve as a platform to study a number of biomolecular and binding interactions[11] to the lipid bilayer. Ultimately, the information gathered from evaluating membrane interactions, may lead to the development of membrane based biomedical devices for conducting novel cell-based assays[12] and potentially high throughput drug screens targeting membranes or membrane associated components[13].

Various materials have been used as a support to form fluid bilayer membranes, including glass surfaces, metal oxide surfaces, flexible polymer cushions, self-assembled monolayers (SAMs), and SAM-supported polycationic layers.[14-16] Among these platforms, SAMs of alkanethiols on gold, provide a well-defined conducting surface that is amenable to several analytical surface techniques to characterize and monitor the formation of bilayer membranes.[17,18] Alkanethiols are synthetically flexible and/or commercially available, providing diverse opportunities for tailoring materials for a range of applications.[19]

Many previous studies have used planar supported fluid lipid bilayers to evaluate ligand-receptor binding interactions where one component, usually the protein, was assembled with a vesicle formation prior to forming planar bilayers.[20,,21] To our knowledge, there has been no quantitative and general chemoselective immobilization strategy to tailor and pattern fluid lipid bilayers with a variety of ligands for bio-interfacial studies.

Herein, we use a microfluidic lithography strategy to pattern two different SAMs on gold followed by the addition of electroactive vesicles for the generation of patterned fluid lipid bilayers capable of immobilizing a variety of ligands and biomolecules. In order to support a fluid lipid bilayer on gold, a patterned siloxane-alkanethiol SAM was used to mimic the properties of glass siloxane surfaces.[22] A SAM of mercaptopropyl trimethoxysilane (HO_3SiSH) was formed, and a solution containing hydroquinone-tethered alkane (H_2Q) lipid vesicles was ruptured, generating a fluid bilayer surface. H_2Q molecules were incorporated into the lipid vesicles prior to the formation of the bilayer. Upon formation of a bilayer the electroactive H_2Q molecules can be electrochemically

oxidized to the corresponding quinone (Q), where the gold substrate is a working electrode. The resulting Q molecules permit the selective coupling of soluble oxyamine-containing ($RONH_2$) ligands.[23,24] As demonstrations of this strategy, oxyamine-rhodamine and glucose-oxyamine ligands were immobilized to electroactive lipid bilayers and characterized by electrochemistry and fluorescence microscopy. Ultimately, this system provides an excellent platform for the chemoselective and biospecific immobilization of ligands to patterned fluid lipid bilayers for studying a variety of biomolecular interactions for a range of biotechnology and cell based applications.

2.2 Materials and Methods

2.2.1 Materials

Egg palmitoyl-oleoyl phosphatidylcholine (egg-POPC) was purchased from Avanti Polar Lipids (Alabaster, AL), ConA-TRITC was obtained from Invitrogen (Carlsbad, CA), and all other chemicals were obtained from Sigma Aldrich.

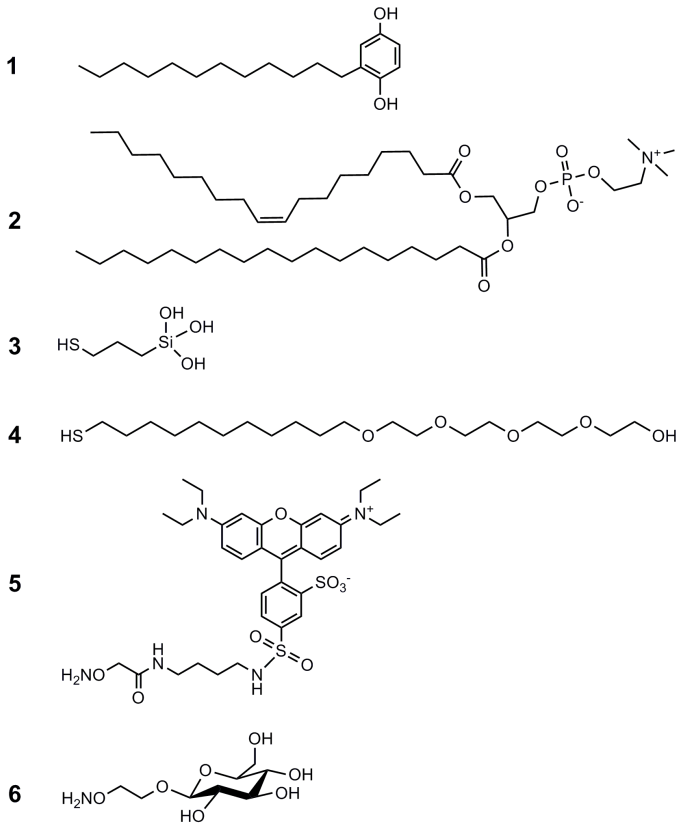

Figure 2.1. List of molecules used in this study. (**1**) Hydroquinone-tethered alkane (H_2Q); (**2**) egg palmitoyl-oleoyl phosphatidylcholine (egg-POPC); (**3**) 3-mercaptopropyl siloxane or siloxane-tethered alkanethiol (HO_3SiSH); (**4**) tetra(ethylene glycol)-tethered alkanethiol (EG_4SH); (**5**) Rhodamine-oxyamine (Rhod-ONH_2); (**6**) Glucose-oxyamine (Glc-ONH_2).

2.2.2 Synthesis of 1,4-bis(tetrahydro-2H-pyran-2-yloxy)benzene (7)

To a solution of hydroquinone (6.0 g, 54.5 mmol) in THF (40 mL) was added 2,3-dihydropuran (44.0 mL, 245.3 mmol, 4.5 eq) and 3 drops of concentrated HCl. The mixture was stirred at room temperature for 8h, diluted with EtOAc (40 mL), washed with $NaHCO_3$ (3 x 50 mL) and brine (1 x 25 mL), dried over $MgSO_4$, and concentrated to a white solid. The solid was then dissolved in EtOAc and recyrstallized with hexanes to afford a white solid 7 (10. 02 g, 66%), ^{1}H NMR (400 Hz, $CDCl_3$, δ): 1.67-1.58 (m, 6H, J=36; -CH_2-), 1.88-1.85 (m, 4H, J=12; -CH_2-), 2.03-2.00 (m, 2H, J=12; -CH_2-), 3.62-3.60

(m, 2H, J=8; -CH_2-), 3.98-3.96 (m, 2H, J=8; -CH_2-), 5.34-5.32 (t, 2H, J=7; -CH-), 7.00 (s, 4H; Ar-H).

2.2.3 Synthesis of 2,2'-(2-dodecyl-1,4-phenylene)bis(oxy)bis(tetrahydro-2H-pyran) (8)

To a solution of 7 (2.00 g, 7.0 mmol) in dry THF (40 mL) at 0°C was added tert-butyllithium (4.6 mL of a 1.7 M solution, 9.1 mmol, 1.3 eq) dropwise over 15 min. The mixture was stirred at 0°C for 60 min and then slowly warmed to room temperature over 3h. At this time, 1-bromododecane (5.08 mL, 21.0 mmol, 3 eq) was added and stirred for 12h. The mixture was diluted with DCM (40 mL) and washed with NH_4Cl (3 x 50 mL) and brine (1 x 25 mL), dried over $MgSO_4$, and concentrated to afford a yellow oil. The mixture was purified by flash chromatography 95:5 Hex:EtOAc to elute a yellow oil 8 (2.23 g, 71%), ^{1}H NMR (400 Hz, $CDCl_3$, δ): 0.91-0.89 (t, 3H, J=8; -CH_3), 1.27-1.23 (m, 18H, J=16; -CH_2-), 1.72-1.68 (m, 10H, J=16; -CH_2-), 2.61-2.58 (t, 2H, J=12; -CH_2-), 3.65-3.63 (m, 4H, J=8; -CH_2-), 5.80-5.78 (t, 2H, J=8; -CH-), 6.68 (s, 1H; Ar-H), 6.81 (s, 1H; Ar-H), 6.84 (s, 1H; Ar-H).

2.2.4 Synthesis of 2-dodecylbenzene-1,4-diol (hydroquinone-tethered alkane, H_2Q) (1)

To a solution of 8 (2.0 g, 4.5 mmol) in 40 mL of a 3:1:1 mixture of AcOH/THF/H_2O was stirred for 16h. The mixture was then concentrated, diluted in EtOAc (20 mL) and washed with 1 mM NaOH (2 x 10 mL), dried over $MgSO_4$, and concentrated to afford a white solid 1 (1.12 g, 90%), ^{1}H NMR (400 Hz, $CDCl_3$, δ): 0.89-0.87 (t, 3H, J=8; -CH_3), 1.30-1.25 (m, 18H, J=20; -CH_2-), 1.57-1.55 (m, 2H, J=7; -CH_2-), 2.58-2.55 (t, 2H, J=12; -

CH_2-), 6.57-6.56 (m, 1H, J=4; Ar-H), 6.67-6.65 (m, 2H, J=7; Ar-H); LRMS (ESI) (*m/z*) $[M\text{-}Na]^+$ calcd for $C_{18}H_{30}O_2$, 301.56, found 301.15.

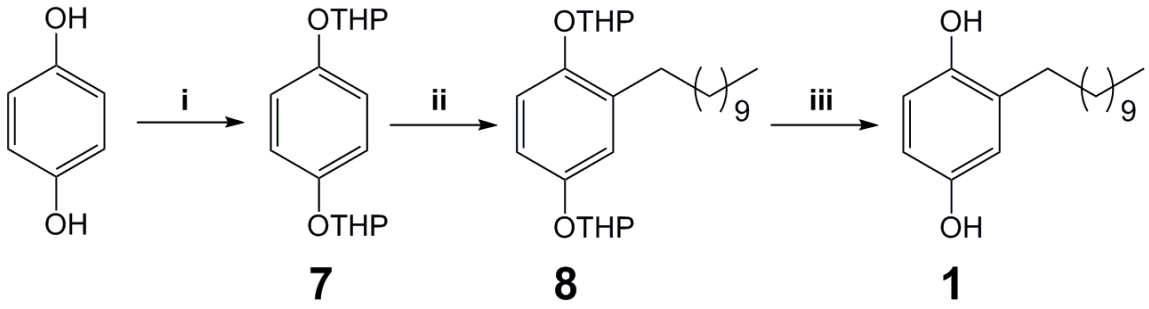

Scheme 2.1. Synthetic route to hydroquinone-tethered alkane (H_2Q, **1**). Reagents and conditions: (i) 2,3-dihydropuran (4.5 eq), HCl (cat), THF, 8h, 66%; (ii) tert-butyllithium (1.3 eq), 1-bromododecane (3 eq), THF, 0°C, 3h, then 25°C, 12h, 71%; (iii) 3:1:1 AcOH/THF/H_2O, 16h, 90%.

2.2.5 Synthesis of 1,2,3,4,6-Penta-O-acetyl-β-D-glucopyranose (9)

To a solution of acetic anhydride (50mL) was added sodium acetate (5.40 g, 66.6 mmol, 3 eq.). The mixture was refluxed at 90°C for 20 minutes to which D-glucose (4.00 g, 22.2 mmol) was added and stirred for 4 hours. The mixture was then concentrated, dissolved in methanol, and recrystallized with cold water. A white solid was then filtered and dried to afford (9) (7.44 g, 85%), ^{1}H NMR (400 Hz, $CDCl_3$, δ): 2.01, 2.03, 2.07, 2.09, 2.13 (s, 15H; CH_3), 4.17-4.14 (m, 2H, J=12; CH_2), 4.40-4.38 (2xm, 1H, J=7; CH), 4.71-4.69 (d, 1H, J=8; CH), 5.32-5.31 (t, 1H, J=4; CH), 5.37-5.36 (t, 1H, J=4; CH), 5.41-4.40 (d, 1H, J=4; CH).

2.2.6 Synthesis of O-(2,3,4,6-tetra-O-acetyl)-β-D-glucopyranosyl-bromoethyloxy (10)

To a solution of 9 (1.00 g, 2.56 mmol, 1 eq.) and $ZnCl_2$ (catalytic) in anhydrous dichloromethane (15 mL) was added 2-bromoethanol (0.24 mL, 3.33 mmol, 1.3 eq.), followed by the addition of boron trifluoride diethyl etherate (0.41 mL, 3.33 mmol, 1.3 eq.) dropwise at 0°C. The mixture was stirred under inert atmosphere (N_2) for 6h at room temperature. Upon completion, the mixture was then washed with water (2x50mL), sodium bicarbonate (1M) (2x50mL), concentrated, and recrystallized in hexanes to afford a white solid 10 (0.93 g, 80%), ^{1}H NMR (400 Hz, $CDCl_3$, δ): 2.01, 2.03, 2.07, 2.09 (s, 12H; CH_3), 3.50-3.49, 3.53-3.51 (2xm, 2H, J=8; CH_2), 3.51-3.49 (m, 2H, J=8; CH_2), 4.11-4.08 (m, 2H, J=12; CH_2), 4.30-4.28 (2xd, 2H, J=8; CH_2), 4.58-4.57 (d, 1H, J=4; CH), 4.99-4.98 (t, 1H, J=4; CH), 5.13-5.12 (t, 1H, J=4; CH), 5.21-5.20 (t, 1H, J=4; CH), (ESI) (*m/z*) [M + H$^+$]: 454.05.

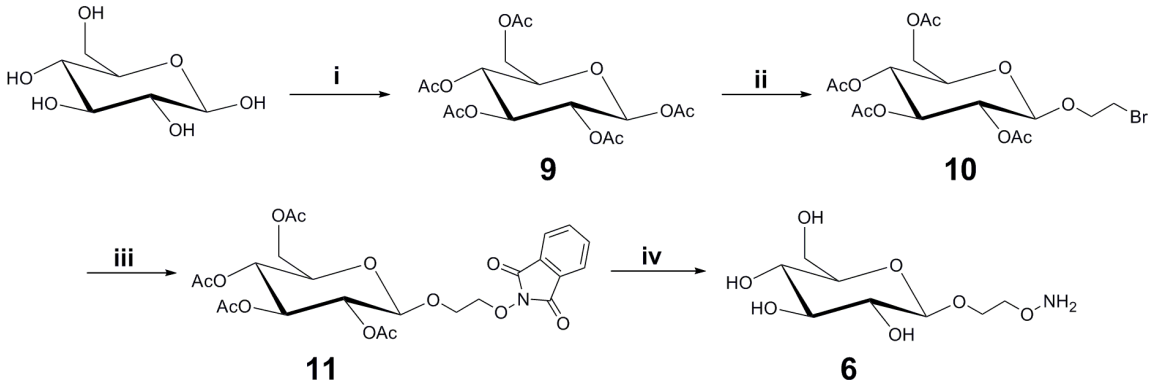

Scheme 2.2. Synthetic route to glucose-oxyamine (Glc-ONH_2, **6**). Reagents and conditions: (i) Ac_2O, NaOAc (3 eq), $ZnCl_2$ (cat), 90°C, 4h, 95%; (ii) 2-bromoethanol (1.3 eq), $ZnCl_2$ (cat), boron trifluoro diethyletherate (1.3 eq), DCM, 0°C-rt, 6h, 80%; (iii) N-hydroxyphthalimide (1.5 eq), $NaHCO_3$ (1.5 eq), DMF, 65°C, 8h, 76%; (iv) hydrazine (6 eq), EtOH, rt, 48h, 67%.

2.2.7 Synthesis of O-(2,3,4,6-tetra-O-acetyl)-β-D-glucopyranosyl-ethyloxy-N-oxyphthalimide (11)

To a solution of N-hydroxyphthalimide (1.07 g, 6.59 mmol, 1.5 eq.) in DMF (20 mL) at 65°C was added sodium bicarbonate (0.55 g, 6.59 mmol, 1.5 eq.). The mixture was then stirred for 30 min until fully deprotonated (brown in color) to which 10 (2.00 g, 4.39 mmol, 1 eq.) was added. The solution was stirred under inert atmosphere (N_2) for 8 hours. After completion, the mixture was diluted with dichloromethane and washed with water (8x100mL) and 1 M $NaHCO_3$ (3x25mL) or until the excess N-hydroxyphthalimide was completely taken up into the aqueous layer. The organic layer was concentrated and purified by flash chromatography (Hex/EtOAc, 3.5:6.5) to afford a pale yellow oil 11 (1.49 g, 63%), ^{1}H NMR (400 Hz, $CDCl_3$, δ): 2.09-2.00 (4xs, 12H; CH_3), 3.78-3.76 (m, 2H, J=8; CH_2), 4.04-4.02, 4.4.39-4.37 (2xm, 2H, J=8; CH_2), 4.09-4.06 (m, 2H, J=12; CH_2), 3.50-3.48 (2xd, 2H, J=8; CH), 4.78-4.77 (d, 1H, J=4; CH), 4.97-4.95 (t, 1H, J=7; CH), 5.09-5.07 (t, 1H, J=7; CH), 5.31-5.29 (t, 1H, J=7; CH), 7.78-7.76 (2xm, 4H, J=8; 4H), (ESI) (*m*/*z*) [M + H^+]: 537.15.

2.2.8 Synthesis of β-D-glucopyranosyl-propyloxy-N-oxyamine (Glucose-oxyamine, Glc-ONH_2) (6)

To a solution of 11 (0.912 g, 1.70 mmol) in ethanol (15 mL) was added hydrazine (0.327 mL, 10.2 mmol, 6 eq). The mixture was stirred under inert atmosphere for up 48h. The mixture was then concentrated and purified by flash chromatography (MeOH/DCM, 3:7) to afford a white solid 6 (0.213 g, 52%), ^{1}H NMR (400 Hz, $CDCl_3$, δ): 3.18-3.16 (t, 1H, J=7; CH), 3.27-3.24 (t, 1H, J=12; CH), 3.36-3.34 (m, 2H, J=8; CH_2), 3.60-3.59, 3.57-3.56

(2xd, 1H, J=4, J=16; CH), 3.75-3.72 (2xm, 2H, J=12; CH_2), 3.78-3.77 (m, 2H, J=8; CH_2), 3.93-3.91 (m, 1H, J=8; CH), 4.36-4.34 (d, 1H, J=8; CH); (ESI) (*m/z*) [$M+H^+$]: 239.10.

2.2.9 Formation of electroactive lipid vesicles

Hydroquinone-tethered alkane (H_2Q) (160 μL at 10 mol %) was reacted with egg-POPC (410 μL at 90 mol %) in chloroform for 4 h, followed by concentration under high vacuum. The dried lipid sample was then reconstituted in 2.43 mL of tris buffer, pH 7.4. The contents of the vial were warmed to 50°C and sonicated at a 70% output for 15 min, with a tip sonifier, until the solution was clear. Large and small unilamelar vesicles (LUVs and SUVs, respectively) were then centrifuged for 30 min at 30,000g to pellet the LUVs, leaving the SUVs suspended in solution.

2.2.10 Preparation of monolayers

Gold substrates were prepared by electron beam deposition of titanium (6 nm) and gold (12-18 nm) on 24 mm × 100 mm glass microscope slides. The slides were cut into 2 × 2 cm^2 pieces and washed with absolute ethanol before use. The slides were then immersed in 1mM solution of 3-mercaptopropyl trimethoxysilane in EtOH for ~12 h.

2.2.11 Generation of solid-supported electroactive lipid bilayers

A 3 mM solution of SUV (egg-POPC/H_2Q, 9:1) in Tris buffer was added to a SAM-modified gold substrate. Lipid bilayers formed by spontaneous fusion on the surface, and the non-adsorbed vesicles were removed by washing with PBS buffer (10 volumes).

2.2.12 Electrochemical characterization

All electrochemical measurements were performed using the Bioanalytical Systems Epsilon potentiostat. An Ag/AgCl electrode (Bioanalytical systems) served as the reference, the Au monolayer acted as the working electrode, and a Pt wire served as the counter electrode. The electrolyte was 1 M $HClO_4$ and the scan rate was 100mV s^{-1}. Measurements were performed in a standard electrochemical cell.

2.2.13 Fluorescence Recovery After Photobleaching (FRAP)

For FRAP experiments, a fluorescent 7-nitrobenz-2-oxa-1,3-diazol-4-yl phosphocoline (NBD-PC) lipid, H_2Q and egg-POPC (3:10:87) ratio bilayer on gold was excited by a Argon laser (488 nm) for a period of 2 min to induce photobleaching. The shutter was then closed after photobleaching and the observed fluorescence recovery was recorded at periodic intervals. To analyze the images to determine fluorescence recovery after photobleaching rates, processing software (LSM 510 Meta, Germany) was used. Approximately >95% of the fluorescence was recovered after 6 min the photobleaching step indicating an electroactive fluid lipid bilayer.

2.2.14 Fluorescence microscopy characterization

Fluorescent and brightfield microscopy was performed using a Nikon TE2000-E inverted microscope. Image acquisition and processing was performed using Metamorph software.

2.2.15 Patterning of SAMs

A polydimethylsilane (PDMS) microfluidic cassette was reversibly sealed to a bare gold surface. In order to pattern a SAM by microfluidic lithography (μFL), a 1 mM solution of

tetra(ethylene) glycol-terminated alkanethiol (EG_4SH) in ethanol was flowed through the channels for 60 s. Without removing the cassette, ethanol was flowed through the channels and suction evacuated to clean the surface. The same cassette was then placed perpendicular to the newly patterned EG_4SH SAM, and μFL was performed with the exact same conditions for a second time, as previously described. The substrate was then rinsed with ethanol, dried, and immersed into a 1 mM solution of HO_3SiSH in EtOH for 16 h, in order to backfill the remaining gold with a SAM.

2.2.16 Electroactive bilayer patterning and ligand immobilization

To generate bilayer patterns, gold surfaces with pre-patterned EG_4SH and HO_3SiSH SAMs were immersed into a 3 mM solution of egg-POPC:H_2Q (9:1) in Tris buffer for 1 h. Substrates were then rinsed with PBS, dried with air, and oxidized electrochemically to present Q-terminated patterned bilayers. Rhod-ONH_2 was reacted with the Q-terminated bilayers (7 mM in MeOH, rt, 4 h). Similarly, glucose-oxyamine (glc-ONH_2) was also immobilized to microarrays of Q-terminated bilayers (20 mM in MeOH, rt, 4 h), and TRITC-conjuagted Concanavalin A (ConA) was added (1 mg/mL in DMSO, rt, 2 h). The resultant microarrays displaying Rhod and ConA were imaged by fluorescence microscopy.

2.3 Results and Discussion

2.3.1 Liposome preparation

The general schematic illustrating the formation of embedded H_2Q (Scheme 1, **1**) lipid vesicles is shown in Figure 1. A solution of H_2Q (1 mg/mL) and egg-POPC (10 mg/mL, **2**) in chloroform ($CHCl_3$) was reacted for 4 h. During mixing, the alkane chain of the H_2Q molecules behaved like lipid tails and spontaneously inserted within the lipid vesicle

membrane. The lipid mixture was then concentrated by speed vacuum for 4 h and reconstituted in Tris buffer, pH 7.4, 3 mM. This solution was then ultrasonicated for 20 min, generating a mixture of small and large unilamellar vesicles (SUVs and LUVs, respectively). The resultant solution was centrifuged (30,000g, 30 min) to pellet out the LUVs, leaving a suspension of H_2Q-containing SUVs.

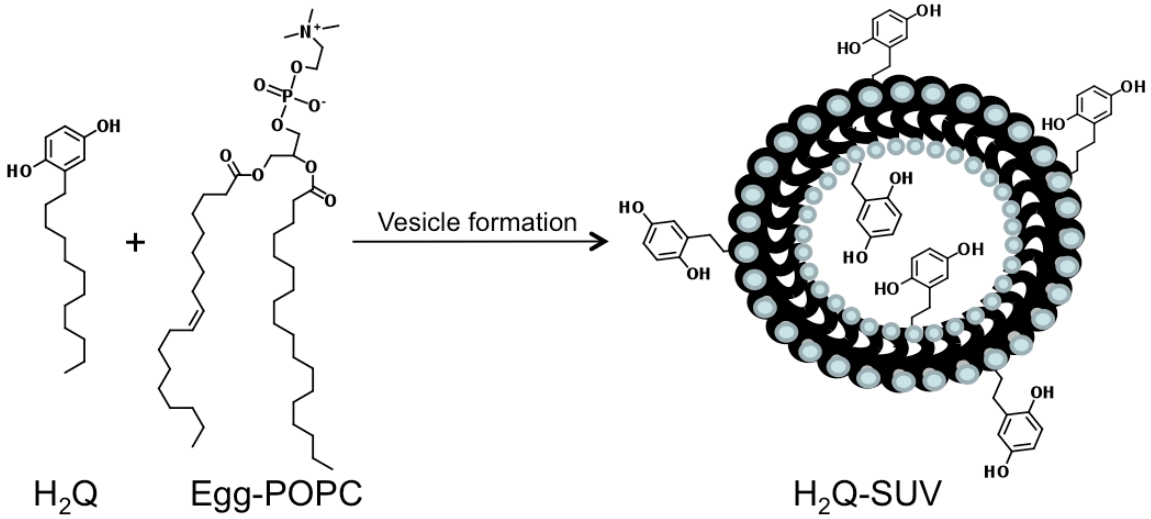

Figure 2.2 General schematic for the formation of chemoselective, electroactive lipid vesicles. Hydroquinone-tethered alkane (H_2Q) was reacted with egg palmitoyl-oleoyl phosphatidylcholine (egg-POPC). The mixture was then concentrated, reconstituted, ultrasonicated, and centrifuged to generate H_2Q containing small unilamellar vesicles (H_2Q-SUVs).

2.3.2 Electroactive bilayer formation

The SUV solution was then ruptured on a SAM of HO_3SiSH generating a fluid bilayer with H_2Q presented from the bilayer surface (Figure 2). Experimentally, a gold substrate was immersed in 1 mM solution of HO_3SiSH (**3**) for 16 h to form a uniform SAM. This particular alkanethiol was selected due to its generation of a 2-dimensional network of silica when assembled on a surface in the presence of water. This in turn produces a model system where the Si-OH head group aids in maintaining bilayer fluidity. The SUV-containing suspension was then added to the SAM surface, resulting in spontaneous

fusion to form a planar bilayer. We have shown previously on gold and indium tin oxide surfaces that the H_2Q molecules are redox active and can be oxidized to the corresponding Q by applying a mild electrochemical potential via the gold supporting electrode. The Q serves as a chemoselective site for ligand conjugation when reacted with an oxyamine-tethered ($RONH_2$) ligand. The resulting oxime linkage is also redox active but with distinct and diagnostic peaks and can be monitored precisely by electrochemistry.[25,26]

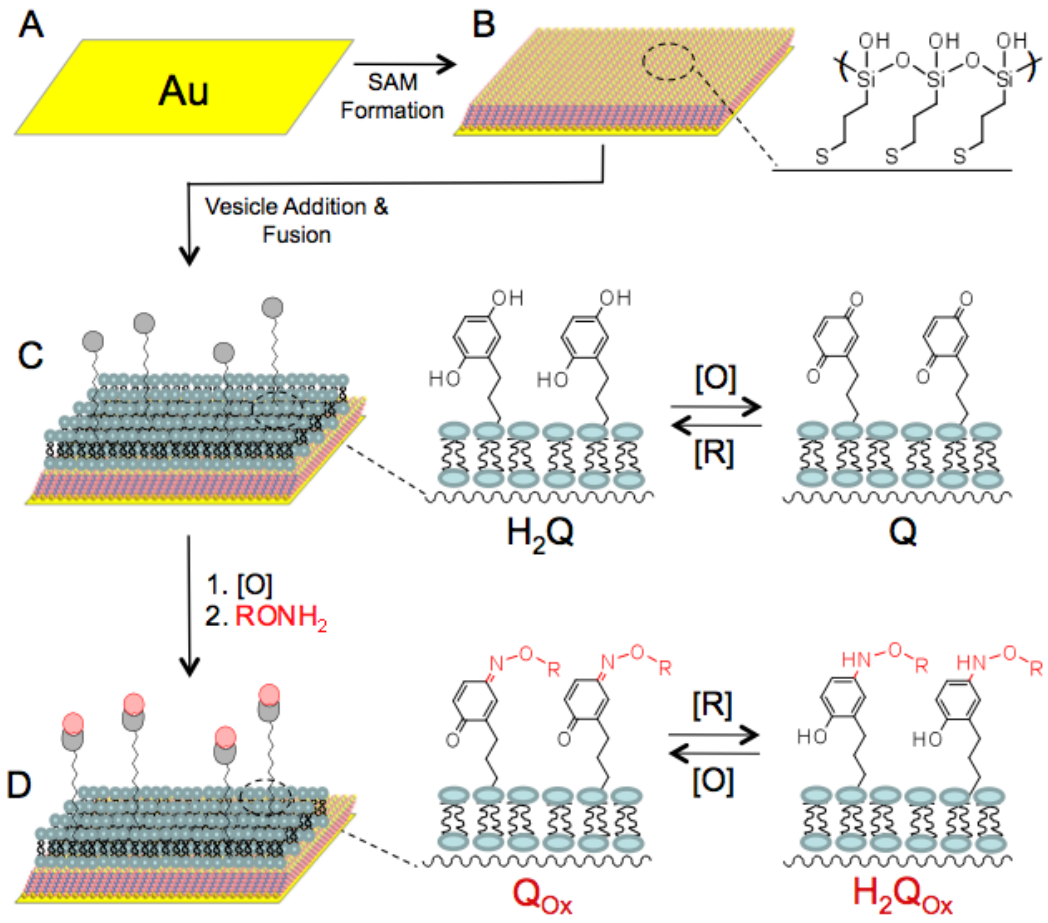

Figure 2.3. Schematic illustrating the formation of a self-assembled monolayer (SAM) supported, electroactive fluid bilayer for chemoselective ligand immobilization. (A) A thin layer of titanium then gold was evaporated onto a glass coverslip. (B) The substrate was immersed in a solution of 3-mercaptopropyl siloxane (HO_3SiSH) in ethanol (EtOH) for ~16 h to form a SAM. (C) To generate a supported planar bilayer, a solution of lipid vesicles containing H_2Q was added to the surface. The H_2Q is electroactive and can

undergo a reversible electrochemical oxidation to generate the corresponding quinone (Q). (D) Addition of an oxyamine-tethered ligand ($RONH_2$) reacts with the Q, generating a covalent interfacial oxime linkage (Q_{Ox}). The resultant oxime product is also redox active and provides a diagnostic electrochemical signal characterizing the amount or yield of reaction to the bilayer.

2.3.3 Electrochemical characterization

Ligand immobilization to H_2Q-containing bilayers was characterized by electrochemistry and specifically cyclic voltammetry (CV) (Figure 3). The H_2Q/Q redox couple, as seen from the blue trace showed unique oxidation and reduction peaks at 500 and 335 mV, respectively. After the surface was oxidized to Q, Rhod-ONH_2 (**5**) was reacted (7 mM in H_2O, 4 h), and the oxime-product (H_2Q_{ox}/Q_{ox}) couple (red trace) displayed redox peaks at 195 mV and 328 mV, respectively. There is a distinct peak potential shift from the H_2Q/Q to the H_2Q_{ox}/Q_{ox} redox couple, indicating that the ligand immobilization had occurred on the fluid lipid bilayer.[27] Electrochemical measurements were performed in PBS pH 7.4, with a scan rate of 100 mV/s, versus a Ag/AgCl reference electrode.

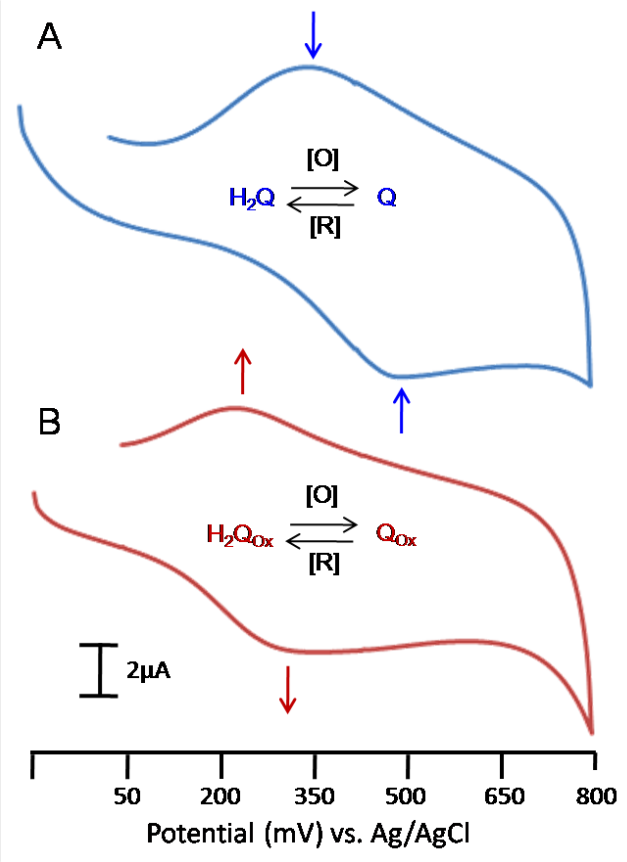

Figure 2.4 Electrochemical characterization of the coupling reaction between a Q-functionalized fluid lipid bilayer and soluble rhodamine-oxyamine (Rhod-ONH_2) by cyclic voltammetry (CV). (A) A CV displaying the diagnostic peak potentials of the H_2Q/Q (blue) redox couple with oxidation [O] at 500 mV and reduction [R] at 335 mV. (B) The resultant CV showing the oxime-product (Q_{Ox}/H_2Q_{Ox}) couple of immobilized Rhod-ONH_2 with peaks at [O] 328 mV and [R] 195 mV (red).

2.3.4 Fluorescence Recovery After Photobleaching

The electroactive bilayer fluidity was confirmed by conducting a fluorescence recovery after photobleaching (FRAP) experiment.[28] Figure 4 shows the sequence of FRAP epifluorescent micrographs obtained after a small area (921 μm x 921 μm) was bleached (Argon laser, 488 nm) from 0 to 6 min. The exposed area was completely dark after photobleaching and gradually recovered its fluorescence (>95%) by 6 min. The extent of

recovery was quantified by comparing the fluorescence intensity of the exposed region normalized to the intensity of the unexposed region.

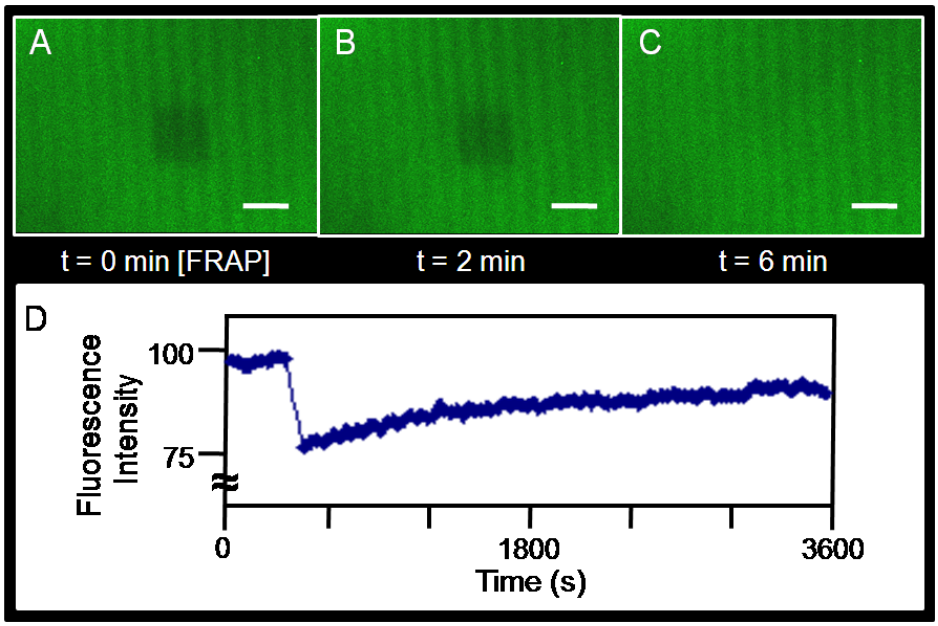

Figure 2.5 Fluorescence recovery after photobleaching (FRAP) experiment of H_2Q containing bilayers to show bilayer fluidity on a HO_3SiSH SAM. (A) t = 1 min after photobleaching; (B) t = 2 min, with partial fluorescence recovery; and (C) t = 6 min, with almost complete recovery (>95%). (D) The recovery profile corresponding to the FRAP data as shown in A-C. Scale bar 200 μm.

2.3.5 Ligand immobilization

In order to spatially control the immobilization of oxyamine-tethered ligands from lipid bilayers on gold, tetra(ethylene glycol)-terminated alkanethiol[29] (EG_4SH, **4**) was patterned by microfluidic lithography (μFL)[30,31] and a SAM of HO_3SiSH was backfilled in the regions containing bare gold (Figure 5). EG_4SH is known to resist nonspecific protein adsorption and also prohibits bilayer formation. Therefore, a microfluidic casette was reversibly sealed to a gold surface, and a solution of EG_4SH (1 mM in EtOH, 60 s) was flowed through the microchannels. The same cassette was then placed perpendicular to the newly patterned EG_4SH SAM, and μFL was performed a second time.

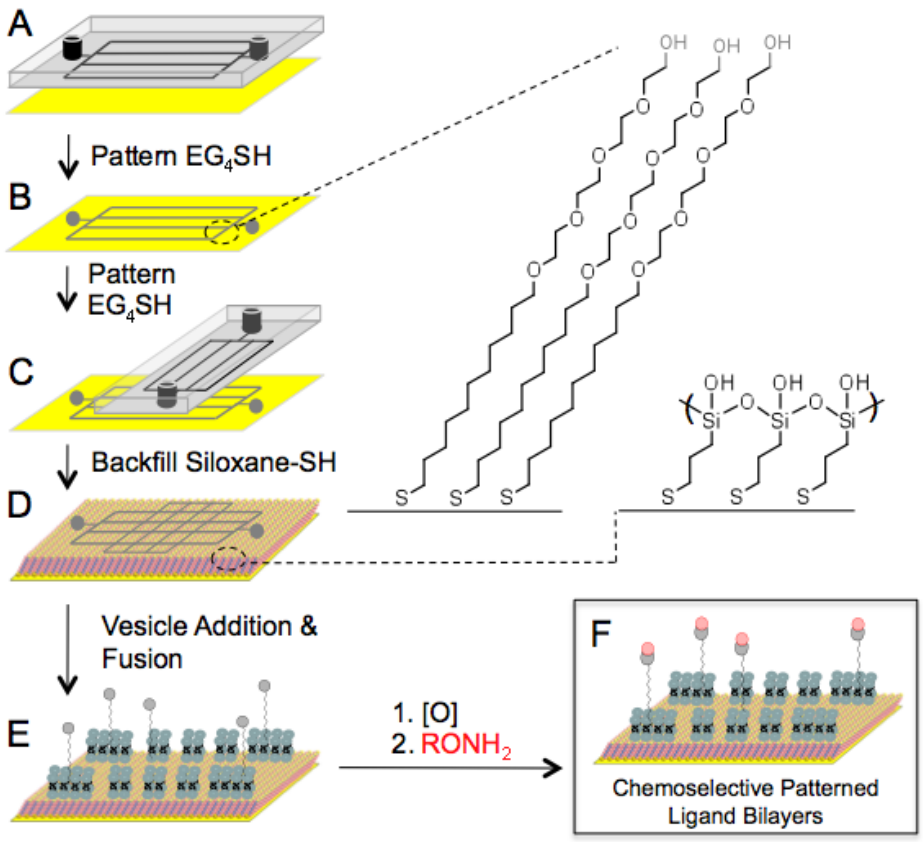

Figure 2.6 Schematic for the generation of a chemoselective, electroactive, and patterned fluid lipid bilayer surface. (A) A PDMS microfluidic cassette was reversibly sealed to a bare gold substrate. (B) A solution of tetra(ethylene) glycol-terminated alkanethiol (EG_4SH) in EtOH was flowed through the channels, forming a patterned EG_4SH SAM by microfluidic lithography (μFL). (C) The same cassette was then removed and placed perpendicular to the newly patterned EG_4SH SAM, and μFL was performed a second time to generate an intersecting EG_4SH pattern. (D) The substrate was then immersed in a solution of HO_3SiSH in EtOH for ~16h, in order to backfill the remaining bare gold regions. (E) A solution of lipid vesicles containing H_2Q (H_2Q-SUVs) was then added to the surface and underwent spontaneous fusion to form fluid bilayers only on the regions containing HO_3SiSH. (F) The H_2Q groups were electrochemically oxidized to Q groups, and an oxyamine-containing ligand ($RONH_2$) was reacted to form a covalent oxime bond, resulting in a chemoselectively, electroactive, and patterned ligand fluid bilayer.

The patterned gold substrate was then rinsed with ethanol, dried, and immersed into a 1 mM solution of HO_3SiSH in EtOH for 16 h, in order to backfill the remaining gold with a siloxane terminated SAM. To generate patterned, fluid bilayers, a pre-patterned surface

with EG_4SH and HO_3SiSH SAMs was immersed into a 3 mM solution of egg-POPC:H_2Q (9:1) in Tris buffer for 1 h. The substrate was then rinsed with PBS, dried in air, and oxidized electrochemically to present a Q-terminated, patterned bilayer. To this surface a Rhod-ONH_2 liagnd was reacted and immobilized (7 mM in MeOH, rt, 4 h). The resultant microarray displaying rhodamine was imaged by fluorescence microscopy (Figure 6). Control experiments were conducted to determine the fidelity of using the H_2Q bilayer immobiliztion strategy. First, a patterned substrate was reacted with rhod-ONH_2 without electrochemical oxidation to Q. A patterned, oxidized surface was also reacted with a non-functionalized rhodamine (does not contain an oxyamine group). For both of these experiments, no fluorescence was observed.

2.3.6 Protein immobilization

This patterning strategy was also shown to be compatible with the chemoselective immobilization of a biospecific ligand to investigate protein-ligand interactions on the bilayer. After patterning an electroactive, fluid lipid bilayer, glucose-oxyamine (glc-ONH_2, Scheme 2, **6**) was immobilized to Q-terminated bilayers (20 mM in MeOH, rt, 4 h).[32] After confirmation of the presence of a gluocose oxime-product by CV, TRITC-conjuagted Concanavalin A (ConA) was added to the surface (1 mg/mL in DMSO, rt, 2 h). ConA is a lectin, or carbohydrate-binding protein, that specifically recognizes and binds to glucose groups.[33] As shown by the fluorescent image in figure 6, glc-ONH_2 was successfully conjugated to patterned bilayers followed by biospecific recognition after treatment with ConA. As a control, no fluorescence was observed when ConA was added to a patterned bilayer, not presenting bound glucose. Importantly, the μFL formed EG_4SH SAMs not only allow for patterning the bilayer but also renders the non-bilayer

regions inert to non specific protein adsorption.[34,35] This feature is critical for extending this system to generate multicomponent ligand bilayers for proteomic and cell adhesion based studies.

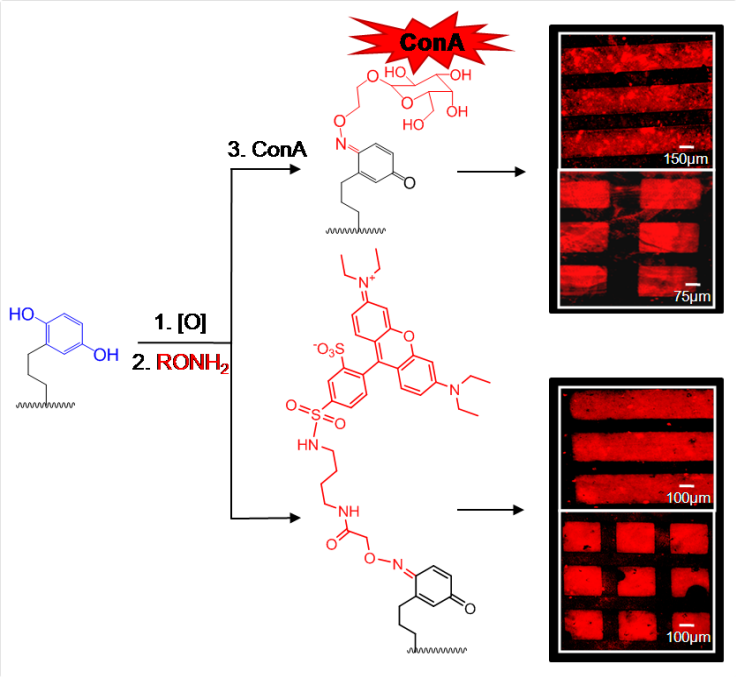

Figure 2.7 Fluorescent micrographs of ligand immobilization on patterned electroactive fluid bilayers. For all surfaces, EG_4SH was first patterned by μFL then the remaining bare gold regions were backfilled with HO_3SiSH. To these surfaces, H_2Q containing lipid vesicles were fused, electrochemically oxidized [O], and then reacted with an oxyamine-tethered ligands ($RONH_2$). (Top) Glucose-oxyamine ($Glc\text{-}ONH_2$) was immobilized to patterned fluid lipid bilayer surfaces, followed by the addition of fluorescent ConA-TRITC. (Bottom) $Rhod\text{-}ONH_2$ was immobilized to patterned fluid lipid bilayers.

2.4 Conclusions

In summary, we have developed a general method to pattern electroactive and chemoselective fluid lipid bilayers on gold surfaces for a range of biospecific ligand-receptor interaction studies on model membranes. To our knowledge, the described

methodology allows for the first time the tailoring of a patterned fluid lipid bilayer post bilayer formation with a range of ligands and/or proteins that can be characterized in situ electrochemically. Importantly, the μFL strategy is rapid and provides the ability to pattern a variety of shapes and feature sizes to generate unique bilayer microarrays.[36] The Si-OH network, as generated by the presence of a HO_3SiSH SAM, aids in maintaining bilayer fluidity, which is important in mimicking the natural cell membrane. The ability to generate fluid bilayer arrays on gold allows for several analytical surface spectroscopy techniques to characterize interfacial associations. In this study, a variety of oxyamine-tethered ligands were successfully immobilized in arrays, indicating that a number of biomolecules can be presented from the surface for subsequent interrogation by other biologically-relevant compounds (proteins, nucleic acids, small molecules). Since the immobilization of ligands results in the formation of an electroactive oxime bond, ligand density and extent of reaction can be quantified and monitored by CV on a fluid lipid bilayer. Since the interfacial reaction is electroactive and quantitative, multiple different ligands may also be immobilized to a single bilayer array. By incorporating existing electrophoretic methods to generate fluid bilayer gradients, a method to generate ligand gradients for cell polarity and cell migration studies may be feasible.[37] Furthermore, the immobilization strategy provides a method to conjugate other materials including, carbon nanotubes, quantum dots, colloids, polymer based nanoparticles and liposomes for a variety of optoelectronic and material applications.[38-41] This platform is rapid and flexible and may be extended to many areas in biochemistry, cell biology and material science to study fundamental membrane activity (lipid microdomains) and enzymology, as well as

provide a high-throughput biotechnology platform for the development of highly integrated biosensors for small molecule screens or cell behavior based assays.

2.5 Acknowledgments

This work was supported by the Carolina Center for Cancer Nanotechnology Excellence (NCI) and grants from the Burroughs Wellcome Foundation (Interface Career Award) and the National Science Foundation (Career Award). We thank Prof. Nancy Thompson and her group (UNC-Chapel Hill) for expertise in bilayer formation and fluorescence microscopy advice.

2.6 References

1. Yoon, T. -Y.; Jeong, C.; Lee, S. -W.; Kim, J. H.; Choi, M. C.; Kim, S. -J.; Kim, M.W.; Lee, S. -D. *Nat. Mater.* **2006**, *5*, 281-285.

2. Parthasarathy, R.; Groves, J. T. *Proc. Natl. Acad. Sci.U.S.A.* **2004**, *101*, 12798-12803.

3. McKiernan, A. E.; Ratto, T. V.; Longo, M. L. *Biophys. J.* **2000**, *79*, 2605-2615.

4. Taylor, J. D.; Phillips, K. S.; Cheng, Q. *Lab on a Chip* **2007**, *7*, 927-930.

5. Hovis, J. S.; Boxer, S. G. *Langmuir* **2000**, *16*, 894-897.

6. Taylor, J. D.; Phillips, K. S.; Cheng, Q. *Lab on a Chip* **2007**, *7*, 927-930.

7. Shi, J.; Chen, J.; Cremer, P. S. *J. Am. Chem. Soc.* **2008**, *130*, 2718-2719.

8. Groves, J. T.; Boxer, S. G.; McConnell, H. M. *Proc. Natl. Acad. Sci.U.S.A.* **1997**, *94*, 13390-13395.

9. Yee, C. K.; Amweg, M. L.; Parikh, A. N. *Adv. Mater.* **2004**, *16*, 1184-1189.

10. Morigaki, K.; Kiyosue, K.; Taguchi, T. *Langmuir* **2004**, *20*, 7729-7735.

11. Brozell, A. M.; Muha, M. A.; Sanii, B.; Parikh, A. N. *J. Am. Chem. Soc.* **2006**, *128*, 62-63.

12. Mossman, K. D.; Campi, G.; Groves, J. T.; Dustin, M. L. *Science* **2005**, *310*, 1191-1193.

13. Fang, Y.; Frutos, A. G.; Lahiri, J. *J. Am. Chem. Soc.* **2002**, *124*, 2394-2395.

14. Sackmann, E. *Science* **1996**, *271*, 43–48.

15. Cremer, P. S.; Boxer, S. G. *J. Phys. Chem. B* **1999**, *103*, 2554-2559. (c). Wagner, L.; Tamm, L. *Biophys. J.* **2000**, *79*, 1400-1414.

16. Srinivasan, M. P.; Ratto, T. V.; Stroeve, P.; Longo, M. L. *Langmuir* **2001**, *17*, 7951-7954.

17. Jenkins, A. T. A.; Neumann, T.; Offenhausser, A. *Langmuir* **2001**, *17*, 265-267.

18. Pale-Grosdemange, C.; Simon, E. S.; Prime, K. L.; Whitesides, G. M. *J. Am. Chem.Soc.* **1991**, *113*, 12-20.

19. Yang, T.; Baryshnikova, O. K.; Mao, H.; Holden, M. A.; Cremer, P. S. *J. Am. Chem. Soc.* **2003**, *125*, 4779-4784.

20. Nam, J. –M.; Nair, P. M.; Neve, R. M.; Gray, J. W.; Groves, J. T. *ChemBioChem* **2006**, *7*, 436-440.

21. Taylor, J. D.; Phillips, K. S.; Cheng, Q. *Lab Chip* **2007**, *7*, 927-930.

22. Chan, E. W. L.; Yousaf, M. N. *J. Am. Chem. Soc.* **2006**, *128*, 15542-15546.

23. Chan, E. W. L.; Yousaf, M. N. *Mol. Biosyst.* **2008**, *4*, 746-753.

24. Luo, W.; Westcott N. P.; Pulsipher, A.; Yousaf, M. N. *Langmuir*, **2008**, *24*, 13096-13101.

25. Westcott, N. P.; Lamb, B. M.; Yousaf, M. N. *Anal. Chem.* **2009**, *81*, 3297-3303.

26.Chan, E. W. L.; Park, S.; Yousaf, M. N. *Angew. Chem. Int. Ed.* **2008**, *47*, 6267-6271.

27. Hovis, J. S.; Boxer, S. G. *Langmuir* **2001**, *17*, 3400-3405.

28. Bailey, F. E., Jr.; Koleske, J. Y. *Poly(ethylene Oxide)*; Academic: New York, 1984

29. Lamb, B. M.; Barrett, D. G.; Westcott, N. P.; Yousaf, M. N. *Langmuir* **2008**, *24*, 8885-8889.

30. Lamb, B. M.; Westcott, N. P.; Yousaf, M. N. *ChemBioChem*, **2008**, *9*, 2628-2632.

31. Chan, E. W.L.; Yousaf, M. N. *ChemPhysChem* **2007**, *8*, 1469-1472.

32. Goldstein, D. E.; Little, R. R.; Wiedmeyer, H. –M.; England, J. D.; MnKenzie, E. *Clin. Chem.* **1986**, *32*, B64-B70.

33. Li, L.; Chen, S.; Zheng, J.; Ratner, B. D.; Jiang, S. *J. Phys. Chem. B.* **2005**, *109*, 2934-2941.

34. Harris, J. M. *Poly(ethylene glycol) Chemistry: Biotechnical and Biomedical Applications*; Plenum: New York, 1992.

35. Feng, Li. *Prostaglandins & other Lipid Mediators* **2005**, *77*, 158-167.

36. Harris, B. P.; Kutty, J. K.; Fritz, E. W.; Webb, C. K.; Burg, K. J. L.; Metters, A. T. *Langmuir*, **2005**, *22*, 4467-4471.

37. Van den Meerakker, J.; Jacobs, J. *J. Electrochem. Soc.* **1996**, *143*, L40-L42.

38. Pokela, R.; Toivanen, R.; Lindroos, V. *Key Eng. Mat.* **1987**, *20-28*, 3863-3873.

39. Lee, S.; Dongfang, Y.; Nikumb, S. *Appl. Surf. Sci.* **2007**, *253*, 4740-4747.

40. Ishikawa, F. N.; Chang, H.-K.; Koungmin, R.; Chen, P.-O.; Badmaev, A.; De Arco, L. G.; Shen, G.; Zhou, C. *ACS Nano,* **2009**, *3*, 73-79.

41. Zhou, X.; Moran-Mirabel, J. M.; Craighead, H. G.; McEuen, P. L. *Nature Nanotechnology* **2007**, *2*, 185-190.

42. Park, S.; Yousaf, M. N. *Langmuir **2008***, *24*, 6201-6207.

43. Westcott, N. P.; Yousaf, M. N. *Langmuir* **2008**, *24*, 2261-2265.

44. Pulsipher, A.; Westcott, N. P.; Luo, W.; Yousaf, M. N. *J. Am. Chem. Soc.* **2009**, *131*, 7626-7632.

CHAPTER 3

Cell-Surface Engineering by Liposome Fusion

3.1 Introduction

Membrane fusion processes are ubiquitous in biology and span multi-cellular communication, extracellular signaling, the reconstruction of damaged organelles, and integration of cells into complex tissues and organs.[1] As a result, there has been much interest in developing model systems to mimic biological membranes to investigate the mechanisms of fusion and for use in various biotechnological applications. For example, cells secrete and display proteins and lipids during vesicle trafficking events that either diffuse into the ECM or become components of the cell membrane after fusion.[2] Naturally, lipid vesicles provide an ideal platform for such studies and have been widely used to examine various membrane-related processes, including fusion.[3-5] In order for fusion to occur, the membranes must be brought into close proximity, followed by bilayer destabilization.[6] Fusion of such lipid vesicles or liposomes can be initiated by using divalent cations, polycations,[7] positively charged amino acids[8] and membrane-disrupting peptides.[9,10] Historically, synthetic chemical agents have also been employed to fuse vesicle membranes[11-14] through non-specific interactions. However, recent exciting efforts to improve selectivity and control over vesicle fusion have been achieved through the use of small, synthetic molecular recognition pairs.[15-16] Since vesicle fusion is a natural process and has been shown to influence the construction of cells into multicellular organisms, much research has focused on using liposomes to deliver

cargoes, reagents, nanomaterials, and therapeutic agents to cells. To our knowledge, there have been very few reports of employing liposome fusion to cell membranes as a method to deliver small chemical functional groups in order to tailor the cell membrane for subsequent bio-orthogonal and chemoselective ligation reactions.[17,18] This platform would find wide use in studying fundamental cell behavior, tissue engineering, and biomedical applications.

Cell-surface receptors that decorate the cell membrane influence a number of biological processes, such as cell adhesion, differentiation, intercellular communication, and tissue formation.[19] As such, methods that selectively engineer the cell surface by introducing chemoselective functional groups will have a significant role in directing and influencing many biological processes for applications in cell-based therapies, drug delivery, and tissue engineering.[20-24] Previous cell-surface modification strategies involve the introduction of chemoselective functional groups through metabolic and genetic engineering approaches.[25-27] However, such strategies may perturb cellular processes by altering cellular physiology.[28]

In this chapter, we present a method to tether chemoselective ketone and oxyamine groups from cell surfaces by liposome delivery toward the goal of rewiring the cell surface. Alkyl ketone and oxyamine molecules spontaneously insert into lipid vesicles upon synthesis. When mixed, chemical recongnition occurs, producing stable oxime bonds under physiological conditions. The reaction is also bio-orthogonal and thus, does not interfere with any other chemical moieties in its cellular surroundings.[29-32] The synthetic ketone and oxyamine molecules fused on the cell membrane serve as cell-surface receptors, providing tools for the attachment of other functional materials,

biomolecules, and probes on the cell surface. Liposome fusion was characterized by matrix-assisted laser-desorption/ionization mass spectrometry (MALDI-MS), dynamic light scattering (DLS), Fourier resonance energy transfer (FRET), isothermal calorimetry (ITC), transmission electron microscopy (TEM), fluorescene-activated cell sorting (FACS), and fluorescene microscopy analyses.

3.2 Materials and Methods

3.2.1 Materials

All chemical reagents were of analytical grade and used without further purification. Lipids egg palmitoyl-oleoyl phosphatidylcholine (POPC), egg 1-palmitoyl-2-oleoyl-phosphatidylglycerol (POPG), 1,2-dioleoyl-3-trimethylammonium-propane (DOTAP), egg 1,2-diphytanoyl-*sn*-glycero-3-phosphoethanolamine-N-(7-nitro-2-1,3-benzoxadiazol-4-yl) (ammonium salt) (NBD-PE), and egg 1,2-dipalmitoyl-*sn*-glycero-3-phosphoethanolamine-N-(lissamine rhodamine B sulfonyl) (ammonium salt) (Rhod-PE) were purchased from Avanti Polar Lipids (Alabaster, AL). Antibodies and fluorescent dyes were obtained from Invitrogen (Carlsbad, CA). FITC labeled beads were purchased from Spherotech, Inc. (Forest Lake, IL) and all other chemicals were obtained from Sigma-Aldrich or Fisher. Swiss 3T3 albino mouse fibroblasts (fbs) were obtained from the Tissue Culture Facility at the University of North Carolina (UNC).

Transmission electron microscopy images were acquired using a TF30He Polara G2 (FEI company) electron cryo microscope, operating at 300 keV. Images were recorded using a Tietz single port model 415 4k×4k CCD camera with a 15-μm pixel size. Fourier resonance energy transfer measurements were performed using a SPEX Fluorolog-3 Research T-format Spectrofluorometer with an excitation wavelength of 471 nm.

Dynamic light scattering was performed using a Nikomp model 200-laser particle sizer with a 5 mW HeNe laser at an excitation wavelength of 632.8 nm and using a Wyatt DynoPro plate reader. Flow cytometry was performed using a Dako CyAn ADP (Beckman-Coulter, Brea, CA), and the data was analyzed with Summit 4.3 software. Phase contrast and fluorescent imaging was performed and processed using a Nikon TE2000-E inverted microscope and Metamorph software, respectively. Scanning electron microscopy images were obtained using a Hitachi S-4700 field emission scanning electron microscope (Hitachi High Technologies America, Inc., Schaumburg, Illinois).

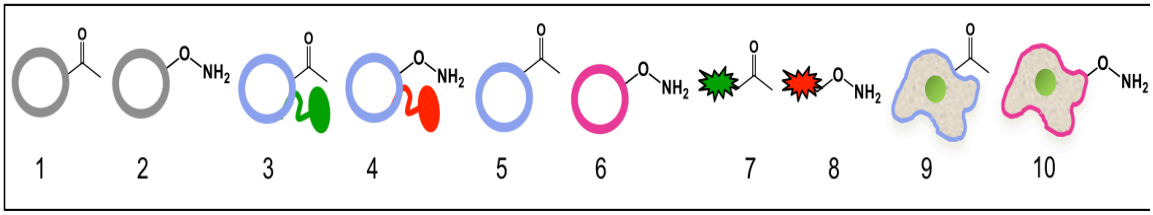

Scheme 3.1. List of liposomes, molecules, and cells used in this study. (**1**) Keto-LUV; (**2**) oxy-LUV; (**3**) keto-NBD-PE LUV; (**4**) oxy-rhod-PE LUV; (**5**) ketone-functionalized liposomes; (**6**) oxyamine-functionalized liposomes; (**7**) fluorescein-ketone; (**8**) rhod-oxyamine; (**9**) ketone-functionalized fbs; and (**10**) oxyamine-functionalized fbs.

3.2.2 2-(dodecyloxy)isoindoline-1,3-dione Synthesis (B)

To a solution of N-hydroxyphthalimide (1.96 g, 12.04 mmol, 1.5 eq) and sodium bicarbonate (10.11 g, 12.04 mmol, 1.5) in DMF (20 mL) at 80°C was added 1-bromododecane (1.93 mL, 8.02 mmol). The mixture was refluxed and stirred for 12 h. The reaction was diluted with DCM and washed with H_2O (6 x 50 mL), 1 M $NaHCO_3$ (3 x 50 mL), and H_2O (2 x 50 mL), dried over $MgSO_4$, and concentrated to afford a white solid, **B** (2.66 g, 87 %). ^{1}H NMR (400 MHz, $CDCl_3$, δ): 1.02 (s, 3H; CH_3), 1.31-1.29 (m, 14H, J = 8; CH_2), 1.47-1.45 (m, 4H, J = 8; CH_2), 1.60-1.57 (m, 2H, J = 12; CH_2), 3.72-3.70 (t, 2H, J = 8; CH_2), 7.80-7.78, 7.85-7.83 (2 x m, 4H, J = 8; Ar-H).

3.2.3 O-dodecyloxyamine Synthesis (A)

To a solution of **B** (2.65 g, 8.00 mmol) in dry DCM (30 mL) under inert atmosphere (Ar) was slowly added hydrazine (1.53 mL, 48.00 mmol, 6 eq). Upon addition, a white precipitate immediately formed. The mixture was stirred for 12 h. The reaction was diluted with DCM and washed with H_2O (6 x 50 mL), dried over $MgSO_4$, and concentrated to afford a pale yellow oil, **A** (1.18 g, 74 %). ^{1}H NMR (400 MHz, $CDCl_3$, δ): 1.03 (s, 3H; CH_3), 1.33-1.31 (m, 14H, J = 8; CH_2), 1.43-1.41 (m, 4H, J = 8; CH_2), 1.50-1.46 (m, 2H, J = 16; CH_2), 3.64-3.62 (t, 2H, J = 7; CH_2). (ESI) (*m*/*z*) [M + H^+]: 201.22.

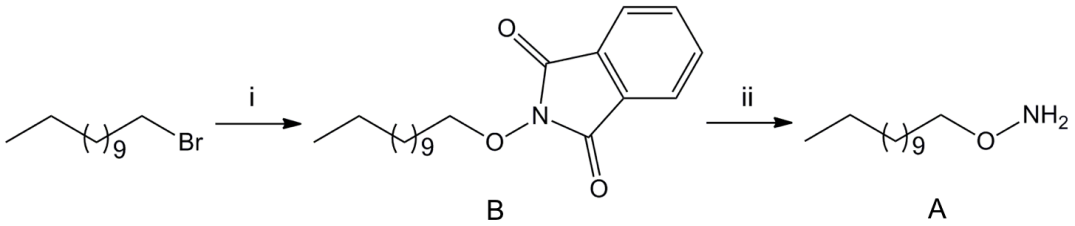

Scheme 3.2. Synthesis of *O*-dodecyloxyamine[a] (**A**). [a] Reagents and conditions. (i) N-hydroxyphthalimide (1.5 eq), $NaHCO_3$ (1.5 eq), DMF, reflux, 80 °C, 12 h; 87 % and (ii) hydrazine (6 eq), dry DCM, N_2, 12 h; 74 %.

3.2.4 (N-(4-(tert-butoxycarbonylamino)butyl)sulfamoyl)-2-(6-(diethylamino)-3-(diethyliminio)-3H-xanthen-9-yl)benzenesulfonate Synthesis (C)

To a solution of rhodamine lissamine (0.880 g, 1.53 mmol) in chloroform ($CHCl_3$, 30 mL) at room temperature (RT) was added N-BOC-1,4-diaminobutane (0.431 g, 2.29 mmol, 1.5 eq) and TEA (0.305 mL, 2.29, 1.5 eq). The mixture was stirred for 8 h and then extracted with H_2O (6 x 25 mL). The organic layers were concentrated to afford a dark purple solid **4**. H^{1}NMR was taken in $CDCl_3$ to confirm **C** (1.045 g, 95 %). TLC

conditions for entire synthesis: $CHCl_3$:MeOH (7.5:2.5). ^{1}H NMR (400 MHz, MeOD, δ): 1.09-1.07 (t, 6H, J = 8; CH_3), 1.36-1.33 (m, 15H, J = 12; CH_3), 1.66-1.64 (m, 4H, J = 8; CH_2), 3.47-3.44 (m, 6H, J = 12; CH_2), 4.20-4.18 (q, 4H, J = 7; CH_2), 5.66 (s, 1H; Ar-H), 5.77 (d, 1H; Ar-H), 6.01 (d, 1H; Ar-H), 6.34-6.30 (m, 2H, J = 16; Ar-H), 7.21 (d, 1H; Ar-H), 7.29 (d, 1H; Ar-H), 7.98 (d, 1H; Ar-H), 8.04 (d, 1H; Ar-H). (ESI) (*m/z*) [M + H^+]: 716.31.

3.2.5 5-(N-(4-aminobutyl)sulfamoyl)-2-(6-(diethylamino)-3-(diethyliminio)-3H-xanthen-9-yl)benzenesulfonate Synthesis (D)

To **C** (0.600 g, 0.837 mmol) was added a solution of TFA, H_2O, and triisopropylsilane (TIPS) in a ratio of 95: 2.5: 2.5 (10 mL). The mixture was stirred at RT under N_2 for 3 h and was then extracted with $CHCl_3$ and H_2O (4 x 25 mL). The organic layers were dried and concentrated to afford a purple solid, **D** (0.45 g, 85 %). ^{1}H NMR (400 MHz, MeOD, δ): 1.11-1.09 (t, 6H, J = 8; CH_3), 1.33-1.31 (m, 6H, J = 7; CH_3), 1.70-1.67 (m, 4H, J = 12; CH_2), 2.63-2.62 (m, 2H, J = 4; CH_2), 3.51-3.49 (m, 6H, J = 8; CH_2), 4.20-4.18 (q, 4H, J = 7; CH_2), 5.64 (s, 1H; Ar-H), 5.71 (d, 1H; Ar-H), 6.02 (d, 1H; Ar-H), 6.32-6.30 (m, 2H, J = 8; Ar-H), 7.24 (d, 1H; Ar-H), 7.30 (d, 1H; Ar-H), 7.98 (d, 1H; Ar-H), 8.04 (d, 1H; Ar-H). (ESI) (*m/z*) [M + H^+]: 628.27.

3.2.6 2-(6-(diethylamino)-3-(diethyliminio)-3H-xanthen-9-yl)-5-(N-(2,2-dimethyl-4,8-dioxo-3,6-dioxa-5,9-diazatridecan-13-yl)sulfamoyl)benzenesulfonate Synthesis (E)

To a solution containing N,N'-dicyclohexylcarbodiimide (DCC, 0.394 g, 1.91 mmol, 2 eq), N-hydroxysuccinimide (NHS, 0.220 g, 1.91 mmol 2 eq), and aminooxy acetic acid (0.356 g, 1.91 mmol, 2 eq) in DMF was stirred under N_2 for 0.5 h. **D** (0.43 g, 0.684

mmol) was then added in DMF (20 mL), followed by TEA (excess). The mixture was strirred for 4 h and then concentrated. Flash chromatography was performed using $CHCl_3$:MeOH (8:2) to elute, **E**. The product was concentrated to afford a purple solid **6** (0.32 g, 60 %). ^{1}H NMR (400 MHz, MeOD, δ): 1.10-1.08 (t, 6H, J = 8; CH_3), 1.39-1.36 (m, 15H, J = 12; CH_3), 1.65-1.63 (m, 4H, J = 7; CH_2), 3.08-3.06 (m, 2H, J = 8; CH_2), 3.48-3.46 (m, 6H, J = 8; CH_2), 4.17-4.15 (q, 4H, J = 7; CH_2), 4.38 (s, 2H; CH_2), 5.61 (s, 1H; Ar-H), 5.73 (d, 1H; Ar-H), 6.02 (d, 1H; Ar-H), 6.31-6.30 (m, 2H, J = 4; Ar-H), 7.24 (d, 1H; Ar-H), 7.32 (d, 1H; Ar-H), 7.96 (d, 1H; Ar-H), 8.09 (d, 1H; Ar-H). (ESI) (*m*/*z*) [M + H$^+$]: 801.31.

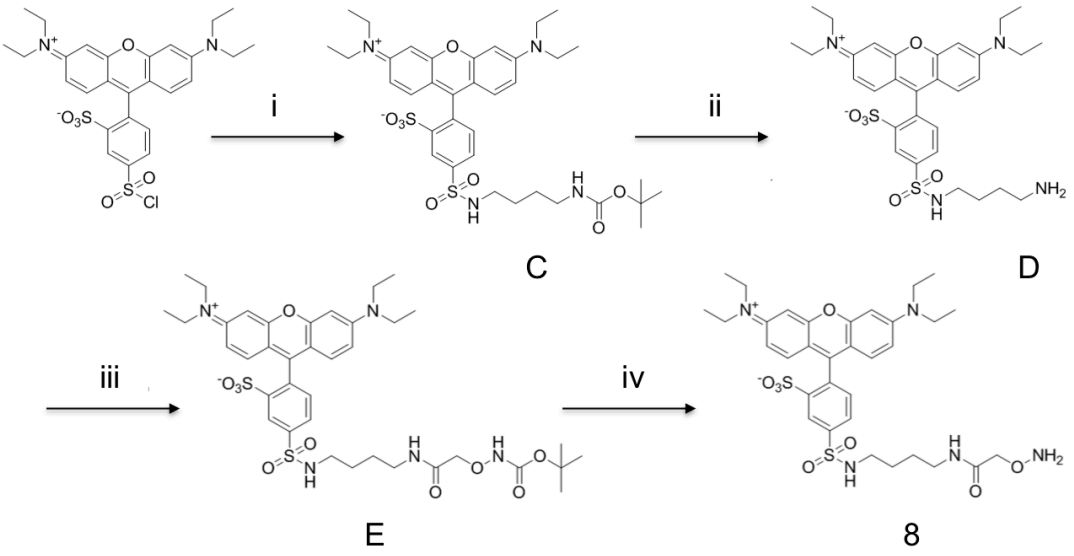

Scheme 3.3. Synthesis of rhod-oxyamine[a] (**8**). [a] Reagents and conditions. (i) N-BOC-1,4-diaminobutane (1.5 eq), TEA (1.5 eq), $CHCl_3$, N_2, 25 ºC, 8 h; 95 %, (ii) triisopropylsilane (TIPS)/H_2O/TFA (2.5 : 2.5 : 95), N_2, 25 ºC, 3 h; 85 %, (iii) N-hydroxysuccinimide (NHS, 2 eq), N,N'-dicyclohexylcarbodiimide (DCC, 2 eq), aminooxy acetic acid (2 eq), TEA (excess), DMF, N_2, 25 ºC, 4 h; 60 %, and (iv) TIPS/H_2O/TFA (2.5 : 2.5 : 95), N_2, 25 ºC, 3 h; 81 %.

3.2.7 5-(N-(4-(2-(aminooxy)acetamido)butyl)sulfamoyl)-2-(6-(diethylamino)-3-(diethyliminio)-3H-xanthen-9-yl)benzenesulfonate (rhod-oxyamine, 7) Synthesis

To **E** (0.30 g, 0.374 mmol) was added a solution of TFA, H_2O, and triisopropylsilane (TIPS) in a ratio of 95: 2.5: 2.5 (10 mL). The mixture was stirred at RT under N_2 for 3 h and was then extracted with $CHCl_3$ and H_2O (4 x 25 mL). The organic layers were dried and concentrated to afford a purple solid and flash chromatography was performed using $CHCl_3$:MeOH (8:2) to elute, **7** (0.21 g, 81 %) ^{1}H NMR (400 MHz, $CDCl_3$, δ): 1.12-1.00 (t, 6H, J = 8; CH_3), 1.42-1.40 (m, 6H, J = 7; CH_3), 1.62-1.60 (m, 4H, J = 7; CH_2), 3.07-3.05 (m, 2H, J = 8; CH_2), 3.45-3.42 (m, 6H, J = 12; CH_2), 4.11-4.09 (q, 4H, J = 8; CH_2), 4.24 (s, 2H; CH_2), 5.64 (s, 1H; Ar-H), 5.75 (d, 1H; Ar-H), 6.02 (d, 1H; Ar-H), 6.29-6.27 (m, 2H, J = 4; Ar-H), 7.28 (d, 1H; Ar-H), 7.31 (d, 1H; Ar-H), 7.92 (d, 1H; Ar-H), 8.05 (d, 1H; Ar-H). (ESI) (*m/z*) [M + H^+]: 701.28.

3.2.8 Formation of Lipid Vesicles. Liposome Fusion Studies

Dodecanone (55 μL, 10 mM in $CHCl_3$ at 5 mol %) was dissolved with egg palmitoyl-oleoyl phosphatidylcholine (POPC) (430 μL, 10 mg/mL in $CHCl_3$, at 95 mol %) and *O*-dodecyloxyamine (60 μL, 10 mM in $CHCl_3$ at 5 mol %) was mixed with POPC (410 μL, 10 mg/mL in $CHCl_3$ at 75 mol %), and egg 1-palmitoyl-2-oleoyl-phosphatidylglycerol (POPG) (92 μL, 10 mg/mL in $CHCl_3$ at 20 mol %). Both lipid sample mixtures were then concentrated under high vacuum for 4 h. The dried lipid samples were reconstituted and brought to a final volume of 3 mL in PBS buffer, pH 7.4. The contents of the vial were warmed to 50˚C and sonicated for 20 min, in a tip sonicator, until the solution became clear and large unilamelar vesicles (LUVs) containing ketone (keto-LUV, **1**) or oxyamine

(oxy-LUV, **2**) groups were formed. **Fourier resonance energy transfer (FRET) fusion studies.** NBD-PE and rhod-PE were added to two separate vials at 2 mol %. The dried lipid samples were then reconstituted in 2.43 mL of PBS buffer, pH 7.4. The contents of the vial were warmed to 50˚C and sonicated for 20 min, in a tip sonicator, until the solution became clear, and LUVs containing ketone (keto-NBD-PE LUVs, **3**) or oxyamine (oxy-rhod-PE LUVs, **4**) groups were formed. **Liposome fusion to cells.** To generate ketone- and oxyamine-containing liposomes for cell fusion studies, dodecanone (55 μL, 10 mM solution in $CHCl_3$ at 5 mol %) and *O*-dododecyloxyamine (60 μL, 10 mM solution in $CHCl_3$ at 5 mol %) were dissolved with egg-POPC (424 μL, 10 mg/mL in $CHCl_3$ at 93 mol %) and 1,2-dioleoyl-3-trimethylammonium-propane (DOTAP, 10 μL, 10 mg/mL in $CHCl_3$ at 2 mol %) in chloroform followed by concentration under high vacuum for 4 h. The dried lipid samples were then reconstituted and brought to a final volume of 3 mL in PBS buffer, pH 7.4. The contents of the vial were warmed to 50 ˚C and sonicated for 20 min, in a tip sonicator, until the solution became clear, and LUVs containing ketone (**5**) or oxyamine (**6**) groups were formed.

3.2.9 Matrix-Assissted Laser-Desorption/Ionization Mass Spectrometry (MALDI-MS)

Preparation of gold-coated MALDI sample plates. Gold-coated MALDI sample plates (123 x 81 mm) (Applied Biosystems, Foster City, CA) were prepared by electron-beam deposition (Thermionics Laboratory Inc, Hayward, CA) of titanium (5 nm) and then gold (12 nm). In order to form self-assembled monolayers (SAM) of alkanethiolates on the plates, the slides were immersed in a 1-mM solution of aminooxyundecanethiol in EtOH

for approximately 1 min, rinsed with EtOH and dried, and then backfilled with a 1-mM solution of mercaptoundecanol in EtOH for 1 h. Once removed from solution, the surfaces were rinsed with EtOH and dried before use. **Liposome preparation.** Keto-LUVs (**1**) were generated as previously described and were then delivered and allowed to react with the oxyamine-terminated MALDI sample plate (90 min). The plates were then washed with water (3 x 3 mL) and EtOH (2 x 3 mL) and dried before use. **MALDI Analysis.** MS analysis was carried out using an AB SCIEX TOF/TOF^{TM} 5800 System (Applied Biosystems, Foster City, CA).

3.2.10 Dynamic Light Scattering (DLS)

Keto- (**1**) and oxy- (**2**) LUVs were generated as previously described and tested by DLS for monodispersity and uniformity. Light scattering experiments were performed using a Nikomp Model 200 Laser Particle Sizer with a 5 mW Helium-Neon Laser at an exciting wavelength of 632.8 nm. Standard deviation determinations were made using Gaussian analysis. A Wyatt DynoPro Dynamic Scattering Plate Reader was used to collect the light scattering data.

3.2.11 Fourier Resonance Energy Transfer (FRET)

Keto- (**3**) and oxy- (**4**) LUVs containing NBD-PE and rhod-PE, respectively, were generated as previously described and tested by FRET. All fluorescence measurements were performed in a SPEX Fluorolog-3 Research T-format Spectrofluorometer. NBD fluorescence was measured at 471 nm (excitation) and 531 nm (emission), maintaining narrow excitation slits to reduce light scattering interference. To obtain FRET

measurements, the NBD dye was excited at 471 nm, and the emission was scanned through 600 nm, and the emission signal for rhod-PE was observed at 578 nm. Fluorescence was followed immediately after mixing oxy-rhod-PE LUV (**4**, 3 mM in PBS, 100 μL) with keto-NBD-PE LUV (**3**, 3 mM in PBS, 100 μL) for approximately 2 h at 2 min intervals. The total lipid concentrations were adjusted to 0.2 mM, and the two LUV populations were had a 1:1 molar ratio. A constant flow of water was passed through the cuvette holder for temperature control. The temperature was maintained at 25 °C.

3.2.12 Isothermal Titration Calorimetry (ITC)

Oxy- (**2**) and keto- (**1**) LUVs were made as previously described. Samples and PBS were degassed before use. Keto-LUV solutions were diluted to 0.02 mM in PBS at pH = 7.4 and were placed in the cell. The oxy-LUV solution was then injected into the cell using a syringe. ITC was performed at 25 °C. No significant heat flow was detected when injecting PBS buffer into keto-LUV or injecting oxy-LUV into PBS buffer. ITC was performed on a MicroCal VP-ITC and data were fit to a single-site binding model using Origin.

3.2.13 Transmission Electron Microscopy (TEM)

Keto- (**1**) and oxy- (**2**) LUVs were made as previously described (0.2 mM in PBS, pH = 7.4). The two vesicle solutions (1:1) were mixed at room temperature for 30 min. 4 μL of vesicles suspended in buffer were applied to standard lacey carbon EM grids were prepared according to published methods. The specimens were blotted from behind and

then submerged into aurenyl acetate solution for staining. The hydrated specimens were then placed into a TF30He Polara G2 (FEI company) electron cryo microscope operating at 300 keV. Images were recorded using a Tietz single port model 415 4k × 4k CCD camera with a 15 micron pixel size on the chip. Pixel sizes at the specimen level were used to calculate accurate dimensions for the specimen.

3.2.14 Rewiring Cell Adhesion

Briefly, mixed self-assembled monolayers (SAMs) presenting oxyamine (OA) or aldehyde (Ald) and tetra (ethylene glycol) (EG_4) groups were patterned using microfluidic lithography and microfluidic oxidation, respectively.[39,40] The percentage of OA and Ald groups were minimal (1/9 OA:EG_4, 1 mM in EtOH total) to ensure resistance to nonspecific protein and cell adhesion and determined by reaction of redox groups by electrochemistry.[44] Swiss 3T3 albino mouse fbs were cultured with keto- (**5**) or oxy- (**6**) LUVs (previously described), separately, and were then seeded (~10^4 cells/mL) to surfaces patterned with OA or Ald, respectively. Over the course of 4 days, cells adhered, spread, and proliferated, filling out the patterned regions of the surface due to the interfacial oxime reaction. Cells cultured with liposomes, not containing the key functional groups, did not attach to the patterned surfaces. Substrates were then stained and imaged by fluorescence microscopy. An exposure time of 400 and 1200 ms were used to image nuclei and actin, respectively.

3.2.15 Fibroblast (Fb) Culture

Swiss 3T3 albino mouse fbs and Rat2 fbs were cultured in Dulbecco's Modified Eagle Medium (Gibco) containing 10 % calf bovine serum (CBS) and 1 % penicillin/streptomycin at 37 °C in 5 % CO_2. **Delivery of functionalized liposomes to cells.** Cells were seeded onto a tissue culture plate and allowed to grow for 48 h at 37 °C in 5 % CO_2 in CBS media. Solutions of keto-LUV (**5**) were reacted with rhod-oxyamine (**7**, 7 mM in H_2O, 100 μL added to 4 mL) for 30 min and then added to cells for 4 h. The cells were then washed with PBS (4 x 4 mL) and imaged under a fluorescence microscope with an exposure time of 1/1200 s. **Cell-surface reaction to ketone-presenting cells.** Solutions of keto-LUV (**5**, 1 mg/mL) were added to the culture to give the desired final ketone concentration of 100 μg/mL in a total volume of 2 mL. The cells were incubated with the keto-LUVs for 4 h and washed with PBS (4 x 25 mL), followed by addition of rhod-oxyamine (**7**, 7 mM in H_2O, 100 μL added to 4 mL) dye and incubation for 30 min. The cells were then washed with PBS (4 x 4 mL) and removed with a solution of 0.05 % trypsin 0.53 mM EDTA and re-suspended in serum-free medium (~10^4 cells/mL). The cells were then seeded to a fibronectin-coated surface for 2 h. After 2 h, serum-containing media was added for cell growth and imaged after 3 days.

3.2.16 Flow Cytometry

Fluorescence activated cell sorting (FACS) analysis was performed in order to quantify the approximate number of ketone and oxyamine groups at the cell surface after membrane fusion. Liposomes (**5**) were prepared as described above and were delivered to Swiss 3T3 albino mouse fbs in culture (3 mM in tris buffer, 400 μL added to 4 mL, 16 h). A time course assay was also conducted using FACS to determine whether the chemistry

was being carried on after cell growth and division. Fbs (**8**) were reacted with hydrazine-conjugated biotin (3 mM in CBS, 1 mL added to 4 mL CBS in cell culture, 1 h) after culture with keto-containing liposome for 1, 3, 5, and 7 d. Fluorescein-conjugated streptavidin (1 mM in CBS, 0.5 mL added to 4 mL CBS in cell culture, 1 h). A control cell population (not displaying ketone groups) was only incubated with biotin-hydrazide and streptavidin-fluorescein for 1 h each, under the same conditions. Cells were then centrifuged (5 min, 1000 rpm), resuspended in RMPI (without phenol red), centrifuged (5 min, 1000 rpm), and resuspended in RPMI (~10^7 cells/2 mL). Fluorescence measurements were calibrated using RCP-5-30 beads (~10^7 beads/mL, Spherotech, Inc., Lake Forest, IL) of known fluorescein equivalent molecule density. Fluorescent intensities based on number of cells counted were compared to the standard bead and control cells lacking fluorescent molecule conjugation and approximate numbers of fluorescent compound bound to the surface was calculated. Flow cytometry was carried out using a Dako CyAn ADP (Beckman-Coulter, Brea, CA), and data was analyzed with Summit 4.3 software.

3.3 Results and Discussion

3.3.1 Fusion Methodology and Dynamic Light Scattering

In previous studies, we have shown how chemoselective oxime chemistry can be used to present biospecific ligands from supported, model fluid lipid bilayer membranes for subsequent recognition by protein receptors.[38] Using this oxime ligation strategy, we generated a number of large unilamellar vesicles (LUVs) that present ketone or oxyamine functional groups and employed them in liposome-liposome fusion, Fourier resonance energy transfer (FRET), and liposome-cell fusion studies. For liposome-liposome fusion

analyses that include matrix-assisted laser-desorption/ionization mass spectrometry (MADLI-MS), dynamic light scattering (DLS), and transmission electron microscopy (TEM), dodecanone and dodecyloxyamine molecules were incorporated, separately, into neutral, egg palmitoyl-oleoyl phosphatidylcholine (POPC) at a ratio of 5:95 to form keto-LUVs (**1**) and oxy-LUVs (**2**), respectively (Figure 1a and 1b). Dodecanone molecules were mixed with POPC and fluorescence donor, egg 1,2-diphytanoyl-*sn*-glycero-3-phosphoethanolamine-N-(7-nitro-2-1,3-benzoxadiazol-4-yl) (NBD-PE) at a ratio of 5:93:2 to form keto-NBD-PE-LUVs (**3**), while dodecyloxyamine molecules were incorporated into POPC, negatively charged, egg 1-palmitoyl-2-oleoyl-phosphatidylglycerol (POPG), and fluorescence acceptor, egg 1,2-dipalmitoyl-*sn*-glycero-3-phosphoethanolamine-N-(lissamine rhodamine B sulfonyl) (rhod-PE) at a ratio of 5:73:20:2 to form oxy-rhod-PE-LUVs (**4**). These chemoselectively tailored liposomes (**3** and **4**) were used to conduct Fourier resonance energy transfer (FRET) studies (Figure 1c). Finally, liposomes that contained dodecanone, POPC, and cationic lipid, 1,2-dioleoyl-3-trimethylammonium-propane (DOTAP) (5:93:2, **5**) and liposomes that composed of dodecyloxyamine, POPC, and DOTAP (5:93:2, **6**) were generated to investigate liposome-cell fusion processes (Figure 1d). Cationic lipid, DOTAP, was incorporated to induce membrane fusion.[39,40] Our general fusion methodology is described in Figure 1a. Two liposome populations (**1** & **2**, **3** & **4**, or **5** & **6**) were mixed, resulting in liposome docking, adhesion, and finally fusion due to the formation of stable, interfacial oxime bonds. Depending on the application, liposomes to each other, forming larger liposomal structures or to cell surfaces, demonstrating non-invasive, cell-surface engineering. Mixing **1** and **2** resulted in a gradual increase in size over a period of 2 h,

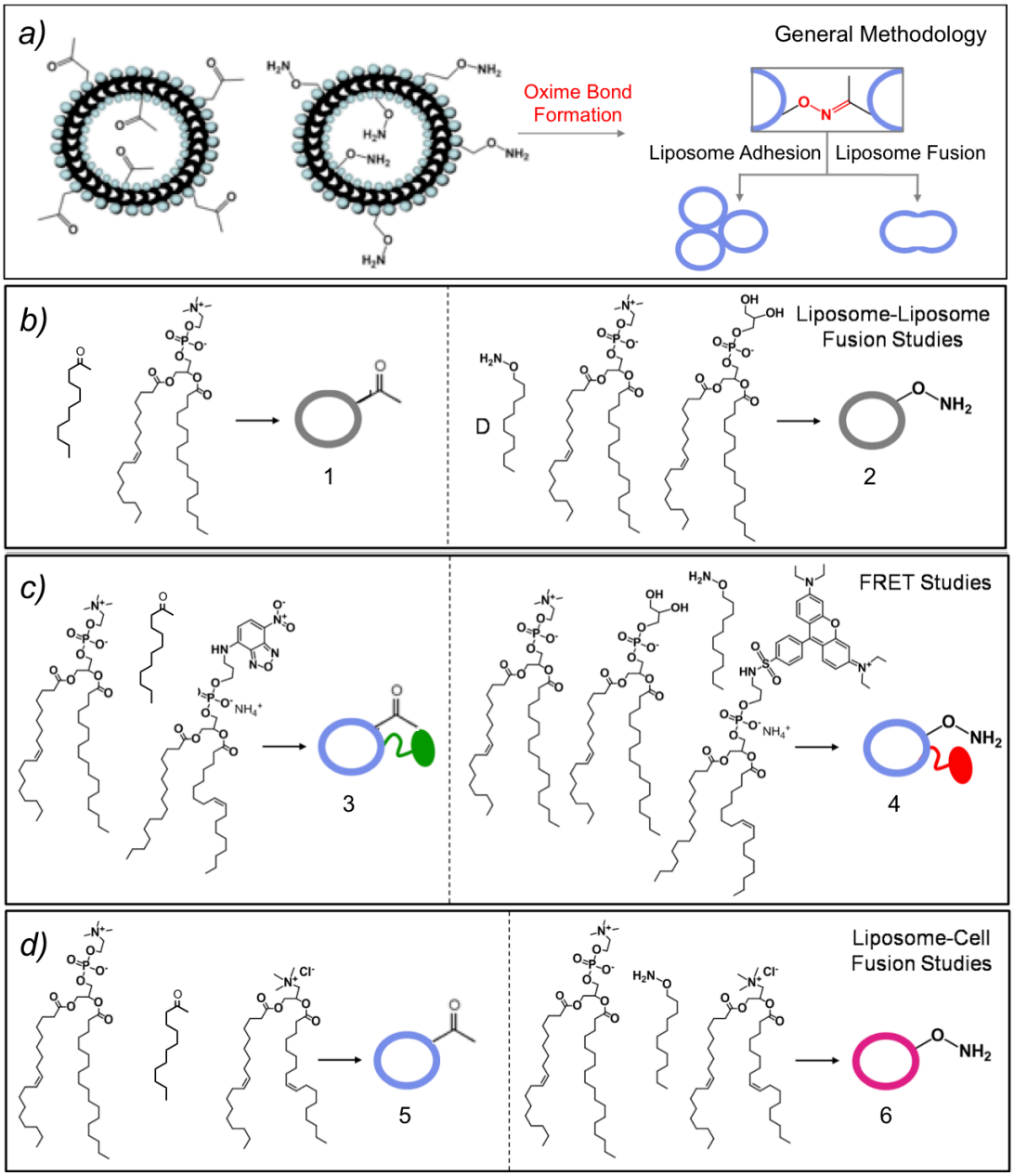

Figure 3.1 General schematic and corresponding lipid components for the formation of fused and adhered liposomes based on chemoselective oxime conjugation. (a) When mixed, ketone- and oxyamine-tethered liposomes react chemoselectively to form an interfacial, covalent oxime linkage, resulting in liposome docking and adhesion. Docked liposomes either fuse or form multi-adherent structures. (b) Dodecanone molecules were incorporated into neutral, POPC at a ratio of 5:95 to form keto-LUVs (**1**), while *O*-dodecyloxyamine molecules were incorporated into POPC and negatively charged, POPG at a ratio of 5:75:20 to form oxy-LUVs (**2**). These liposomes were used for liposome-liposome fusion studies. (c) Dodecanone molecules were incorporated into POPC and fluorescence donor, NBD-PE at a ratio of 5:93:2 to form keto-NBD-PE LUVs (**3**). *O*-Dodecyloxyamine molecules were incorporated into POPC, POPG, and

fluorescence acceptor, rhod-PE at a ratio of 5:73:20:2 to form oxy-rhod-PE LUVs (**4**). These liposomes were used for FRET studies. (d) Dodecanone molecules were incorporated into POPC and positively charged, DOTAP at a ratio of 5:97:2 to form ketone-presenting liposomes (**5**). *O*-Dodecyloxyamine molecules were incorporated into POPC and DOTAP at a ratio of 5:93:2 to form oxyamine-presenting liposomes (**6**). These liposomes were used for cell-liposome fusion studies.

followed by no change in size (Figure 2d). In a control reaction, LUVs not presenting ketones were reacted with LUVs containing oxyamines (**1**). Likewise, LUVs containing ketone groups (**2**) were mixed with LUVs that did not display oxyamines. For both of these control experiments, no size change was observed over time. This result strongly supports that liposome adhesion and fusion are driven by chemoselective oxime bond formation between the ketone- and oxyamine-alkanes.

3.3.2 MALDI-MS

Oxime conjugation, after keto-LUV (**1**) fusion, was confirmed by MALDI-MS analysis. Self-assembled monolayers (SAMs) of aminooxyundecanethiol were formed on a gold-coated, sample plate. A solution containing keto-LUVs (**1**) was then allowed to fuse and react with the surface for 90 min, followed by MALDI-MS examination. A mass of 387 units was detected, confirming successful oxime conjugation, resulting from liposome fusion on the surface (Figure 2a).

3.3.3 TEM

Structural insight into the formation of different adhered and fused liposomes was observed through TEM (Figure 2b).[41] Vesicles of different sizes and shapes result after 2 h of liposome mixing (keto-LUV, **1** and oxy-LUV, **2**). The liposome size gradually increases with time and is consistent with the data collected from other sizing experiments (e.g., DLS). Upon reaction, the following three structures were observed:

multi-adherent liposomes that were not fused, partially fused liposomes, and completely fused, large uni- and multi-lamellar liposomes (Figure 2b).

3.3.4 DLS

DLS was performed upon mixing liposomes (**1** and **2**) to monitor vesicle size change as a function of time. Increases in vesicle size were observed due to aggregation, adhesion, or fusion (blue trace, Figure 2d). Liposome saturation was reached ~80 min after mixing. Without the presence of ketone and oxyamine functional groups, the LUV size remains constant (red trace, Figure 2d).

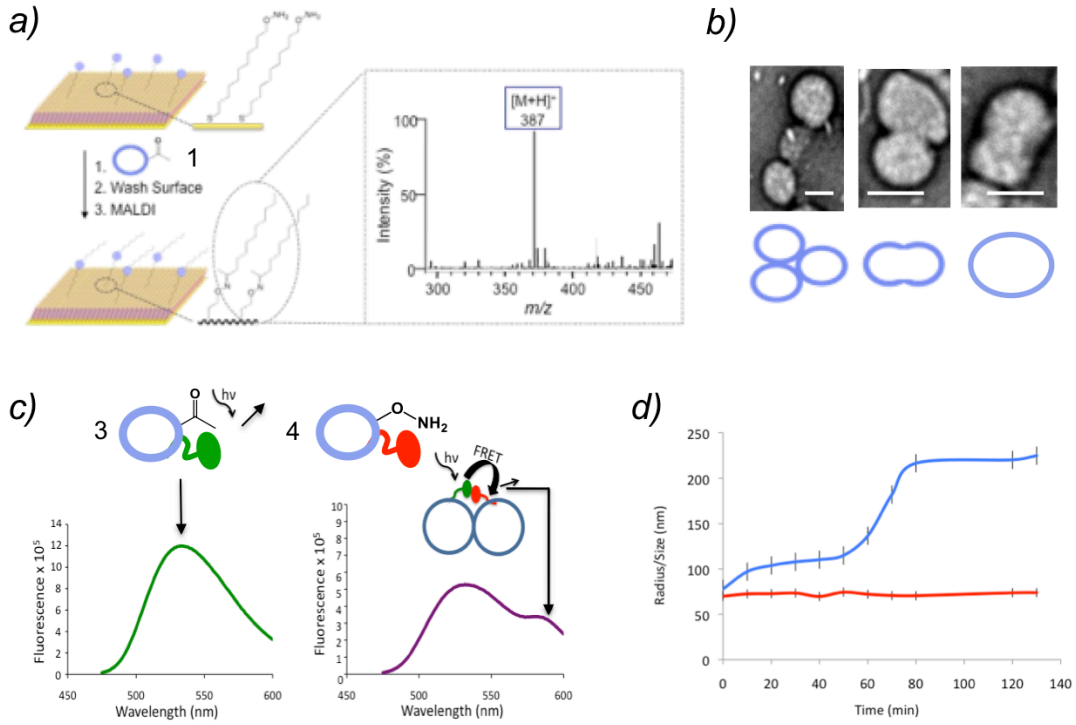

Figure 3.2 Characterization of the formation of fused and adhered liposomes based on chemoselective oxime conjugation. (a) Mass spectrometry (MS) data representing the oxime ligation of keto-LUVs to self-assembled monolayers (SAMs) of oxyamine-terminated alkanethiol on a gold surface is displayed. Matrix-assisted laser desorption/ionization (MALDI) was performed after keto-LUVs were delivered to the surface, and a mass of 387 units was detected, confirming oxime conjugation. (b) Structural analyses using transmission electron microscopy (TEM), representing the adhesion and fusion of keto- (**1**) and oxy- (**2**) LUVs over time. The following images are shown from left to right: multi-adherent liposomes that are not fused; partially fused liposomes; and a single, large liposome after complete fusion. The scale bars represent 60

nm. (c) Fourier resonance energy transfer (FRET) analysis of liposome adhesion and fusion was monitored over 2 h. Fluorescence emission of keto-NBD-PE/PC LUVs (**3**), excited at 460 nm, was observed by scanning 475-600 nm (green trace). Fluorescence emission of keto-NBD-PE/PC LUVs (**3**) mixed with oxy-rhod-PE/PC/POPG LUVs (**4**) is represented (purple trace). A new FRET emission peak is observed at 578 nm showing mixed liposome adhesion. (d) Dynamic light scattering (DLS) was performed upon mixing liposomes (**1** and **2**) to monitor vesicle size change as a function of time. Increases in vesicle size were observed due to aggregation, adhesion, or fusion (blue trace). Liposome saturation was reached ~80 min after mixing. Without the presence of ketone and oxyamine functional groups, the LUV size remains constant (red trace).

3.3.5 FRET

Figure 2c shows a liposome fusion assay involving FRET characterization. A lipid-bound FRET pair, NBD-PE (donor) and rhod-PE (acceptor), were incorporated at 2 mol % concentration during liposome generation to produce keto-NBD-PE LUVs (**3**) and oxy-rhod-PE LUVs (**4**), respectively. Hypothetically, fusion of these vesicles should result in a gradual decrease in the donor emission peak and an increase in acceptor emission peak[40] due to the close proximity of these dyes. As shown, vesicle mixing resulted in this FRET fusion signature. Fusion was observed immediately upon mixing **3** and **4**, slowing within 2 h to a stable population, which is similar to earlier sizing results. An emission peak was not observed for the acceptor rhodamine dye when performing control experiments that tested the energy transfer with an LUV that did not contain oxyamines. Similar results were observed when LUVs that did not contain ketones or oxyamines were mixed. This data further supports that liposome aggregation and fusion is based on chemoselective oxime bond formation.

3.3.6 Cell-Surface Labeling

Chemical approaches to engineer cell surfaces have emerged as powerful tools for a variety of biomedical and biotechnological applications, including tissue engineering, drug delivery, and cell-based therapies.[24] Several metabolic and genetic approaches to

display small molecular recognition pairs at cell surfaces for further covalent modification have been achieved through Click chemistry[42] and Staudinger ligation.[20] However, such strategies may alter cellular physiology and interfere with normal biochemical pathways.[28] In this report, we use oxime chemistry to tailor and fluorescently label cell surfaces via a novel liposome fusion strategy. As mentioned, cationic lipid, DOTAP, was incorporated within keto- and oxy-LUVs to initiate electrostatic destabilization and subsequent fusion to the cell membrane.[39] As such, the minimum DOTAP concentration required to facilitate liposome-cell fusion was determined to be 2 % through fluorescence labeling optimization. Keto-LUVs were generated using DOTAP and POPC concentrations that ranged from 0.5 % to 5 % and 90 % to 94.5 %, respectively, while maintaining a 5-% ketone concentration. These liposomes were incubated with fibroblasts (fbs) for 4 h, conjugated with an oxyamine-tethered rhodamine (rhod-oxyamine, **8**) (0.7 mM, 2 h), and the cell fluorescence intensities were then compared. From 2 % to 5 % DOTAP, the intensities were almost identical, indicating that 2 % DOTAP is sufficient to initiate fusion.

Given this optimized lipid ratio (POPC/ketone or oxyamine/DOTAP at 93:5:2), two cell-surface engineering methods were employed to fluorescently label fbs. Similar to our optimization experiments, a solution of keto-LUVs (**5**, 200 μL, 0.6 mM) was added to fbs in culture for 2 h, resulting in membrane fusion and subsequent display of ketones from the cell surface (**9**) (Figure 3d). Rhod-oxyamine (**8**, 100 μL, 0.7 mM in H_2O) was then added the cells for 2 h. After oxime formation, the fbs were washed with PBS, trypsinized, diluted with CBS-containing media (~10^2/mL), seeded to a glass substrate, and imaged under a fluorescent microscope. As observed in figure 3f, the conjugation of

rhod-oxyamine with ketone-presenting fbs resulted in the red fluorescence labeling of cells. When the control fbs (i.e., no ketone groups present) were reacted with rhod-oxyamine (**8**) and then imaged, no fluorescence was observed (Figure 3e). Demonstrating the flexibility of this liposome-based surface labeling strategy, we modified fb surfaces to present a ketone-functionalized fluorescein dye (**7**) after oxy-LUV-ketone-fluorescein conjugation and subsequent membrane fusion (Figure 3a). A solution of oxy-LUVs (**6**, 3 mM) was incubated with a ketone-functionalized fluorescein (**7**, 0.15 mM, 1 eq, 2 h), generating fluorescently labeled liposomes. The liposomes were then added to fbs in culture for 2 h. After fusion, the cells were washed with PBS, trypsinized, diluted with CBS-containing media (~10^2/mL), seeded to a glass substrate, and imaged under a fluorescent microscope. Figure 3c presents green fluorescently labeled fbs after fusion with fluorescein-functionalized LUVs. When liposomes, not containing oxyamine groups were incubated with fluorescein-ketone and added to fbs in culture for 2 h, no fluorescence was observed (Figure 3b). Thus, our control images indicated that reaction and labeling does not occur without the proper oxime recognition pair (Figure 3b and 3e). Furthermore, under these conditions, we observed no changes in cell behavior upon liposome fusion to cells. This is a very important feature for future *in vivo* applications. Thus, by combining liposome fusion and oxime chemistry, we were able to tailor the cell surface with either ketone groups or oxyamine groups, which may act as chemoselective cell-surface receptors for a range of small molecules, ligands, biomolecules, and nanoparticles.

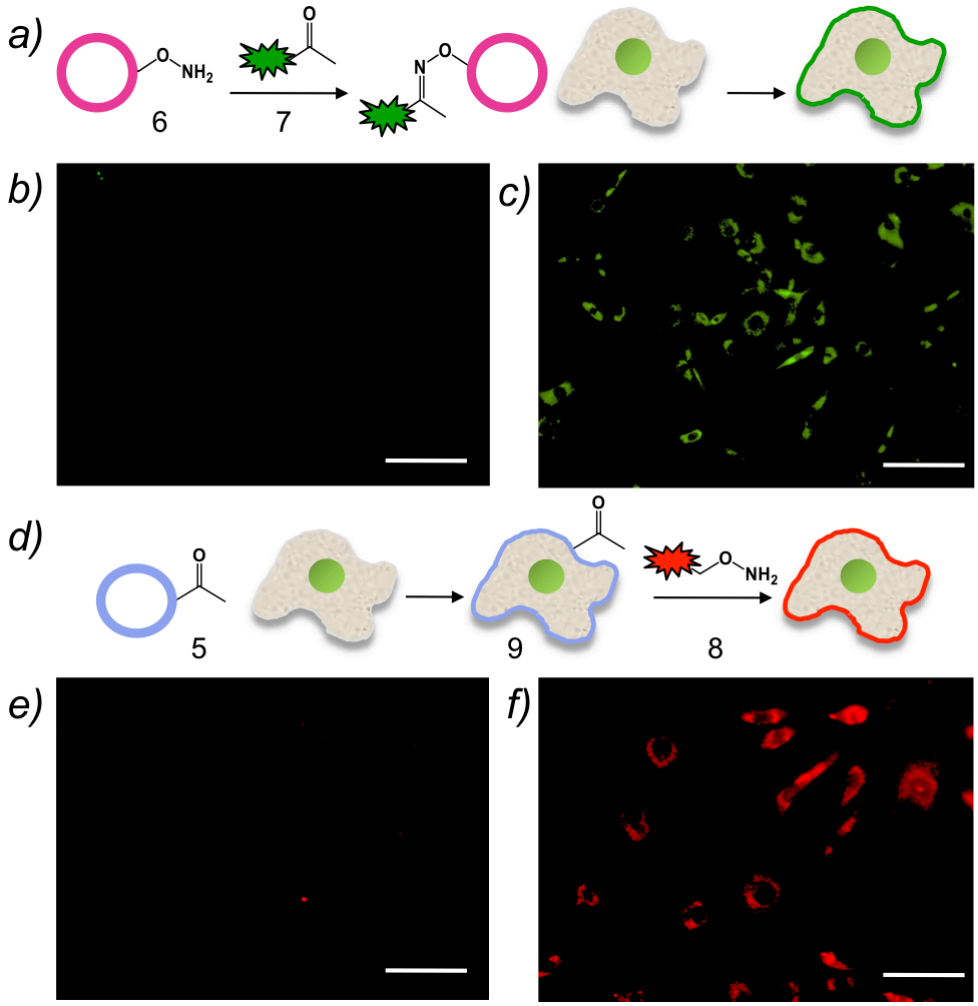

Figure 3.3 (Top) Schematic describing the delivery and subsequent fusion of fluorescent liposomes to cell surfaces with corresponding brightfield and fluorescent images. (a) Oxy-LUVs (**6**, 3 mM) were reacted with fluorescein-ketone (**7**, 0.15 mM, 2 h) to generate green fluorescent liposomes. The fluorescent liposomes were then added to fbs in culture, resulting in the fluorescent labeling of cells after liposome fusion to the cell membrane. Micrographs show (b) control cells where liposomes not containing oxyamine groups were incubated with fluorescein-ketone and added to fbs in culture for 2 h. and (c) green fluorescently labeled cells after oxyamine-functionalized liposomes were incubated with fluorescein-ketone and delivered to fbs (2 h). (Bottom) General schematic and images for cell-surface tailoring using liposome fusion and chemoselective oxime chemistry. (d) Keto-LUVs (**5**, 3 mM) were added and fused with the cells to display these groups from the cell surface (**9**). Addition of rhod-oxyamine (**8**, 0.7 mM in H_2O, 2 min) resulted in chemoselective oxime formation and red fluorescent labeling of the cells. Images display (e) control fbs where liposomes not displaying ketones were fused to the membrane (2 h) and rhod-oxyamine was added and no fluorescence was observed and (f) fluorescently labeled cells after ketone-functionalized liposomes were fused to fbs (2 h) and cells were -incubated with rhod-oxyamine. Scale bars for b and c and d and e represent 50 and 30 μm, respectively.

3.3.7 Cell Patterning: Rewiring Adhesion

The ability to pattern and adhere cells to different materials, such as thin metal films, polymer scaffolds, and nanoparticles, with a simple and straightforward chemoselective and bio-orthogonal approach would be beneficial for cell biology, tissue engineering, and biotechnology. Thus, we employed our liposome fusion-based toward cell-surface engineering to modify and rewire cell surface to adhere to patterned 2D substrates, directed through stable oxime bond conjugation. Figure 4a and 4b illustrate the strategy to rewire cell surfaces for the goal of cell adhesion to self-assembled monolayers (SAMs) of alkanethiolates on gold substrates. Employing microfluidic oxidation[34] and lithography,[35] aldehyde and oxyamine SAMs, respectively, were patterned at a ratio of 10 %. The remaining 90 % of the surface was backfilled with tetra(ethylene glycol) alkanethiol, which is known to pacify biomaterials against nonspecific protein adsorption and cell adhesion.[36] Meanwhile, fbs were cultured separately with keto- (**5**) and oxy-LUVs (**6**, 3 mM, 4 h), resulting in membrane fusion and subsequent display of ketones (**9**) and oxyamines (**10**) from cell surfaces. The resulting ketone- and oxyamine-presenting fbs were then seeded (~10^2 cells/mL, 2 h) to the patterned oxyamine and aldehyde substrates, respectively, and allowed to react and form stable oxime linkages in the patterned regions. The cells were cultured for 4 d on these substrates, growing and proliferating in the patterned regions. The results of patterned keto-fbs on oxyamine SAMs are shown in figure 4c; patterned oxy-fbs on aldehyde SAMs are displayed in figure 4d and 4e. Furthermore, unmodified cells did not attach to the surface. Thus, this strategy allows for a bottom-up, bio-orthogonal synthetic approach to rewire how cells adhere to materials and does not require metabolic or genetic cell manipulations.

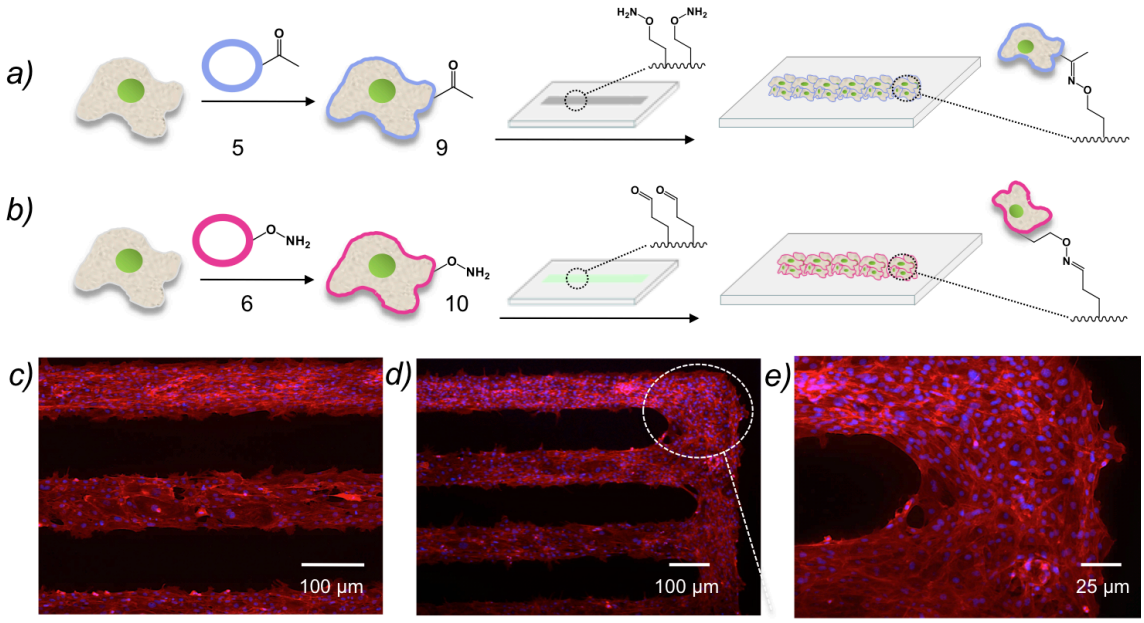

Figure 3.4 Schematics and fluorescent micrographs of rewired cells adhered to patterned self-assembled monolayers (SAMs) of alkanethiolates on gold substrates. (a and b) Keto- (**5**) and oxy-LUVs (**6**, 3 mM, 4 h) were cultured with separate fb populations, producing ketone- and oxyamine-presenting fbs (**9** and **10**, respectively). These cells were then seeded (~10^2 per mL, 2 h) to patterned, oxyamine- and aldehyde-terminated SAMs (10 %), respectively, and allowed to adhere through stable oxime conjugation. The unpatterned surface regions present tetra(ethylene glycol), which resists cell and protein adsorption. The cells then grew and proliferated only filling out the oxyamine- and aldehyde-tethered surface regions, respectively. (c) A fluorescent micrograph of patterned ketone-fbs (**9**), adhered to an oxyamine-terminated SAM is shown. (d and e) Fluorescent micrographs of patterned oxyamine-fbs (**10**), adhered to an aldehyde-terminated SAM are demonstrated. Cells were stained with DAPI (blue, nucleus) and phalloidin (red, actin).

3.3.8 Flow Cytometry

Flow cytometry was performed to further verify the ability of tailoring small molecules to cell surfaces through covalent oxime bond formation. This method also enables the quantification of ketone and oxyamine molecules that are present at the cell surface after liposome delivery and subsequent membrane fusion. Liposomes that incorporated

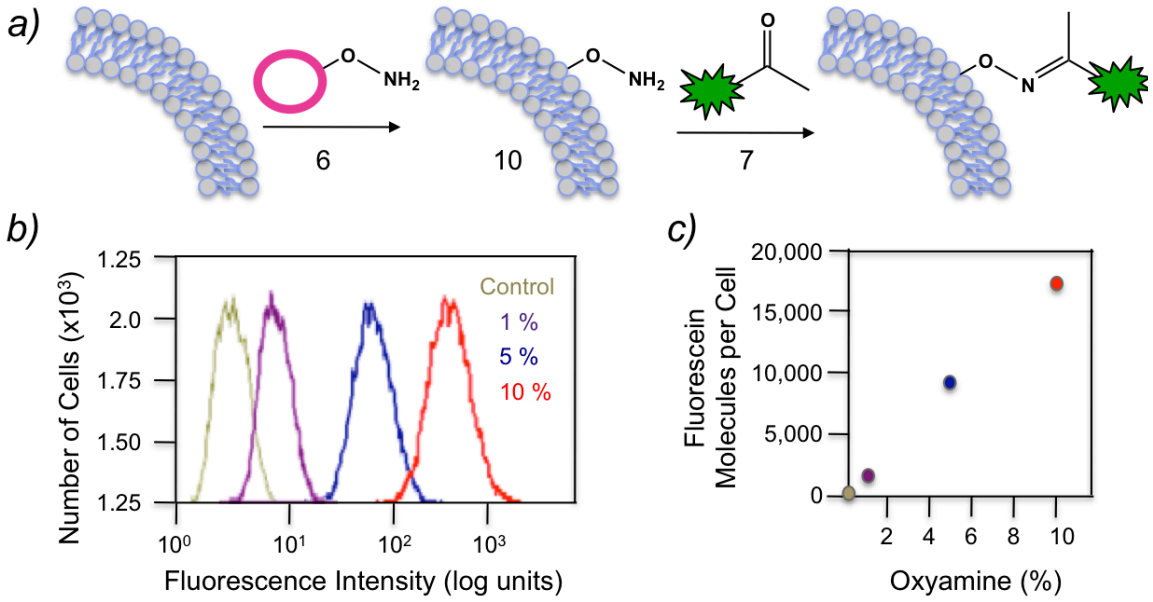

Figure 3.5 Cell surface molecule quantification using flow cytometry. (a) Oxy-LUVs (**6**, 3 mM) were added to fbs in culture (4 h), resulting in membrane fusion and subsequent display of oxyamine groups from cell surfaces (**10**). Ketone-functionalized fluorescein (**7**, 0.15 mM 2 h) was then reacted with the fbs, generating fluorescently labeled cells. (b) Liposomes with varying oxyamine mol % (0 %, 1 %, 5 %, and 10 %) were generated and cultured with separate populations of fbs. After reacting with ketone-fluorescein, the cell populations were washed with PBS, trypsinized, centrifuged, resuspended in RPMI media, and tested using FACS analyses. As shown, the fluorescence intensity increased with increasing oxyamine concentration. (c) The number of present molecules at the cell surface with respect to oxyamine concentration was quantified using flow cytometry. A bead with a known FITC molecule density was employed as a standard comparison to calculate the number of oxyamines after oxy-LUVs (**6**) with 0 %, 1 %, 5 %, and 10 % oxyamine was cultured with cells. As the oxyamine concentration increased, the molecules per cell increased linearly (0 %, 128; 1 %, 1600; 5 %, 9800; and 10 %, 17400). Twenty thousand cells were counted for each sampling.

varying oxyamine concentrations of (i.e., 0, 1, 5, and 10 mol %) were generated (**6**, 3 mM) cultured with separate fb populations for 4 h, resulting in membrane fusion and oxyamine display (**10**, Figure 5a). A ketone-modified fluorescein dye (**7**, 0.15 mM, 2 h) was then conjugated to the cell surfaces in each population, producing green fluorescently labeled fbs. The FACS analyses results are demonstrated in figure 5b. Twenty thousand cells were counted for all samples. As shown, the fluorescence intensity

increases with increasing number of oxyamine molecules present for fluorescein conjugation. Additionally, the control cell population that was fused with unmodified liposomes and reacted with ketone-fluorescein (**7**) demonstrated the lowest intensity. Furthermore, a bead with known FITC molecule density was calibrated and used as a standard comparison to quantify the number of oxyamine molecules present at the cell surface after fusion.[37] Figure 5c displays the correlation between oxyamine mol % and oxyamine molecules per cell counted by FACS analyses. The calculated molecules per cell for the control fbs and oxyamine-presenting fbs that were fused with 1 %, 5 %, and 10 % oxyamine were approximately 128, 1300, 9800, and 17400, respectively. A linear trend was observed; as the molecule concentration increased, the fluorescence intensity and number of molecules at the cell surface increased. Thus, the density of molecules that decorate cell surfaces can be controlled and quantified using this liposome fusion-based methodology for cell-surface engineering.

3.4 Conclusion

In summary, we developed a chemoselective synthetic cell receptor system based on a liposome delivery and fusion strategy. Ketone and oxyamine groups were introduced to a liposomal system and chemoselective vesicle fusion was achieved using molecular recognition and interfacial oxime bond formation. Subsequent delivery of the decorated liposomes to cells lead to fusion and modification of a cell surface by bio-orthogonal reactive groups that serve as synthetic chemoselective cell receptors. Ketone and oxyamine modified cells were patterned on solid surfaces, displaying oxyamine and ketone groups respectively. Thus, rewiring cell adhesion was achieved using chemoselective oxime bond formation and without using any cell adhesive ligands, such

as Arg-Gly-Asp (RGD) and fibronectin. Since no biomolecules are used with this strategy, no long-term stability and degradation issues in complex cell culture media or *in vivo* will affect cell targeting or cell assembly. This methodology may have diverse applications in biomedical technologies including tissue engineering and regenerative medicine. Cells displaying ketone and oxyamine groups can react chemoselectively to form three-dimensional (3D) and tissue-like structures as directed through *in situ* oxime bond formation. This method can be extended to generate 3D cell co-culture systems and study cell-cell interactions. The ketone- and oxyamine-functionalized liposomes may have extensive applications in drug delivery and diagnostic applications, in which the interior of the liposome contains cargo while the exterior surface can be simultaneously functionalized with the tracking agent.

3.5 Acknowledgements

The authors thank Dr. Nancy Thompson and her lab group for use of equipment and expertise in liposome chemistry, Lisa Bixby for help with FACS analysis, and Brian Lamb for aid with MS data collection. This work was supported by the Carolina Center for Cancer Nanotechnology Excellence, the Burroughs Wellcome Foundation (Interface Career Award), and the National Science Foundation.

3.6 References

(1) Mayer, A. *Annu. Rev. Cell. Develop. Biol*. **2002**, *18*, 289.

(2) Rowan, A. *Nat. Rev. Mol. Cell Biol.* **2006***, 7*, 555-561.

(3) Ellens, H., Bentz, J., Szoka, F. *Biochemistry*, **1985**, *24*, 3099-3106.

(4) Dennison, S. M., Greenfield, N., Lenard, J., Lentz, B. R. *Biochemistry*, **2002**, *41*, 14925-14934.

(5) Evans, K. O., Lentz, B. R. *Biochemistry*, **2002**, *41*, 1241-1249.

(6) Jahn, R., Lang, T., Sudhof, T. C. *Cell*, **2003,** *112*, 519-533.

(7) McNew, J. A., Weber, T., Parlati, F., Johnston, R. J., Melia, T. J., Sollner, T. H., Rothman, J. E. *J. Cell Biol.* 2000, *150*, 105-117.

(8) Soolner, T. H. *Curr. Opin. Biol.* **2004**, *16*, 429- 435.

(9) Parlati, F., Weber, T., McNew, J. A., Westermann, B., Sollner, T. H., Rothman, J. E. *Proc. Natl. Acad. Sci. U.S.A.* **1999**, *96*, 12565-12570.

(10) Paumet, F., Rahimian, V., Rothman, J. E. *Proc. Natl. Acad. Sci. U.S.A.* **2004**, *101*, 3376-3380.

(11) Richard, A., Marchi-Artzner, V., Lalloz, M-N., Brienne, M-J., Artzner, F., Gulik-Krzywicki, T., Guedeau-Boudeville, M-A., Lehn, J.-M. *Proc. Natl. Acad. Sci. U.S.A.* **2004**, *101*,15279-15284.

(12) Marchi-Artzner, V., Gulik-Krzywicki, T., Guedeau-Boudeville, M-A., Gosse, C., Sanderson, J. M., Dedieu, J.-C., Lehn, J-M. *ChemPhysChem* **2001,** *2*, 367-376.

(13) Marchi-Artzner, V., Jullien, L., Gulik-Krzywicki, T., Lehn, J.-M. *Chem. Commun.* **1997***, 1***,** 117-118.

(14) Paleos, C. M., Tsiourvas, D. *J. Mol. Recognition*, **2006**, *19*, 60-67.

(15) Chan, Y.-H. M., Lengerich, B., Boxer, S. G. *Proc. Nat. Acad. Sci. U.S.A.* **2009***, 106*, 979-984.

(16) Gong, Y., Luo, Y., Bong, D. *J. Am. Chem. Soc.* **2006,** *128*, 14430-14431.

(17) Sarkar, D., Vemula, P. K., Zhao, W., Gupta, A., Karnik, R., Karp, J. M. *Biomaterials*, **2010**, *31*, 5266-5274.

(18) Winans, K. A., Bertozzi, C. R. *Chem. Biol.* **1995**, *5*, R313-R315.

(19) Kellam, B., De Bank, P. A., Shakesheff, K. A. *Chem. Soc. Rev.* **2003**, *32*, 327-337.

(20) Saxon, E., Bertozzi, C. R. *Science,* **2000**, *287*, 2007-2010.

(21) Lin, C. W., Ting, A. Y. *J. Am. Chem. Soc.* **2006**, *128*, 4542-4543.

(22) Liu, W., Brock, A., Chens, S., Chen, S., Schultz, P. G. *Nat. Methods*, **2007**, *4*, 239-244.

(23) Wilson, J.T., Krishnamurthy, V. R., Cui, W., Qu, Z., Chaikof, E. L. *J. Am. Chem. Soc.* **2009**, *131*, 18228-18229.

(24) Prescher, J. A., Bertozzi, C. R. *Nat. Chem. Biol.* **2005**, *1*, 13-21.

(25) Chen, I., Howarth, M., Lin, W., Ting, A. Y. *Nat. Methods*, **2005**, *2*, 99-104.

(26) Boonyarattanakalin, S., Martin, S. E., Sun, Q., Peterson, B. R. *J. Am. Chem. Soc.* **2006**, *128*, 11463-11470.

(27) Rabuka, D., Forstner, M. B., Groves, J. T., Bertozzi, C. R. *J. Am. Chem. Soc.* **2008**, *130*, 5947-5953.

(28) Rose, K. *J. Am. Chem. Soc.* **1994***, 116*, 30-33.

(29) Rideout, D., Calogeropoulou, T., Jaworski, J., McCarthy, M. *Biopolymers*, **1990**, *29*, 247-262.

(30) Rideout, D. *Cancer. Invest.* **1994***, 12*, 189-202.

(31) Shao, J., Sham, J. P. *J. Am. Chem. Soc.* **1995**, *117*, 3893-3899.

(32) Pale-Grosdemange, C., Simons, E. E., Prime, K. L., Whitesides, G. M. *J. Am. Chem. Soc.* **1991***, 113*, 12-20.

(33) Park, S., Yousaf, M. N. *Langmuir,* **2008***, 24*, 6201-6207.

(34) Westcott, N. P.; Pulsipher, A.; Lamb, B. M.; Yousaf, M. N. *Langmuir,* **2008***, 24*, 9237-9240.

(35) Lamb, B. M.; Barrett, D. G.; Westcott, N. P.; Yousaf, M. N. *Langmuir,* **2008***, 24*, 8885-8889.

(36) Harder, P., Grunze, M., Dahint, R., Whitesides, G. M., Laibinis, P. E. *J. Phys. Chem. B*, **1998**, *102*, 426-436.

(37) Hsiao, S. C., Shum, B. J., Onoe, H., Douglas, E. S., Gartner, Z., Mathies, R. A., Bertozzi, C. R., Francis, M. B. *Langmuir*, **2009**, *25*, 6985-6991.

(38) Dutta, D., Pulsipher, A., Yousaf, M. N. *Langmuir*, **2010**, *26*, 9835-9841.

(39) Csiszar, A., Hersch, N., Dieluweit, S., Biehl, R., Merkel, R., Hoffmann, B. *Bioconjugate Chem.* ***2010****, 21*, 537-543.

(40) Beigel, M., Keren-Zur, M., Laster, Y., Loyter, A. *Biochemistry* **1988**, *27*, 660-666.

(41) Beck, P., Liebi, M., Kohlbrecher, J., Ishikawa, T., Ruegger, H., Fischer, P., Walde, P., Windhab, E. *Langmuir*, **2010**, *26*, 5382-5387.

(42) Chang, M., Prescher, J. A., Sletten, E. M., Baskin, J. M., Miller, I. A., Agard, N. J., Lo, A., Bertozzi, C. R. *Proc. Natl. Acad. Sci. U.S.A.* **2010***, 107*, 1821-1826.

CHAPTER 4

Synthetic Chemoselective Rewiring of Cell-Surfaces: Generation of Three-Dimensional Tissue Structures

4.1 Introduction

Cells that make up tissues and organs exist and communicate within a complex, three-dimensional (3D) environment. The spatial orientation and distribution of extracellular matrix (ECM) components directly influences the manner in which cells receive, integrate, and respond to a range of input signals.[1] As such, cellular interactions with ECM molecules and/or other cells have been extensively investigated for fundamental studies in development, cell motility, differentiation, apoptosis, paracrine signaling, and applications in tissue engineering.[2,3] There has been tremendous effort toward the design and fabrication of 3D scaffolds that mimic ECM properties and induce tissue formation *in vitro*, utilizing various biomaterials, biodegradable polymers,[4] collagen,[5] and hydrogels.[6,7] Among the major challenges facing the use of these technologies for tissue engineering are the abilities to force contact between multiple cell types in 3D to control the spatial and temporal arrangement of cellular interactions and tailor and mold the biomaterial to recapitulate the 3D, *in vivo* environment under laboratory constraints. Without the use of engineered scaffolds in culture, most cells are unable to form the necessary higher-order 3D structure required for the anatomical mimicry of tissue and are limited to random migration, generating two-dimensional (2D) monolayers. As a result, several approaches, including the use of dielectrophoretic forces,[8,9] laser-guided

writing,[10-12] surface manipulation,[13] and a number of lithographic printing techniques[14-17] have been integrated with 3D scaffold designs to produce multi-type cellular arrays[9,11,17] or 3D cell clusters or spheroids.[7,8,13] In a recent pioneering study by Bertozzi and Gartner, 3D aggregates consisting of multiple cell types were formed within a hydrogel matrix through DNA hybridization after cell surfaces were engineered with complementary short oligonucleotides via a metabolic labeling approach.[7] However, for some applications, the presentation of cell-surface DNA may not be stable for extended time periods in cell culture or *in vivo*.[18]

Other approaches to cell-surface engineering have also been undertaken to incorporate a functional group into a target biomolecule, such as an endogenous protein, utilizing a cell's biosynthetic machinery.[19,20] These strategies aim to produce a site that can then be covalently modified with its delivered counterpart or probe. However, most of these protein-based tags are large and bulky and become problematic when interacting with the other glycans and biomolecules on the cell suface.[21,22] Additionally, the perturbation of cellular physiology with biomolecules at the cell surface may result in the interference of significant biochemical pathways or cellular functions.[23,24] Thus, a methodology that combines cell-surface modification, without the use of molecular biology techniques or biomolecules, and a simple, stable bio-orthogonal conjugation bottom-up approach that is capable of directing tissue formation would greatly benefit a range of medical applications such as wound healing and burn treatment.

Herein, we develop and employ a novel strategy to induce specific and stable cell-cell contacts through chemoselective cell-surface engineering based on liposome delivery and fusion of bio-orthogonal functional groups to cell membranes.[25] Using a cationic lipid,

membrane fusion,[26,27] rather than the endocytotic cellular uptake of vesicle contents, is induced. This enables the presentation of bio-orthogonal ketone and oxyamine molecules from cell surfaces for subsequent chemoselective oxime ligation. No proteins or large biomolecules are used in this strategy, and therefore, cellular physiology is not perturbed. We demonstrate how this method may be used in several applications including, the delivery of reagents to cell surfaces, formation of 3D spheroid assemblies of cells with controlled inter-connectivity, and patterned multi-layered cell tissues. Furthermore, 3D multi-layered stem cell and fbroblast (fb) co-cultures were generated, and differentiation was induced to form tissue-like structures of adipocytes and fbs. To our knowledge, this is the first report utilizing tailored liposomes to modify a living cells surface through membrane fusion for subsequent bio-orthogonal tailoring to generate 3D tissue-like structures.

4.2 Materials and Methods

4.2.1 Materials

All chemical reagents were of analytical grade and used without further purification. Lipids egg palmitoyl-oleoyl phosphatidylcholine (POPC) and 1,2-dioleoyl-3-trimethylammonium-propane (DOTAP), egg were purchased from Avanti Polar Lipids (Alabaster, AL). Antibodies and fluorescent dyes were obtained from Invitrogen (Carlsbad, CA). Trypan blue viability dye was obtained from Hyclone (Fisher Sci, Pittsburgh, PA), and all other chemicals were obtained from Sigma-Aldrich or Fisher. Swiss 3T3 albino mouse fibroblasts (fb) were obtained from the Tissue Culture Facility at the University of North Carolina (UNC). Rat2 fb transfected with m-cherry were

obtained from the Bear Lab (UNC Chapel Hill, NC). Human Mesenchymal stem cells (hMSCs) were purchased from Lonza (Basel, Switzerland).

Phase contrast and fluorescent imaging was performed and processed using a Nikon TE2000-E inverted microscope and Metamorph software, respectively. Scanning electron microscopy images were obtained using a Hitachi S-4700 field emission scanning electron microscope (Hitachi High Technologies America, Inc., Schaumburg, Illinois). Confocal micrographs were taken and processed using a Nikon Eclipse TE2000-E inverted microscope (Nikon USA, Inc., Melville, NY) and Volocity software, respectively.

4.2.2 2-(dodecyloxy)isoindoline-1,3-dione Synthesis

To a solution of N-hydroxyphthalimide (1.96 g, 12.04 mmol, 1.5 eq) and sodium bicarbonate (10.11 g, 12.04 mmol, 1.5) in DMF (20 mL) at 80°C was added 1-bromododecane (1.93 mL, 8.02 mmol). The mixture was refluxed and stirred for 12 h. The reaction was diluted with DCM and washed with H_2O (6 x 50 mL), 1 M $NaHCO_3$ (3 x 50 mL), and H_2O (2 x 50 mL), dried over $MgSO_4$, and concentrated to afford a white solid (2.66 g, 87 %). ^1H NMR (400 MHz, $CDCl_3$, δ): 1.02 (s, 3H; CH_3), 1.31-1.29 (m, 14H, J = 8; CH_2), 1.47-1.45 (m, 4H, J = 8; CH_2), 1.60-1.57 (m, 2H, J = 12; CH_2), 3.72-3.70 (t, 2H, J = 8; CH_2), 7.80-7.78, 7.85-7.83 (2 x m, 4H, J = 8; Ar-H).

4.2.3 O-dodecyloxyamine Synthesis

To a solution of *2-(dodecyloxy)isoindoline-1,3-dione* (2.65 g, 8.00 mmol) in dry DCM (30 mL) under inert atmosphere (Ar) was slowly added hydrazine (1.53 mL, 48.00 mmol, 6 eq). Upon addition, a white precipitate immediately formed. The mixture was stirred for 12 h. The reaction was diluted with DCM and washed with H_2O (6 x 50 mL), dried over

$MgSO_4$, and concentrated to afford a pale yellow oil (1.18 g, 74 %). ^{1}H NMR (400 MHz, $CDCl_3$, δ): 1.03 (s, 3H; CH_3), 1.33-1.31 (m, 14H, J = 8; CH_2), 1.43-1.41 (m, 4H, J = 8; CH_2), 1.50-1.46 (m, 2H, J = 16; CH_2), 3.64-3.62 (t, 2H, J = 7; CH_2). (ESI) (*m/z*) [M + H^+]: 201.22.

4.2.4 Liposome Fusion to Cells

To generate keto-LUV and oxy-LUV, dodecanone (55 μL, 10 mM solution in $CHCl_3$ at 5 mol %) and alkane-tethered oxyamine (60 μL, 10 mM solution in $CHCl_3$ at 5 mol %) were dissolved with egg-POPC (424 μL, 10 mg/mL in $CHCl_3$ at 93 mol %) and 1,2-dioleoyl-3-trimethylammonium-propane (DOTAP, 10 μL, 10 mg/mL in $CHCl_3$ at 2 mol %) in chloroform followed by concentration under high vacuum for 4 h. The dried lipid samples were then reconstituted and brought to a final volume of 3 mL in PBS buffer, pH 7.4. The contents of the vial were warmed to 50˚C and sonicated for 20 min, in a tip sonicator, until the solution became clear, and LUVs containing ketone or oxyamine groups were formed.

4.2.5 3D Spheroid Generation

Keto-LUV and oxy-LUV were added to two separate fb populations in culture for (3 mM in tris buffer, 400 μL added to 4 mL, 16 h), resulting in fusion and display of ketones and oxyamines from the cell surface. Oxyamine-presenting Rat2 fb contained an m-cherry label (nucleus) for enhanced visualization, while the ketone-presenting Swiss 3T3 albino mouse fb contained no fluorescent label. These two cell populations were then trypsinized and mixed together (~20^4 cells/mL, 4 mL total) in serum containing (10 % CBS, pH of 7.4) media in a 10 mL-flask and incubated at 37 °C and 5 % CO_2 for 3 h.

After mixing, the cells were seeded on a glass surface (~20^4 cells/mL, 1 mL) and visualized under a Nikon TE2000-E inverted microscope or by scanning electron microscopy. Image acquisition and processing was performed using Metamorph software. An exposure time of 75 ms was used to image all spheroids.

4.2.6 Scanning Electron Microscopy (SEM) of 3D Spheroids

After spheroids were assembled in solution (reaction for 3 h as described above) and delivered to a glass slide (~20^4 cells/mL, 1 mL, 0.8 x 0.8 cm^2) and the fixed with 10 % formalin in PBS for 15 min. The substrate was then washed with water (15 min), and cells were then dehydrated stepwise in 30, 50, 70, 90, and 100 % ethanolic solutions for 15 min each. After critical point drying and sputtering 2 nm of gold, the sample was ready for imaging using a Hitachi S-4700 field emission scanning electron microscope (Hitachi High Technologies America, Inc., Schaumburg, Illinois).

4.2.7 Fibroblast (Fb) Culture

Swiss 3T3 albino mouse fb and Rat2 fb were cultured in Dulbecco's Modified Eagle Medium (Gibco) containing 10 % calf bovine serum (CBS) and 1 % penicillin/streptomycin at 37 °C in 5 % CO_2. **Delivery of functionalized liposomes to cells.** Cells were seeded onto a tissue culture plate and allowed to grow for 48 h at 37 °C in 5 % CO_2 in CBS media. Solutions of keto-LUV were reacted with rhod-oxyamine (7 mM in H_2O, 100 μL added to 4 mL) for 30 min and then added to cells for 4 h. The cells were then washed with PBS (4 x 4 mL) and imaged under a fluorescence microscope with an exposure time of 1/1200 s.

4.2.8 hMSC (human mesenchymal stem cell) culture

hMSCs and basic, growth, and differentiation media were obtained from Lonza (Basel, Switzerland). hMSCs were cultured in Dulbecco's Modified Eagle Medium (Gibco) containing 10 % fetal bovine serum (FBS) and 1 % penicillin/streptomycin at 37°C in 5 % CO_2. Adipogenic differentiation was induced by culturing with induction medium as described in the Lonza protocol.

4.2.9 Immunhistochemistry

After the growth of 3D tissue-like structures and co-culture with Swiss 3T3 albino mouse fb, surfaces were fixed with formaldehyde (4 % in PBS, 30 min). Substrates were then immersed in a solution containing water and 60 % isopropyl alcohol (3-5 min), followed by staining with Oil Red O (5 min) and Harris Hemotoxylin (1 min) (6,7). Substrates were visualized by phase contrast microscopy using a Nikon TE2000-E inverted microscope. Image acquisition and processing was performed using Metamorph software. An exposure time of 75 ms was used to image all HMSCs.

4.2.10 Directed 3D Tissue-like Multi-Layers

Ketone-functionalized fibroblast cells were seeded (~10^4 cells/mL) to microcontact printed patterned (1 mM hexadecanethiol in EtOH, printed on gold 5 s, backfilled with 1 mM EG_4 in EtOH, 16 h) surfaces presenting fibronectin (10 mg/mL, 2 h) for 2 h. The cells were allowed to grow for 3 days (serum-free media, 37 ºC in 5 % CO_2).[29] Oxyamine-functionalized fibroblast cells (~10^4 cells/mL) were then seeded to surfaces for 2 h followed by addition of serum-containing (10 % CBS) media to promote cell growth.

The cells were cultured for 3 more days before imaging. Controls showed no multi-layer formation when oxyamine or ketone groups were not presented on the cell surfaces or when two ketone-presenting cells interacted with each other or when two oxyamine-presenting cells interacted with each together. Only when the correct oxime pair is combined do multi-layers of cells form. After generation, substrates were fixed, stained, and imaged by confocal microscopy as described below.

4.2.11 Cell Staining for Imaging

Cells were fixed with formaldehyde (4 % in PBS) and permeated (PBS containing 0.1 % Triton X–100). A fluorescent dye mixture, containing phalloidin-TRITC (actin) and DAPI (nucleus) was then made in PBS containing 5 % normal goat serum and 0.1 % Triton X –100. Cells were incubated with the dye solution for 2 h. The substrates were then secured in fluorescence mounting medium (Dako, Carpinteria, CA, USA), which enhances the visualization of cells when viewed under a fluorescent microscope on a glass cover slip. An exposure time of 400 and 1200 ms were used to image nuclei and actin, respectively.

4.2.12 Confocal Microscopy

Cell clusters and tissue formation were visualized with a Nikon Eclipse TE2000-E inverted microscope (Nikon USA, Inc., Melville, NY). Data was analyzed by Leica software and a spectral confocal microscope (LeicaMicrosystems, Bannockburn, IL). An average of 84 image scans were used to generate the 3D reconstructions with Volocity software.

4.2.13 3D Co-Culture Spheroid and Multi-Layer Generation

Spheroids: Keto- and oxy-LUVs were generated as previously reported and were added to hMSC and Swiss 3T3 albino mouse fb (3 mM in tris buffer, 400 μL added to 4 mL, 16 h), respectively, and were cultured, resulting in fusion and display of ketones and oxyamines from the cell surface. These two cell populations were then trypsinized and mixed together in serum containing (10 % FCS, pH of 7.4) media in a 10 mL flask and incubated at 37 °C and 5 % CO_2 for 1, 2, 3, and 5 h. After mixing for the allotted time, cells were seeded onto a glass surface and visualized under a Nikon TE2000-E inverted microscope under the brightfield setting (75 ms exposure time). Controls were also performed where hMSCs displaying ketone groups were co-cultured with fbs (not displaying oxyamine groups) for each of the corresponding time points, 1, 2, 3, and 5 h, seeded onto glass, and imaged under the brightfield setting (75 ms). Image acquisition and processing was performed using Metamorph software. **Multi-layers**: Ket- and oxy-LUVs were added to hMSC and Swiss 3T3 albino mouse fb (3 mM in tris buffer, 400 μL added to 4 mL, 16 h), respectively, and were cultured, resulting in fusion and display of ketones and oxyamines from the cell surface. hMSCs displaying ketone groups were trypsinized and cultured on glass slides (10^5 cells/mL) and allowed to grow for 2 days. Fibroblasts presenting oxyamines were then trypsinized and added (10^5 cells/mL) to the hMSCs. These cells were co-cultured in media (10 % FCS) for 3, 5, and 7 d, resulting in the formation of 3D multi-layered, tissue-like structures of hMSC and fb.

4.2.14 Cell Viability Assay

Cell viability of 3D spheroid and multi-layered tissue-like structures was assessed by performing a trypan blue viability assay (Hyclone, Fisher Sci, Pittsburgh, PA). Fb spheroid and multi-layer structures were prepared as previously described. A solution of 0.4 % trypan blue in PBS was made and diluted in CBS (1:1) containing the spheroids (1, 3, and 5 h after mixing, 20^4 cells/mL) in solution and multi-layer cell sheets (3, 5, and 7 d after a second fb population was added, 10^5 cells/mL) on a glass slide. Trypan blue was allowed to react with the cells for 2 min, at which time spheroids and surfaces were imaged and false colored with blue for enhanced visualization using a Nikon TE2000-E inverted microscope. As a control, cells were cultured for 7 days to generate a multilayer and were then fixed as mentioned above. Trypan blue was allowed to react for 2 min, and cells were imaged. For phase contrast and fluorescent imaging, exposure times of 75 and 400 ms were used, respectively.

4.3 Results and Discussion

4.3.1 Overview of the Method

Vesicle fusion was directed through the use of molecular recognition and chemoselective ligation toward the goal of rewiring cell adhesion to generate 3D multi-layers of cells. Using liposomes as the simplest model of a cell, we previsouly demonstrated and extensively characterized the parameters for chemoselectively driven liposome fusion. Vesicles were tailored with ketone (dodecanone) or oxyamine (*O*-dodecyloxyamine) molecules. The resulting two populations of vesicles were used to

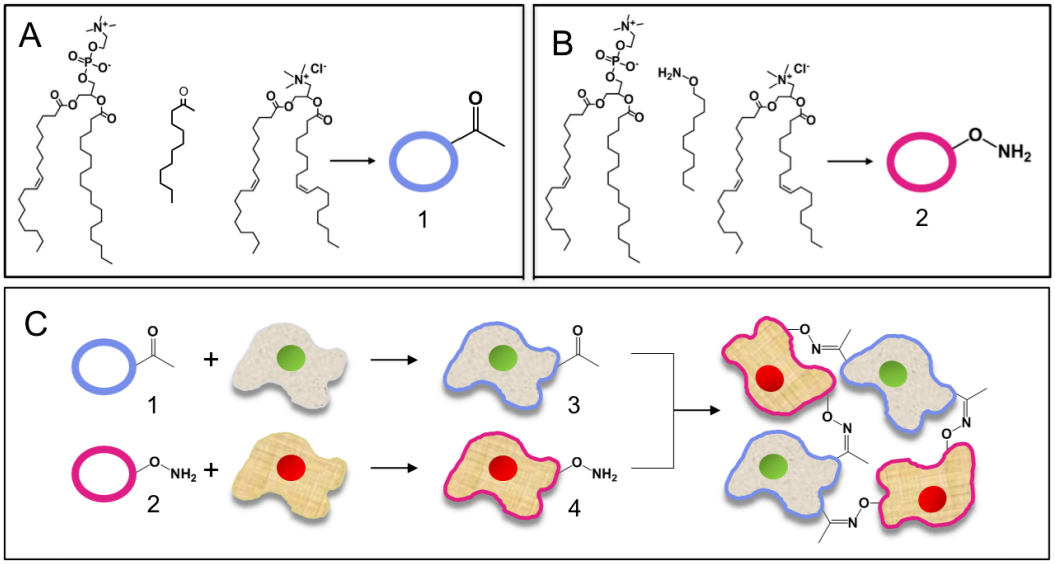

Figure 4.1 General schematic describing 3D tissue formation via liposome fusion and chemoselective cell-surface tailoring. (A) Dodecanone molecules were incorporated into neutral, egg palmitoyl-oleoyl phosphatidylcholine (POPC) and positively charged, 1,2-dioleoyl-3-trimethylammonium-propane (DOTAP) at a ratio of 5:93:2 to form ketone-presenting liposomes (**1**). (B) Dodecyloxyamine molecules were incorporated into POPC and DOTAP at a ratio of 5:93:2 to form oxyamine-presenting liposomes (**2**). (C) Two fibroblast (fb) populations were cultured separately with ketone- (**1**) or oxyamine- (**2**) containing liposomes. Due to the presence of a positively charged liposome fusion occurs, producing ketone- (**3**) and oxyamine- (**4**) tethered fbs. Upon mixing these cell populations, clustering and tissue-like formation, based on chemoselective oxime conjugation, occurred.

study liposome adhesion or fusion to one another via oxime conjugation. This system was then integrated with mammalian cells in culture to fuse liposomes to cell membranes for applications in small molecule delivery and cell-surface engineering. In this study, we used this membrane modification strategy to direct the assembly of 3D spheroid clusters and tissue-like structures by culturing two cell populations functionalized with oxyamine- and ketone-containing groups. Since this method is general, bio-orthogonal, chemically stable (oxime bond), and non-cytotoxic, patterned multi-layered tissue-like structures of different geometric shapes could also be fabricated without the use of 3D scaffolds to

confine the cell populations. We also show that this method has promising use in stem cell transplantation by co-culturing human mesenchymal stem cells (hMSCs) with fibroblasts (fbs) and inducing adipocyte differentian while in a 3D multi-layered tissue-like structure.

For membrane fusion studies, dodecanone and dodecyloxyamine were incorporated separately into netual, egg palmitoyl-oleoyl phosphatidylcholine (POPC) and cationic, 1,2-dioleoyl-3-trimethylammonium-propane (DOTAP) lipids at a ratio of 5:93:2 (Figure 1A and 1B). The alkane-tethered ketone and oxyamine molecules spontaneously insert themselves into the vesicles during syntheses.[28] Cationic lipid, DOTAP, was added to favor and enhance membrane fusion, and subsequent display of lipid components at the cell surface, rather than endocytosis of the vesicle contents.[26,27] Our general fusion strategy to generate 3D tissue-like structures is represented in figure 1C. When cells are incubated with ketone- (**1**) or oyamine- (**2**) containing liposomes, membrane fusion occurs, resulting in the presentation of ketone and oyamine groups from cell surfaces (**3** and **4**). When these cell populations are cultured together, interconnected, 3D tissue-like structures form, mediated through chemoselective oxime conjugation. These stable tissue stuctures can be generated in solution or on a solid support.

4.3.2 3D Spheroid Assembly

The ability to generate multicellular connected tissues of multiple cell types *in vitro* is crucial for studying the complex interplay of cells in a range of organs *in vivo* and for developing strategies for synthetic tissue transplantation. With varying successes, a number of current strategies to generate 3D cell connections rely on forcing mixed cell

populations into complex microfabricated wells or vessels. Therefore, we extended this liposome fusion, oxime-based strategy to generate 3D spheroid assemblies of interconnected cells using two different cell-type populations (Figure 2). The oxyamine-presenting rat2 fbs (**4**) contained a nuclear m-cherry fluorescent label so that the cell clustering to non-fluorescent ketone-tethered cells (**3**) could be easily observed. During a 3-hour period of mixed-culturing (~10^4 cells/mL) in solution, cells formed spheroid structures due to the presence of complementary recognition groups (Figure 2B and 2C). Furthermore, when oxyamine-presenting fbs (**4**) were cultured with control fbs (cells not functionlized with ketone groups), spheroid assembly did not occur (Figure 2A). Studies were also performed to test whether spheroid size and cell composition could be controlled (Supporting Information, Figure S1). Ketone-presenting hMSCs (**6**) were co-cultured with oxyamine-functionalized fbs (**5**) for 1, 2, 3, and 5 h. After 1 h, clusters comprised with only a few cells were observed. As the co-culturing duration increased, larger spheroid structures were seen. Notably, control experiments were performed simultaneously to ensure that spheroid generation was being directed through chemoselective oxime conjugation. Shown as insets in figure S1A-D, tissue structure formation did not occur without the proper complementary pair displayed from cell surfaces, regardless of the mixing duration (1-5 h). Thus, size and composition of 3D cell assemblies in solution could be controlled, showing great promise for applications in stem cell transplantation and regenerative medicine.

Spheroid formation was also characterized by scanning electron microscopy (SEM) (Figure 2E-G and *S*2). Cells functionalized with oxyamine (**5**) and ketone (**3**) groups were able to generate clusters when mixed in solution as displayed in figure 4F and 4G

(Supporting Information, Figure *S*2). However, spheroid assemblies were not observed when ketone-presenting fibroblasts were reacted with non-functionalized cells; fbs spread out on the surface, migrated, but remained alone (Figure 4E). It is important to note that cells were able to form stable, interconnected 3D structures in solution simply upon mixing two tailored cell populations. Currently, methods to generate these structures require the support of a 3D hydrogel matrix and/or assisted assembly through an external stimulus.[5,7-9,13]

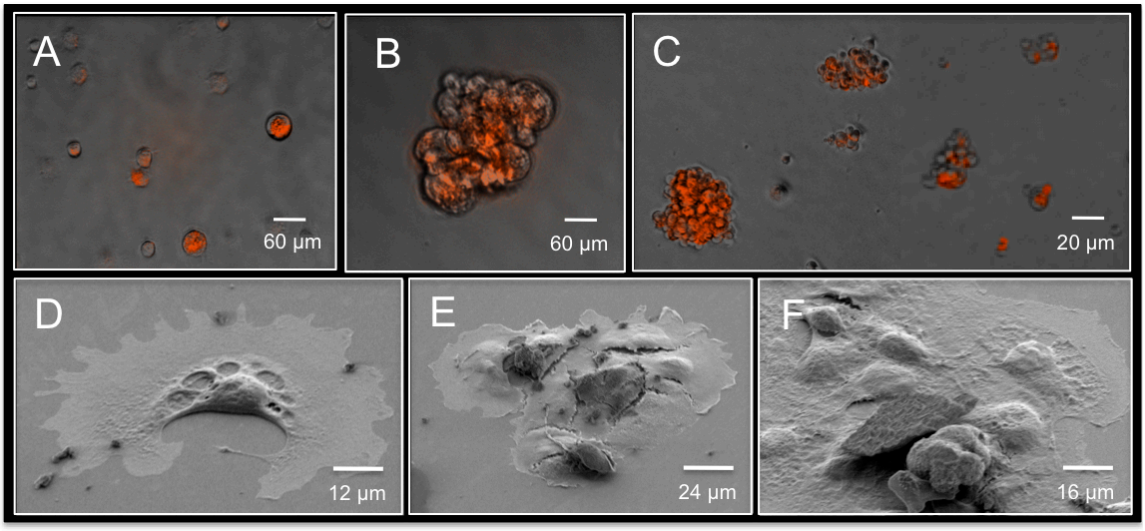

Figure 4.2 Fluorescent, phase contrast, and scanning electron micrographs (SEM) describing 3D spheroid formation via liposome fusion and chemoselective cell-surface tailoring. Two fibroblast populations were cultured separately with ketone- (**1**) or oxyamine- (**2**) containing liposomes, resulting in membrane fusion and subsequent tethering of ketones and oxyamines from the cell surface. The oxyamine-tethered rat2 fbs (**4**) contained a fluorescent m-cherry nuclear label. The ketone-presenting Swiss albino 3T3 fbs (**3**) were not fluorescently labeled. (A) Control experiments (overlay image) demonstrate no spheroid formation for cells that did not contain either ketone or oxyamine groups. (B and C) However, when two cell populations displaying ketone (**3**) and oxyamine (**4**) recognition groups are mixed, interconnected spheroid assemblies form (overlay images). (D-F) Representative SEM images of control cells and (E and F) spheroid assemblies, as described above, are displayed. For all spheroid assemblies depicted, cell populations were mixed and cultured together for 3 h before imaging at ~10^4 cells/mL.

4.3.3 3D Multi-Layered Tissues

In addition to forming small, 3D cell clusters or spheroid structures in solution, this strategy may be employed to direct larger, dense 3D tissue-like networks on a surface with geometric control (Figure 3). We used full substrates, as well as surfaces that were patterned with cell adhesive and non-adhesive regions to generate multi-layered sheets and patterned tissue structures, respectively.[43] Ketone- (**1**) and oxyamine- (**2**) tailored liposomes were cultured with separate fb populations, resulting in membrane fusion and subsequent presentation of chemoselective sites for oxime conjugation from the surface (**3** and **5**, respectively) (Figure 3A). Culturing these groups on a solid support (~10^5 cells/mL), in a layer-by-layer deposition manner, gave rise to multi-layered, tissue-like cell sheets, which were characterized by confocal microscopy as shown in figure 3E and 3F. Fbs naturally only form a single monolayer once they become contact-inhibited. However, we have successfully induced fb-fb clustering though oxime-mediated, cell-surface engineering based on liposome fusion.

To ensure that oxime chemistry was aiding in the formation of 3D tissue-like structures, several control experiments were performed. Cells that did not present ketone or oxyamine functionality were seeded onto separate surfaces. A second cell population presenting oxyamine (**5**) or ketone (**3**) groups from the cell surface was added, resulting in the formation of only a 2D monolayer of cells (Figure 3B- and 2C). Similarly, two different cell populations that were tethered with oxyamine (**5**) groups were mixed together, and only a 2D monolayer was generated after 4 d of culture. The same results were observed after culturing two different ketone-functionalized cell populations for 4 d. These results further support the hypothesis that multi-layered cell interconnectivity is

driven by complementary, oxime chemistry. We also extended this strategy toward the generation of 3D multi-layered co-cultures with hMSCs and fbs (Supporting Information, Figure S3). Ketone-functionalized hMSCs (**6**) were first cultured on a substrate (~10^5 cells/mL), and the stem cells were allowed to spread out and grow for 2 d. Oxyamine-presenting fbs (**5**) were then added (~10^5 cells/mL) and co-cultured for an additional 2 d. As shown by the confocal images in figure S3B and S3C, 3D multi-layered cell sheets (4

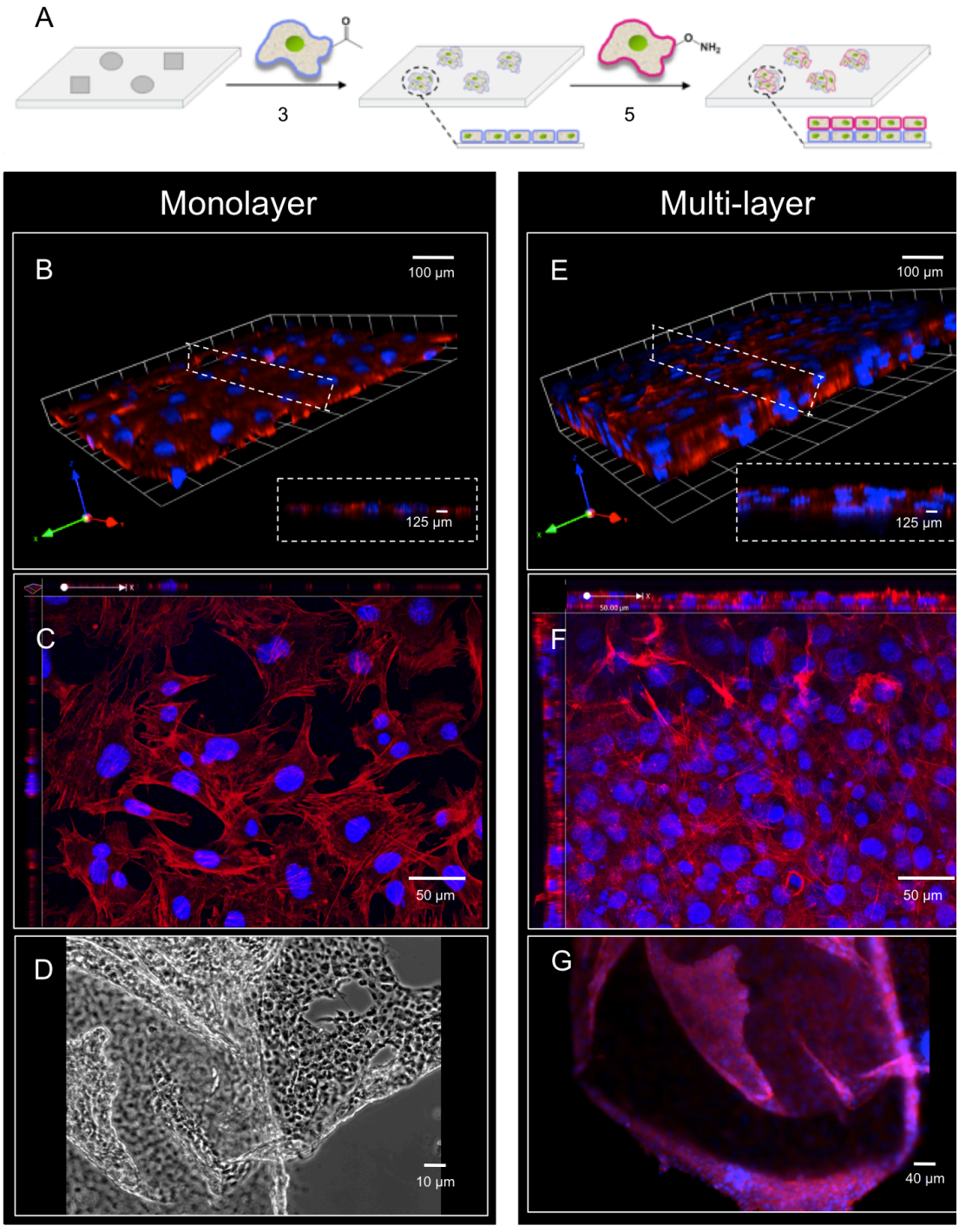

Figure 4.3 General schematic and images of oxime-mediated, 3D tissue-like structure formation with controlled interconnectivity. (A) Ketone- (**1**) and oxyamine- (**2**) containing liposomes were added to two separate fb populations, resulting in membrane fusion and subsequent presentation of the ketone (**3**) and oxyamine (**5**) groups from cell surfaces. By culturing these cells on substrates, alternating cell population seeding layer-by-layer, gave rise to multi-layered, tissue-like cell sheets through stable oxime

chemistry. (B) A 3D reconstruction and (C) confocal micrograph showing only a monolayer of cells after oxyamine-presenting cells (**5**) were cultured with adhered non-functionalized cells. (D) A 3D reconstruction and (E) confocal micrograph of multiple cell layers after oxyamine-presenting cells (**5**) were added to substrates presenting ketone-containing cells (**3**). (H and I) Intact, 3D multi-layered cell sheets can be removed from the surface by gentle agitation as displayed by brightfield and fluorescent images. The insets in B and E show a z-plane cross-section that indicates the thickness of the cell layers. Cells were stained with DAPI (blue, nucleus) and phalloidin (red, actin).

layers) were formed. The proper controls were conducted; without the oxime pair, only a 2D monolayer of stem cells and fbs was formed (Supporting Information, Figure S3A).

4.3.4 3D Tissue Release and Cell Viability

During multi-layer culture, it was possible to control the release of the tissues from the surface with gentle agitation (Figure 3D and 5G). The ability to release tissue after surface-supported growth *in vitro* shows great potential for applications in tissue engineering and cellular transplantation. Cell viability was also tested for 3D spheroid and multi-layered structures of fbs and hMSC/fibroblast co-cultures using the trypan blue assay (Supporting Information, Figure S4).[29] After spheroid (1, 2, 3, and 5 hours of mixing in solution) and multi-layer (3, 5, and 7 days on a surface) formation, cells were incubated with trypan blue (0.4 %, 2 min). No cells were observed dead in spheroid (1-5 hours) and multi-layers (3 days). However, after 5 and 7 days of multi-layer generation, cells showed an approximate viability of 91 % and 84 %, respectively. The blue intensity (fluorescence false colored for enhanced visualization) was compared to a control cell population by linescan analysis (Figure S4). The control cells were cultured for 7 days to generate a 3D multi-layer and were then fixed. Trypan blue was allowed to react for 2 min, followed by imaging and quantification. Overall, the viability of cells in conducting

membrane fusion to generate 3D tissue-like structures in solution and on a solid support is high. Therefore, this method may be very useful for applications in tissue engineering and stem cell transplantation.

4.3.5 3D Tissue Patches with Geometrical Control

We further demonstrated spatial control by generating a number of 3D multicellular micropatterns. Microcontact printing[30] was used to produce a variety of patterns and geometries on a gold substrate. Employing SAM and microfabrication technologies, hexadecanethiol (1 mM in EtOH) was printed on a gold surface for 5 s using a patterened, polydiemthylsiloxane (PDMS) stamp. The surface was then backfilled with tetra(ethylene glycol)-alkanethiol (EG_4) (1 mM in EtOH, 16 h) to render the remaining regions inert to nonspecific protein absorption. Fibronetin, a cell-adhesive protein was then added (10 mg/mL in CBS, 2 h), adhering only to the hydrophobic, patterned areas. As shown by the confocal image in figure 4A, only a 2D, circular cell pattern arises after ketone-presenting fbs (**3**) were cultured with fbs, not functionalized with oxyamine molecules. However, when liposome fusion occurs to display complementary ketone and oxyamine groups from cell surfaces (**3** and **5**, respectively), multi-layered 3D cell patterns were formed (Figure 4B-D). Bar, square, and circular tissue-like structures are depicted in figure 4B-D. The ability to generate 3D tissues with controlled geometry would find great use in tissue transplantation, in which specifically tailored patches are required.

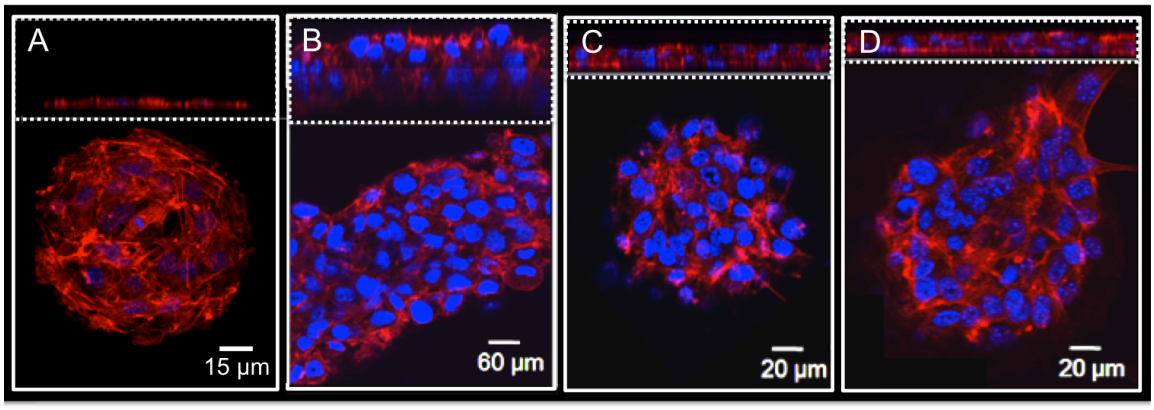

Figure 4.4 Confocal images representing 2D monolayer and 3D multi-layered tissue-like structures of fbs with spatial control. (A) A circular, 2D monolayer of fbs (control) result after ketone-functionalized fbs (**3**) and fbs (not functionalized with oxyamines) are patterned on a circular, microcontact printed region, presenting fibronectin and allowed to grow for 5 days. (B-D) Fbs, functionalized with ketone groups (**3**) were seeded onto microcontact printed regions containing fibronectin and allowed to grow for 2 days. Fbs, functionalized with oxyamine groups (**5**) were then seeded and allowed to grow for 2-3 more days. Confocal images demonstrating 3D tissue formation in (B) bar, (C) square, and (C) circle geometries are depicted. The corresponding z-plane cross-sections that indicate the thickness of the cell layers are shown as an inset. Cells were stained with DAPI (blue, nucleus) and phalloidin (red, actin).

4.3.6 3D Stem Cell Co-Cultures with Induced Adipocyte Differentiation

We have explored the general use of this liposome fusion method and have delivered ketone and oxyamine groups to a range of cell lines and have demonstrated that 3D spheroid and multi-layer can be generated using co-cultures of human mesenchymal stem cells (hMSCs) and fibroblasts (Supporting Information, Figures S1 and S3, respectively). We next extended our methodology toward stem cell differentiation to determine whether 3D multi-layered co-cultures could be induced to generate tissues of differentiated hMSCs and fbs. As shown in figure 5A, ketone-functionalized hMSCs (**6**) were first cultured on a substrate for 3 d, producing a 2D monolayer of cells (Figure 5B).

Oxyamine-tethered fbs (**5**) were then co-cultured with the hMSCs, and the cells were allowed to grow and proliferate for 2 d (Figure 5C). Adipogenic induction media was then added, the 3D multi-layered co-culture was stained for nuclei (purple) and lipid vacuoles (red), which are characteristic of adipocytes (fat cells). The phase contrast images in figure 5D and 5E demonstrate the successful generation of tissue-like structures, comprising induced adipocytes and fbs. The ability to co-culture stem cells with many other cell types and induce differentiation shows great promise in the field of regenerative medicine and stem cell transplantation.

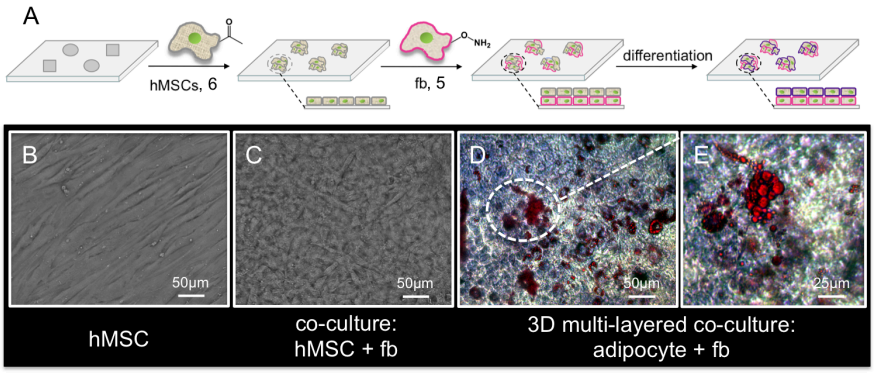

Figure 4.5 General schematic and brightfield images representing oxime-mediated, 3D tissue-like structure formation with hMSC/fb co-cultures and subsequent induced adipocyte differentiation to generate 3D adipocyte/fb co-culture structures. (A) Ketone-tethered hMSCs (**6**) were seeded onto a surface, followed by the addition of oxyamine-functionalized fbs (**5**). The co-culture was allowed to grow and divide for 3 d at which point, adipogenic differentiation was induced with the addition of the appropriate media. This resulted in a 3D multi-layer of adipocytes and fb. (B) A confluent 2D monolayer of ketone-presenting hMSCs is represented. (C) A brightfield image displaying a 3D multi-layer co-culture of hMSCs (**6**) and oxyamine-functionalized fbs (**5**) is shown. (D) Adipogenic differentiation was induced with media resulting in 3D multi-layered adipocyte and fb co-culture structures, represented by low and (E) high-resolution brightfield images (after 10 days in culture). Adipocytes were stained with Oil Red O (lipid vacuoles) and Harris Hemotoxylin (nucleus).

4.4 Conclusions

In summary, we developed a liposome delivery and fusion method to display ketone or oxyamine functional groups from cell surfaces for applications in bio-orthogonal ligand conjugation, rewiring cell adhesion, and the generation of stable, 3D spheroid assemblies and multi-layered tissue-like structures. This strategy may have diverse applications in the field of tissue engineering and regenerative medicine, from growing biocompatible tissues and organs *in vitro* to their cellular transplantation *in vivo*.[31,32] For example, assembled tissue patches with geometrically defined shape can be grown in culture and transplanted or grafted to specific locations.[33] Furthermore, this strategy may allow for time-lapse observation of cell movement *in vivo* by using a pulse (delivery of labeled cells via liposome fusion) followed by a chase (bio-orthogonal reagent to target only the labeled cells). When applied *in vivo*, this method may allow for the monitoring of many spatio-temporal developmental events and tumor metastasis. Since the liposome fusion method is general, many other types of chemistries in a single liposome can be delivered to the membrane surface simultaneously. For example, liposomes containing ketones, alkynes, dienes, azides, hydrazides, or dienophiles in varying combinations may be delivered to a cell surface for iterative or simultaneous post-functionalization via bio-orthogonal ligation reactions.

We have also been able to perform liposome fusion to the same cells several times, which may be important to tailor the membrane with multiple groups or to increase the concentration of a particular surface functional group (data not shown). By rewiring cell adhesion, a number of materials, surfaces, nanoparticles, and biomedical devices for various biotechnological applications may be decorated with cells. Since, no

biomolecules are used with this strategy, no long-term stability and degradation issues in complex cell culture media or *in vivo* will affect cell targeting or cell assembly. By combining this strategy with polymer scaffolds, 3D tissues and organs may be generated for paracrine signaling studies, tissue replacement therapies, stem cell plasticity studies, or as a model platform for various high-throughput screening studies.[34-37] Finally, integrating this strategy with traditional liposome delivery, where the interior of the liposome contains small molecules or nanoparticle cargoes, a multiplex system where the delivery of reagents to the interior of cells and simultaneous labeling of the exterior of the cells may be possible for entirely new diagnostic and biomedical applications.

4.5 Acknowledgements

The authors thank Dr. Jim Bear for his generous donation of m-cherry labeled cells, Dr. Nancy Thompson and her lab group for use of equipment and expertise in liposome chemistry, and Dr. Michael Chua for aid with confocal imaging. This work was supported by the Carolina Center for Cancer Nanotechnology Excellence, the Burroughs Wellcome Foundation (Interface Career Award), and the National Science Foundation.

4.6 References

1. Nelson, C. M.; Bissel, M. J. *Annu. Rev. Cell Dev. Biol.* **2006**, *22*, 287-309.

2. Meshel, A. S.; Wei, Q.; Adelstein, R. S.; Sheetz, M. P. *Nat. Cell Biol.* **2005**, *7*,157-164.

3. Isenberg, B. C.; Williams, C.; Tranquillo, R. T. *Annu. Biomed. Eng.,* **2006**, *34*, 971-985.

4. Hollister, S. J. *Nature Mater.* **2005**, *4*, 518-524.

5. Gillette, B. M.; Jensen, J. A.; Tang, B.; Yang, G. J.; Bazargan-Lari, A.; Zhong, M.; Sia, S. K. *Nat. Mater.* **2008**, *7*, 636-640.

6. Tanaka, H.; Murphy, C. L.; Murphy, C.; Kimura, M.; Kawai, S.; Polak, J. M. *J. Cell Biochem.* **2004**, *93*, 454-462.

7. Gartner, Z. J.; Bertozzi, C. R. *Proc. Natl. Acad. Sci. U.S.A.* **2009**, *106*, 4606-4610.

8. Albrecht, D. R.; Underhill, G. H.; Wassermann, T. B.; Sah, R. L.; Bhatia, S.N. *Nat. Methods* **2006**, *3*, 369-375.

9. Gray, D. S.; Tan, J. L.; Voldman, J.; Chen, C. S. *Biosens. Bioelectron.* **2004**, *19*, 1765-1774.

10. Odde, D. J, Renn, M. J. *Biotechnol. Bioeng.* **2000**, *67*, 312-318.

11. Nahmias, Y.; Odde, D.J. *Nat. Protocol* **2006**, *1*, 2288-229626.

12. Barron, J. A.; Krizman, D. B.; Ringeisen, B. R. *Annu. Biomed. Eng.* **2005**, *33*, 121–130.

13. Inaba, R.; Khademhosseini, A.; Suzuki, H.; Fukuda, J. *Biomaterials* **2009**, *30*, 3573-3577.

14. Ringeisen, B. R.; Othon, C. M.; Barron, J. A.; Young, D.; Spargo, B. *J. Biotechnol.* **2006**, *1*, 930-948.

15. Chiou, P. Y.; Ohta, A.T.; Wu, M. C. *Nature* **2005**, *436*, 370-372.

16. Falconnet, D.; Csucs, G.; Grandin, H. M.; Textor, M. *Biomaterials* **2006**, *27*, 3044-3063.

17. Khademhosseini, A.; Langer, R.; Borenstein, J.; Vacanti, J. P. *Proc. Natl. Acad. Sci. U.S.A.* **2006**, *103*, 2480-2487.

18. Rice, J. *MIT Technol. Rev.* **2009**, March 11.

19. Prescher, J. A.; Bertozzi, C. R. *Nat. Chem. Biol.* **2005**, *1*, 13-21.

20. Chen, I.; Howarth, M.; Lin, W.; Ting, A. Y. *Nat. Methods* **2005**, *2*, 99-104.

21. Keppler, A.; Pick, H.; Arrivoli, C.; Vogel, H.; Jonhsson, K. *Proc. Natl. Acad. Sci. U.S.A.* **2004**, *101*, 9955-9959.

22. Miller, L. W.; Sable, J.; Goelet, P.; Sheetz, M. P.; Cornish, V. W. *Angew. Chemie. Int. Ed.* **2004**, *43*, 1672-1675.

23. Kellam, B.; De Bank, P. A.; Shakesheff, K. M. *Chem. Soc. Rev.* **2003**, *32*, 327-337.

24. Rabuka, D.; Forstner, M. B.; Grovers, J. T.; Bertozzi, C. R. *J. Am. Chem. Soc.* **2008**, *130*, 5947-5953.

25. Sarkar, D.; Vemula, P. K.; Zhao, W.; Gupta, A.; Karnik, R.; Karp, J. M. *Biomaterials*, **2010**, *31*, 5266-5274.

26. Wilson, J. T.; Krishnamurthy, V. R.; Cui, W.; Qu, Z.; Chaikof, E. L. *J. Am. Chem. Soc.* **2009**, *131*, 18228-18229.

27. Csiszar, A.; Hersch, N.; Dieluweit, S.; Biehl, R.; Merkel, R.; Hoffmann, B. *Bioconjugate Chem.* **2010**, *21*, 537-543.

28. Dutta, D.; Pulsipher, A.; Yousaf, M. N. *Langmuir* **2010**, *26*, 9835-9841.

29. Hsiao, S. C.; Shum, B. J.; Onoe, H.; Douglas, E. S.; Gartner, Z.; Mathies, R. A.; Bertozzi C. R.; Francis, M. B. *Langmuir* **2009**, *25*, 6985-6991.

30. Love, J. C.; Estroff, L. A.; Kriebel, J. K.; Nuzzo, R. G.; Whitesides, G. M. *Chem. Rev.* **2005**, *105*, 1103-1170.

31. Mueller-Klieser, W. *Am. J. Physiol.* **1997**, *273*, C1109-C1123.

32. Khademhosseini, A.; Vacanti, J.; Langer, R. *Sci. Am.* **2009**, *300*, 64-71.

33. Badylak, S. F.; Nareem, R. M. *Proc. Natl. Acad. Sci. U.S.A.* **2010**, *107*, 3285-3286.

34. Khetani, S. R.; Bhatia, S. N. *Nat. Biotechnol.* **2008**, *26*, 120-126.

35. Zeisberg; Yang, C.; Martino, M.; Duncun, M. B.; Rieder, F. Tanjore, H.; Kalluri, R. *J. Biol. Chem.* **2007**, *282*, 23337-23347.

36. Bhatia, S. N.; Balis, U.; Yarmush, M. L.; Toner, M. *Biotechnol. Prog.* **1998**, *14*, 378-387.

37. Kunz-Schughart, L. A.; Freyer, J. P.; Hofstaedter, F.; Ebner, R. *J. Biomol. Screen* **2004**, *9*, 273-285.

38. Pale-Grosdemange, C.; Simons, E. E.; Prime, K. L.; Whitesides, G. M. *J. Am. Chem. Soc.* **1991**, *113*, 12-20.

CHAPTER 5

Dynamic Control on Cell-Tissue Interactions.

5.1 Introduction

Controlling cell-cell interactions and cellular architecture in three-dimensional (3D) space and time is critical for the proper development (*1*) and survival of higher-order organisms (*2*). These dynamic interactions are complex but essential for correct cell behavior and tissue function based on a myriad of physical, mechanical, and hydroynamic forces, as well as autocrine and paracrine signaling (*3,4*). However, to recapitulate these processes *in vitro* while maintaining these dynamic and discrete cell-cell contacts is difficult and requires a multidisciplinary coordinated effort, intersecting several research fields (*5*). Thus, the ability to modulate cell-cell interactions in space and time would in turn allow for unprecedented control of cell behavior and enable the design and utility of new dynamic tissue engineering scaffolds, *in vivo* imaging capabilities, high-throughput tissue-based screening assays, and drug delivery therapies (*6,7*).

Several recent approaches to generate co-culture tissue structures in 2D and 3D have been developed and employed, including dielectrophoresis (8), microfabrication (*9,10*), hydrogel (*11,12*), and cell patterning techniques (*13,14*). Tailoring cell membranes by cell-surface engineering methods have also proven to be important for the development of co-culture and multicellular micro-tissues (*15*). In particular, the integration of bio-orthogonal chemical strategies (*16*) with cell surfaces may allow for a

range of cell-surface modifications for control of lignd presentation, ligand density, and potentially spatio-temporal control of cell-cell interactions. Bio-orthogonal chemical reactions have been extensively developed and utilized due to their ability to be performed at physiological conditions (Diels-Alder, Oxime, Huisgen cycloaddition, Staudinger, etc…), without side reactions, and in complex protein mixtures, cell lysates, and *in vivo*. Furthermore, these chemistries have been applied in many fundamental cell studies (*17*), drug delivery therapies (*18*), and diagnostic measuring applications (*19*). However, the delivery and incorporation of a range of these chemical groups to a cells surface for a variety of cell types remains challenging and not straightforward (*20*).

The development of synthetic liposomes and liposome fusion methods have proven very useful for numerous studies as cell membrane model systems and as microarray platforms to study cell membrane dynamics and for biotechnology applications (*21,22*). Additionally, liposome-to-liposome and liposome-to-cell fusion methods have also been developed to deliver therapeutic agents to cells and organelles, and to study cellular interactions (*23*). However, until now, there has been no report utilizing liposome-to-cell fusion to deliver dynamic and bio-orthogonal groups directly to cell surfaces for subsequent chemoselective conjugation and release of ligands or for the temporal programming of controlled cell-cell assembly. A strategy that combines cell-surface modification, without the use of molecular biology techniques or biomolecules, with a stable, dynamic, and switchable bio-orthogonal ligand conjugation and release approach to direct tissue formation and subsequent disassembly, would greatly benefit fundamental cell behavioral studies and tissue engineering research.

Herein, we report a novel liposome fusion based methodology to tailor cell surfaces with dynamic and switchable bio-orthogonal chemistries and to direct the assembly and disassembly of 3D tissues for applications in stem cell differentiation and tissue engineering. We show that this strategy is redox responsive and allows for multiple rounds of the controlled conjugation and release of molecules to and from cell surfaces *in situ.* This chemical methodology can simultaneously be used as an analytical probe for monitoring cellular interactions, as well as a trigger to alter cell-surface ligands and cell-cell contacts.

5.2 Materials and Methods

5.2.1 Materials

All chemical reagents were of analytical grade and used without further purification. Lipids egg palmitoyl-oleoyl phosphatidylcholine (POPC), egg 1-palmitoyl-2-oleoyl-phosphatidylglycerol (POPG), 1,2-dioleoyl-3-trimethylammonium-propane (DOTAP), egg 1,2-diphytanoyl-*sn*-glycero-3-phosphoethanolamine-N-(7-nitro-2-1,3-benzoxadiazol-4-yl) (ammonium salt) (NBD-PE), and egg 1,2-dipalmitoyl-*sn*-glycero-3-phosphoethanolamine-N-(lissamine rhodamine B sulfonyl) (ammonium salt) (Rhod-PE) were purchased from Avanti Polar Lipids (Alabaster, AL). Antibodies and fluorescent dyes were obtained from Invitrogen (Carlsbad, CA). FITC labeled beads were purchased from Spherotech, Inc. (Forest Lake, IL), trypan blue viability dye was obtained from Hyclone (Fisher Sci, Pittsburgh, PA), and all other chemicals were obtained from Sigma-Aldrich or Fisher. Swiss 3T3 albino mouse fibroblasts (Fb) were obtained from the Tissue Culture Facility at the University of North Carolina (UNC). Rat2 Fb transfected

with m-cherry were obtained from the Bear Lab (UNC Chapel Hill, NC). Human Mesenchymal stem cells (hMSCs) were purchased from Lonza (Basel, Switzerland).

5.2.2 2-dodecylbenzene-1,4-diol (Hydroquinone Alkane, HQ, A) Synthesis.

*1,4-bis(tetrahydro-2H-pyran-2-yloxy)benzene **(B)***: To a solution of hydroquinone (6.0 g, 54.5 mmol) in THF (40 mL) was added 2,3-dihydropuran (44.0 mL, 245.3 mmol, 4.5 eq) and 3 drops of concentrated HCl. The mixture was stirred at room temperature for 8h, diluted with EtOAc (40 mL), washed with $NaHCO_3$ (3 x 50 mL) and brine (1 x 25 mL), dried over $MgSO_4$, and concentrated to a white solid. The solid was then dissolved in EtOAc and recyrstallized with hexanes to afford a white solid **B** (10. 02 g, 66 %), ^{1}H NMR (400 Hz, $CDCl_3$, δ): 1.67-1.58 (m, 6H, J = 36; -CH_2-), 1.88-1.85 (m, 4H, J = 12; -CH_2-), 2.03-2.00 (m, 2H, J = 12; -CH_2-), 3.62-3.60 (m, 2H, J = 8; -CH_2-), 3.98-3.96 (m, 2H, J = 8; -CH_2-), 5.34-5.32 (t, 2H, J = 7; -CH-), 7.00 (s, 4H; Ar-H).

*2,2'-(2-dodecyl-1,4-phenylene)bis(oxy)bis(tetrahydro-2H-pyran) **(C)***: To a solution of **B** (2.00 g, 7.0 mmol) in dry THF (40 mL) at 0°C was added tert-butyllithium (4.6 mL of a 1.7 M solution, 9.1 mmol, 1.3 eq) dropwise over 15 min. The mixture was stirred at 0°C for 60 min and then slowly warmed to room temperature over 3h. At this time, 1-bromododecane (5.08 mL, 21.0 mmol, 3 eq) was added and stirred for 12h. The mixture was diluted with DCM (40 mL) and washed with NH_4Cl (3 x 50 mL) and brine (1 x 25 mL), dried over $MgSO_4$, and concentrated to afford a yellow oil. The mixture was purified by flash chromatography 95:5 Hex:EtOAc to elute a yellow oil **C** (2.23 g, 71 %),

^{1}H NMR (400 Hz, $CDCl_3$, δ): 0.91-0.89 (t, 3H, J = 8; -CH_3), 1.27-1.23 (m, 18H, J = 16; -CH_2-), 1.72-1.68 (m, 10H, J = 16; -CH_2-), 2.61-2.58 (t, 2H, J = 12; -CH_2-), 3.65-3.63 (m, 4H, J = 8; -CH_2-), 5.80-5.78 (t, 2H, J = 8; -CH-), 6.68 (s, 1H; Ar-H), 6.81 (s, 1H; Ar-H), 6.84 (s, 1H; Ar-H).

2-dodecylbenzene-1,4-diol **(A)**: To a solution of **C** (2.0 g, 4.5 mmol) in 40 mL of a 3:1:1 mixture of AcOH/THF/H_2O was stirred for 16h. The mixture was then concentrated, diluted in EtOAc (20 mL) and washed with 1 mM NaOH (2 x 10 mL), dried over $MgSO_4$, and concentrated to afford a white solid **A** (1.12 g, 90 %), ^{1}H NMR (400 Hz, $CDCl_3$, δ): 0.89-0.87 (t, 3H, J = 8; -CH_3), 1.30-1.25 (m, 18H, J = 20; -CH_2-), 1.57-1.55 (m, 2H, J = 7; -CH_2-), 2.58-2.55 (t, 2H, J = 12; -CH_2-), 6.57-6.56 (m, 1H, J = 4; Ar-H), 6.67-6.65 (m, 2H, J = 7; Ar-H); (ESI) (*m/z*) $[M + Na]^+$ = 301.15.

5.2.3 O-dodecyloxyamine (Aminooxy Alkane, AO, D) Synthesis.

2-(dodecyloxy)isoindoline-1,3-dione ***(E).*** To a solution of N-hydroxyphthalimide (1.96 g, 12.04 mmol, 1.5 eq) and sodium bicarbonate (10.11 g, 12.04 mmol, 1.5) in DMF (20 mL) at 80°C was added 1-bromododecane (1.93 mL, 8.02 mmol). The mixture was refluxed and stirred for 12 h. The reaction was diluted with DCM and washed with H_2O (6 x 50 mL), 1 M $NaHCO_3$ (3 x 50 mL), and H_2O (2 x 50 mL), dried over $MgSO_4$, and concentrated to afford a white solid (2.66 g, 87 %). ^{1}H NMR (400 MHz, $CDCl_3$, δ): 1.02 (s, 3H; CH_3), 1.31-1.29 (m, 14H, J = 8; CH_2), 1.47-1.45 (m, 4H, J = 8; CH_2), 1.60-1.57 (m, 2H, J = 12; CH_2), 3.72-3.70 (t, 2H, J = 8; CH_2), 7.80-7.78, 7.85-7.83 (2 x m, 4H, J = 8; Ar-H).

O-dodecyloxyamine ***(D).*** To a solution of **E** (2.65 g, 8.00 mmol) in dry DCM (30 mL) under inert atmosphere (Ar) was slowly added hydrazine (1.53 mL, 48.00 mmol, 6 eq).

Upon addition, a white precipitate immediately formed. The mixture was stirred for 12 h. The reaction was diluted with DCM and washed with H_2O (6 x 50 mL), dried over $MgSO_4$, and concentrated to afford a pale yellow oil (1.18 g, 74 %). ^{1}H NMR (400 MHz, $CDCl_3$, δ): 1.03 (s, 3H; CH_3), 1.33-1.31 (m, 14H, J = 8; CH_2), 1.43-1.41 (m, 4H, J = 8; CH_2), 1.50-1.46 (m, 2H, J = 16; CH_2), 3.64-3.62 (t, 2H, J = 7; CH_2). (ESI) (*m/z*) [M + H^+]: 201.22.

5.2.4 Lipid Vesicle Formation for Fusion Studies

HQ-tethered alkane (160 μL, 10 mM in $CHCl_3$ at 10 mol %, (**A**)) and POPC (410 μL, 10 mg/mL in $CHCl_3$ at 90 mol %) were mixed and then concentrated for 4 hours under high vacuum. Likewise, OA-tethered alkane (60 μL, 10 mM in $CHCl_3$ at 5 mol %, (**D**)), POPG (92 μL, 10 mg/mL in $CHCl_3$ at 20 mol %), and POPC (410 μL, 10 mg/mL in $CHCl_3$ at 75 mol %) were mixed and then concentrated for 4 hours at high vacuum. The dried lipid samples were then reconstituted in 3 mL in PBS buffer, pH 7.4. The contents of the vial were warmed to 50˚C and then sonicated for 15 min with a tip sonicator until the solution became clear, forming small and large and small unilamelar vesicles (LUVs and SUVs, respectively). Vesicle-containing solutions were then centrifuged at 30,000 rpm for 30 min, pelleting out the LUVs and leaving the SUVs in solution. The HQ- or OA-SUVs ((**1**) and (**3**), respectively) were then used in further vesicle (liposome) fusion studies.

5.2.5 Chemical Oxidative Activation of HQ-SUVs

HQ-SUVs were prepared as previously described. To a solution of HQ-SUVs (3 mM in PBS, 4 mL) was added $CuSO_4 \cdot 5H_2O$ (20 μL, 5 μM in PBS) for 5 min, producing quinone-tethered vesicles (Q-SUVs, (**2**)).

5.2.6 Transmission Electron Microscopy

HQ- (**1**) and Q- (**2**) SUVs were prepared and activated, respectively, as previously mentioned OA- (**3**) SUVs were also made as described above. Q- (**2**) and OA-(**3**) SUVs (0.2 mM in PBS) were mixed in a 1:1 ratio at room temperature for 30 min. A 4-μL vesicle suspension mixture was then applied to standard lacey carbon EM grid as prepared according to published methods. The specimens were blotted from behind and then submerged into aurenyl acetate solution for staining. The hydrated specimens were then placed into a TF30He Polara G2 (FEI company) electron cryo microscope operating at 300 keV. Images were recorded using a Tietz single port model 415 4k × 4k CCD camera with a 15 micron pixel size on the chip. Pixel sizes at the specimen level were used to calculate accurate dimensions for the specimen.

5.2.7 Fourier Resonance Energy Transfer (FRET) Characterization

HQ- (**16**) and OA- (**17**) SUVs were prepared as described above with the addition of NBD-PE (20 μL, 10 mg/mL in $CHCl_3$ at 2 mol %) and Rhod-PE (28 μL, 10 mg/mL in $CHCl_3$ at 2 mol %), respectively. HQ-SUVs were then activated to Q-SUVs as reported. NBD fluorescence was measured at 471 nm (excitation) and 531 nm (emission) maintaining narrow excitation slits to reduce light scattering interference. Q- and OA-SUVs containing NBD-PE and Rhod-PE, respectively, were then mixed (1:1) to obtain FRET measurements. The NBD dye was excited at 471 nm, and the emission was scanned through 600 nm. An emission signal for Rhod-PE was observed at 578 nm. All fluorescence measurements were performed in a SPEX Fluorolog-3 Research T-format Spectrofluorometer. Fluorescence was followed immediately after mixing OA-SUV (**17**)

with Q-SUV (**16**) for approximately 2 hours at 2 min intervals. A constant flow of water was passed through the cuvette holder for temperature control. The temperature was maintained at 25°C.

5.2.8 Dynamic Light Scattering (DLS) Characterization

Q- (**2**) and OA- (**3**) SUVs were prepared as described and mixed at a 1:1 ratio and were monitored over 80 min. DLS experiments were performed using a Nikomp model 200 laser particle sizer with a 5mW HeNe laser at an excitation wavelength of 632.8 nm. Standard deviation determinations were made using Gaussian analysis. A Wyatt DynoPro dynamic scattering plate reader was used to collect the data.

5.2.9 Liposome Fusion to Cells (Cell-Surface Engineering)

HQ-tethered alkane (160 μL, 10 mM in $CHCl_3$ at 10 mol %, (**A**)), DOTAP (10 μL, 10 mg/mL in $CHCl_3$ at 2 mol %), and POPC (398 μL, 10 mg/mL in $CHCl_3$ at 88 mol %) were mixed and then concentrated for 4 hours under high vacuum. Similarly, OA-tethered alkane (60 μL, 10 mM solution in $CHCl_3$ at 5 mol %, (**D**)), DOTAP (10 μL, 10 mg/mL in $CHCl_3$ at 2 mol %), and POPC (424 μL, 10 mg/mL in $CHCl_3$ at 93 mol %) were mixed and then concentrated for 4 hours under high vacuum. The above-mentioned procedure for forming HQ- (**4**) and Q- (**12**) SUVs was then performed. A 400-μL aliquot of HQ- (**4**) and OA- (**12**) SUVs were then added separate populations of Fbs, m-cherry labeled Fbs, and hMSCs (3 mM in PBS, 400 μL added to 4 mL cells in culture) and were cultured for 16 hours, resulting in vesicle fusion to the cell membrane and subsequent presentation of HQ (**A**) and OA (**D**) groups from the cell surface ((**5**), (**13**), (**14**), and (**15**)).

5.2.10 Chemical Oxidative Activation of HQ-Presenting Cells

HQ-SUVs (**4**) were prepared and fused to cells as previously described. $CuSO_4 \cdot 5H_2O$ (20 μL, 5 μM in PBS) was then added to cells in culture (4 mL of CBS-containing media) for 5 min, producing Q-presenting cells ((**6**) and (**11**)).

5.2.11 Flow Cytometry Characterization and Quantification of HQ (A) and OA (D) on the Cell Surface

Fluorescence activated cell sorting (FACS) analysis was performed in order to quantify the approximate number of HQ (**A**) and OA (**D**) groups on the cell surface after membrane fusion. HQ-SUVs were generated as previously mentioned and cultured with Fbs (3 mM in PBS, 400 μL added to 4 mL cells in culture) for 1, 3, 5, and 7 days, resulting in the fusion and display of HQ (**A**) from the cell surface (**5**). HQ (**A**) was activated to Q, as mentioned, before testing. Q-presenting Fbs (**6**) were then reacted with hydrazide-conjugated biotin (3 mM in CBS, 1 mL added to 4 mL CBS in cell culture, 1 h, (**9** and **10**)). Fluorescein- conjugated streptavidin (1 mM in CBS, 0.5 mL added to 4 mL CBS in cell culture, 1 h) was then added. A control cell population (not functionalized with HQ groups) was only incubated with biotin-hydrazide and streptavidin-FITC for 1 h, respectively, under the same conditions as described above. Cells were then centrifuged (5 min, 1000 rpm), re-suspended in RMPI (without phenol red), centrifuged (5 min, 1000 rpm), and re-suspended in RPMI (10^7 cells in 2 mL). Fluorescence measurements were calibrated using RCP-5-30 beads (10^7 beads/mL, Spherotech, Inc., Lake Forest, IL) of known fluorescein equivalent molecule density (*4*). Fluorescent intensities based on number of cells counted (at least 10^5/sample) were compared to the standard bead and control cells lacking fluorescent molecule conjugation and approximate numbers of fluorescent compound bound to the surface was calculated. Flow cytometry was carried

out using a Dako CyAn ADP (Beckman-Coulter, Brea, CA), and data was analyzed with Summit 4.3 software.

5.2.12 Electrochemical Oxidative Activation, Conjugation, and Release of HQ-Presenting Cells (5 and 13)

HQ-SUVs (**4**) were prepared and fused to cells (**5**) as previously described. These cells were then treated with trypsin (1 mL, 2 min, 37 °C) and seeded onto a gold surface (10^5 cells, 2 x 2 cm^2) for 2 h in serum-free-containing media, and then 16 h in CBS-containing media. Linear sweep voltammetry (LSV) was then performed to oxidize HQ to Q using an Ag/AgCl reference, Pt wire auxiliary, and the gold surface containing the HQ-presenting cells (**5**) as the working electrode (-100 to 650 mV). PBS was used as the electrolyte solution (10 mM, pH 7.4), and the scan rate was 100 mVs^{-1}. OA-tethered ligands were then reacted with Q-presenting cells (**6**) to form an interfacial oxime linkage on the cell surface. This reaction can be monitored using cyclic voltammetry (CV) with a sweeping potential of -100 to 650 mV at 100 mVs^{-1}. To release ligands or cells, the working electrode was subject to a reducing potential (-100 mV, 10 s, PBS, pH = 7.4), resulting in a cleavage of oxime bond. Measurements were performed in a standard electrochemical cell. All electrochemical measurements were performed using a Bioanalytical Systems potentiostat.

5.2.13 Fluorescent Characterization of Liposome Fusion to Cells (Cell-Surface Engineering).

A solution of HQ-SUV (**4**) (1 mg/mL) was added Fbs in culture to give the desired final HQ concentration of 100 μg/mL in a total volume of 2 mL and were incubated 4 h. The cells (**5**) were then washed with PBS, followed by activation of HQ to Q as mentioned.

Rhod-OA (100 µL added to 4 mL cell culture, 7 mM in H_2O) was added to Q-displaying cells (**6**) in culture and was incubated at 37 °C for 30 min, resulting in oxime bond formation and Rhod-presenting Fbs (**7** and **8**). The cells were then washed with PBS buffer and removed with a solution of 0.05 % trypsin 0.53 mM EDTA and re-suspended in serum-free medium (10^5 cells/mL). The cells were then seeded to a fibronectin-coated surface for 2 h and visualized by fluorescence microscopy under the Texas Red channel with an exposure time of 1200 ms. Similarly, a solution containing biotin-hyrdazide (1 mg/mL in PBS, 0.5 mL added to 2 mL CBS) was added to Q-presenting Fbs (**6**) for 2 h, followed by addition of FITC-streptavidin for 1 h to produce biotin/streptavidin-presenting Fbs (**9** and **10**). After 1 h, serum-containing media was added for cell growth and imaged after 3 days under the FITC channel with an exposure time of 600 ms.

5.2.14 Electrochemical Characterization of Ligand Conjugation and Release to Cell Surfaces (cell-surface engineering).

Rhod-OA was conjugated to Q-presenting Fbs (**6**) as described above. CV was performed to determine the presence of the oxime bond (**7** and **8**), scanning from -100 to 650 mV, with a scan rate of 100 mVs^{-1}, in PBS (pH = 7.4). To release Rhod-OA, a constant reducing potential (-100 mV, 10 s) was applied, and CV was then used to determine the regeneration of HQ and Q redox peaks (-100 to 650 mV). The cells were then activated to Q by conducting LSV, and biotin-hydrazide was conjugated as reported above (**9** and **10**). CV was again performed after conjugation to determine the presence of the hydrazide bond (-100 to 650 mV, 100 mVs^{-1}).

5.2.15 Fibroblast (Fb) Culture

Swiss 3T3 albino mouse Fbs and m-cherry labeled, Rat2 Fbs were cultured in Dulbecco's Modified Eagle Medium (Gibco) containing 10 % calf bovine serum (CBS) and 1 % penicillin/streptomycin at 37°C in 5 % CO_2. When ready for experimentation, cells are removed from the tissue culture plastic using a solution of 0.05 % trypsin 0.53 mM EDTA and re-suspended in serum-free medium (10^5 cells/mL).

5.2.16 Cell Patterning Characterization of Liposome Fusion to Cell Surfaces

Mixed self-assembled monolayers (SAMs) presenting OA and EG_4 alkanethiolates were patterned using microfluidic lithography (*5*). The percentage of OA groups was minimal (1/9 OA:EG_4, 1 mM n EtOH total) to ensure resistance to nonspecific protein and cell adhesion. Fbs were first cultured with HQ-SUVs (**4**) and then activated to Q (**6**) as previously described. Cells were then treated with trypsin (1 mL) and seeded on the OA-patterned surface (10^5 cells/mL) in serum-free medium for 2 h and then CBS-containing medium for 3 days. During this time, cells adhered, spread, and proliferated, filling out the patterned regions of the surface due to the interfacial oxime reaction and were then stained and imaged. As a control, Fbs were cultured with SUVs, not displaying HQ, and were then seeded to OA-patterned substrates (1:9 OA/EG_4); the cells did not attach. Fbs were then released from the surface by application of a reductive potential (-100 mV, 10 s, PBS, pH = 7.4), which cleaves the interfacial oxime linkage. Substrates were then stained and imaged by fluorescence microscopy.

5.2.17 Mass Spectrometry (MS) Characterization

Preparation of gold-coated MALDI sample plates. Gold-coated MALDI sample plates (123 x 81 mm) (Applied Biosystems, Foster City, CA) were prepared by electron-beam

deposition (Thermionics Laboratory Inc, Hayward, CA) of titanium (5 nm) and then gold (12 nm). In order to form self-assembled monolayers (SAM) of alkanethiolates on the plates, the slides were immersed in a 1-mM solution of aminooxyundecanethiol in EtOH for approximately 1 min, rinsed with EtOH and dried, and then backfilled with a 1-mM solution of mercaptoundecanol in EtOH for 1 h. Once removed from solution, the surfaces were rinsed with EtOH and dried before use. **Liposome preparation.** HQ-containing liposomes (**4**) were generated as previously described, activated to Q (**5**) (10 μL, 5 μM $CuSO_4 \cdot 5H_2O$ in PBS added to 2 mL), and were then delivered to and allowed to react with the AO-terminated MALDI sample plate (90 min). The plates were then washed with water (3 x 3 mL) and EtOH (2 x 3 mL) and dried before use. **Cell preparation.** Swiss 3T3 albino mouse Fbs were incubated with HQ-LUVs (3 mM in tris buffer, 1 mL added to 4 mL culture media, 37 °C in 5 % CO_2, 16 h, **4**). HQ-presenting Fbs (**5**) were then treated with trypsin (1 mL) and seeded (10^7 cells/mL) to the MALDI sample plates in serum-free medium (droplet on the surface). HQ was then oxidized (2 μL, 5 μM $CuSO_4 \cdot 5H_2O$ in PBS) to Q (**5**) and cells were allowed to react with the surface for 3 h. Plates were then rinsed thoroughly with 0.1 % SDS in PBS (2 x 3 mL) and EtOH (2 x 3 mL) and dried before testing to remove the cells and proteins. **MALDI Analysis.** MS analysis was carried out using an AB SCIEX TOF/TOF^{TM} 5800 System (Applied Biosystems, Foster City, CA).

5.2.18 human Mesenchymal Stem Cell (hMSC) Culture

hMSCs and basic, growth, and differentiation media were obtained from Lonza (Basel, Switzerland). hMSCs were cultured in Dulbecco's Modified Eagle Medium (Gibco) containing 10 % fetal bovine serum (FBS) and 1 % penicillin/streptomycin at 37°C in 5

% CO_2. Adipogenic differentiation was induced by culturing with induction medium as described in the Lonza protocol.

5.2.19 3D Spheroid Co-Culture Generation

HQ-SUVs (**4**) and OA-SUV (**12**) were added to two separate Fb or hMSC populations in culture for 16 h, resulting in fusion and display of HQ and OA groups from the cell surface (**5**, **13**, **14**, and **15**). The HQ-displaying cells (**5** and **13**) were activated by chemical oxidation as previously described before co-culturing. **Fluorescence imaging.** OA-presenting Rat2 Fbs (**14**) contained an m-cherry label (nucleus) for enhanced visualization, while the Q-presenting Swiss 3T3 albino mouse Fbs (**6**) contained no fluorescent label. These two cell populations were treated with trypsin and mixed together (100 μL, 1:1) in serum-containing (10 % CBS) media in a 10 mL-flask and incubated at 37 °C and 5 % CO_2 for 1, 2, 3, and 5 h. After mixing, the cells were seeded on a glass surface and visualized under a Nikon TE2000-E inverted microscope in the Texas Red channel with an exposure time of 1200 ms. Image acquisition and processing was performed using Metamorph software.

5.2.20 Co-Culture Spheroids for Phase Contrast and SEM Imaging

Similarly, activated Q-presenting hMSCs (**11**) were co-cultured with OA-displaying Fbs (**15**) in solution. These two cell populations were treated with trypsin and mixed together (100 μL, 1:1) in serum-containing (10 % FBS) media in a 10 mL-flask and incubated at 37 °C and 5 % CO_2 for 1, 2, 3, and 5 h. After mixing, the cells were seeded on a glass surface and visualized under a Nikon TE2000-E inverted microscope (Brightfield channel, 75 ms) or by scanning electron microscopy (described below). Control experiments were also performed in which Q-hMSCs (**11**) were mixed and co-cultured

with Fbs (not functionalized with OA groups) under the same conditions as described above, and images were taken. Image acquisition and processing was performed using Metamorph software.

5.2.21 Scanning Electron Microscopy (SEM) of 3D Spheroids

After spheroids co-cultures of Fbs (**15**) and hMSCs (**11**) were generated in solution as described above, cells were delivered to a glass slide (0.8 x 0.8 cm^2) and then fixed with 10 % formalin in PBS for 15 min. The substrate was then washed with water (15 min), and cells were then dehydrated stepwise in 30, 50, 70, 90, and 100 % ethanolic solutions for 15 min each. After critical point drying and sputtering 2 nm of gold, the sample was ready for imaging using a Hitachi S-4700 field emission scanning electron microscope (Hitachi High Technologies America, Inc., Schaumburg, Illinois).

5.2.22 3D Multi-Layered Co-Culture Cell Tissue Generation

HQ-SUVs (**4**) were cultured with hMSCs (3 mM in PBS, 400 μL added to 4 mL cells in culture, 16 h), resulting in membrane fusion and display of HQ from the cell surface (**13**). HQ-hMSCs (**13**) were then treated with trypsin (1 mL), seeded on a gold surface as mentioned above (10^5 cells/mL), and were allowed to grow and proliferate for 3 days. The HQ groups were then activated to Q by performing LSV (-100 to 650 mV) and were incubated for 4 hours before adding OA-functionalized Fbs (10^5 cells/mL) (**15**) that had been treated with trypsin (1 mL). The Fbs (**15**) were seeded to Q-presenting hMSCs (**11**) for 2 h in serum-free medium, followed by the addition of serum-containing media (4 mL) to promote cell growth. The cells were cultured for 3, 5, and 7 days before staining and confocal imaging. Controls showed no multi-layer formation when OA or Q groups were not presented on the cell surfaces or when two Q- or OA-displaying cells interacted

with one another. Only when the correct oxime pair is combined do multi-layered co-cultures. After generation, substrates were fixed, stained, and imaged by confocal microscopy as described below.

5.2.23 3D Spheroid and Multi-Layered Co-Culture Generation and Release. Spheroids. HQ- (**4**) and OA- (**12**) SUVs were generated as previously reported, added to hMSCs and Fbs (3 mM in PBS, 400 μL added to 4 mL cells in culture), respectively, and cultured for 16 h. After activation, these two cell populations (**11** and **15**) were then treated with trypsin (1 mL) and mixed together (100 μL, 1:1) in serum containing (10 % FCS) media in a 10 mL flask and incubated at 37 °C and 5 % CO_2 for 1, 2, 3, and 5 h. After mixing for the allotted time, cells were seeded onto a gold surface and visualized under a Nikon TE2000-E inverted microscope under the brightfield setting (75 ms). Image acquisition and processing was performed using Metamorph software. **Multi-layers**: HQ- (**4**) and OA- (**12**) SUVs were added to hMSC and Fb (3 mM in PBS, 400 μL added to 4 mL cells in culture), respectively, and were cultured for 16 h. hMSCs displaying HQ (**13**) groups were treated with trypsin (1 mL) and cultured on gold slides (10^5 cells/mL) and allowed to grow for 2 days and then activated by conducting LSV (-100 to 650 mV). OA-presenting Fbs (**15**) were then treated with trypsin (1 mL) and added (10^5 cells/mL) to Q-hMSCs (**11**). These cells were co-cultured for 3, 5, and 7 d, resulting in the formation of 3D multi-layered co-cultured structures of hMSC and Fb. To selectively release cells in either spheroid or multi-layered tissue structures, a reduction potential of -100 mV was applied for 1 min in serum-free medium and cells were imaged by phase contrast or confocal microscopy as described.

5.2.24 Cell Staining for Imaging.

Cells were fixed with formaldehyde (4 % in PBS, 10 min), permeated (PBS containing 0.1 % Triton X–100, 10 min), and rinsed in PBS (2 x 5 min). **Fluorescence imaging-** A fluorescent dye mixture containing phalloidin-TRITC (red, actin) and anti-vinculin (green, focal adhesions) was made in PBS with 5 % normal goat serum and 0.1 % Triton X –100. Cells were incubated with the dye solution for 1 h and were then rinsed in PBS for 5 min. A second fluorescent dye mixture consisting of phalloidin-TRITC (red, actin), DAPI (blue, nucleus), and Cy-2 (green, focal adhesions) was then made in PBS with 5 % normal goat serum and 0.1 % Triton X –100. Cells were incubated with the dye solution for 1 h and were then rinsed in PBS for 5 min. The substrates were secured in fluorescence mounting medium (Dako, Carpinteria, CA, USA), which enhances the visualization of cells when viewed under a fluorescent microscope on a glass cover slip. Exposure times for imaging DAPI, actin, and focal adhesions were 400, 1200, and 600 ms, respectively. **Confocal imaging-** A fluorescent dye mixture containing phalloidin-TRITC (red, actin) and DAPI (blue, nucleus) was then made in PBS containing 5% normal goat serum and 0.1% Triton X –100. Cells were incubated with the dye solution for 2 h. The substrates were then secured in fluorescence mounting medium (Dako, Carpinteria, CA, USA), which enhances the visualization of cells when viewed under a fluorescent microscope on a glass cover slip. An average of 84 scans were taken to generate 3D reconstruction images.

5.2.25 hMSC Differ5entiation and Immunhistochemistry

Adipogenic differentiation of Q-hMSCs (**11**) was induced after the growth of 3D tissue-like structures and co-culture with AO-Fb (**15**) by culturing substrates with induction

medium as described in the Lonza protocol. Surfaces were then fixed with formaldehyde (4 % in PBS, 30 min), immersed in a solution containing water and 60 % isopropyl alcohol (3-5 min) and stained with Oil Red O (red, lipid vacuoles, 5 min) and Harris Hemotoxylin (purple, nucleus, 1 min). Substrates were visualized by phase contrast microscopy using a Nikon TE2000-E inverted microscope. Image acquisition and processing was performed using Metamorph software.

5.2.26 Confocal Microscopy

Cell clusters and tissue formation were generated, stained, and secured on a glass slide as previously described above and were visualized with a Nikon Eclipse TE2000-E inverted microscope (Nikon USA, Inc., Melville, NY). Data was analyzed by Metamorph software and a spectral confocal microscope (LeicaMicrosystems, Bannockburn, IL). 3D reconstructions of fluorescent images were generated using Volocity software with an average of 84 scans/image.

5.2.27 Cell viability assay of 3D spheroid and multi-layered co-culture structures

Cell viability of 3D spheroid and multi-layered tissue-like structures was assessed by performing a trypan blue viability assay (Hyclone, Fisher Sci, Pittsburgh, PA). Fb (**15**) and hMSC (**11**) spheroid and multi-layer co-culture structures were prepared as previously described. A solution of 0.4 % trypan blue in PBS was made and diluted in CBS (1:1) containing the spheroids (1, 2, 3, and 5 h after mixing) in solution and multi-layer cell sheets (3, 5, and 7 d after a second cell population was added) on a glass slide. Trypan blue was allowed to react with the cells for 2 min, at which time spheroids and surfaces were imaged for blue fluorescence using a Nikon TE2000-E inverted microscope. A control experiment was performed in which 3D multilayered hMSC and

Fb co-cultures were generated for 7 days and then fixed with paraformaldehye and stained with trypan blue as described above. Images were compared to the control to approximate the % viability of cells in multilayers.

5.2.28 Cell Viability Assay of Cells After Potential Application

HMSCs and Fbs were cultured with HQ-functionalized liposomes for 1, 3, 5, and 7 d as mentioned (**5** and **13**) and tested for viability after being subject to varying potentials. All cell populations maintained viability > 95 %. Measurements were performed in PBS, pH = 7.4. Each potential was held for 10 s, ranging from -100 to 650 mV, in ~185 mV increments. Cell viability was approximated by conducting a trypan blue assay after being subject to different potentials.

5.3 Results and Discussion

5.3.1 Overview of the Method

In order to deliver and tailor cell surfaces with dynamic and bio-orthogonal chemical groups for cell membrane manipulation and control of cell-cell interactions, we first developed a liposome fusion-based model system. Hydroquinone (**1**, HQ) and aminooxy alkanes (**3**, AO) were synthesized and incorporated into liposomes (fig. S1-S5). We have previously shown in solution and on conducting substrates how HQ is in the ‘off state’ and can be activated to the ‘on state’ quinone (Q) by mild chemical or electrochemical oxidation. Q can then chemoselectively react with AO-tethered ligands to form stable oxime linkages at physiological conditions (fig. S1) (*24-26*). The oxime linkage can then be selectively cleaved under reductive conditions to regenerate HQ with simultaneous release of the AO-tethered groups. This redox-active, oxime-based conjugation and release chemistry is bio-orthogonal and can be carried out in complex

protein mixtures, cell lysates, and in cell culture (*26*). Thus, our rationale was to combine this dynamic, switchable, and bio-orthogonal conjugation and release strategy with liposome fusion to tailor cell surfaces *in vitro* for studies in cell-surface manipulation and tissue engineering.

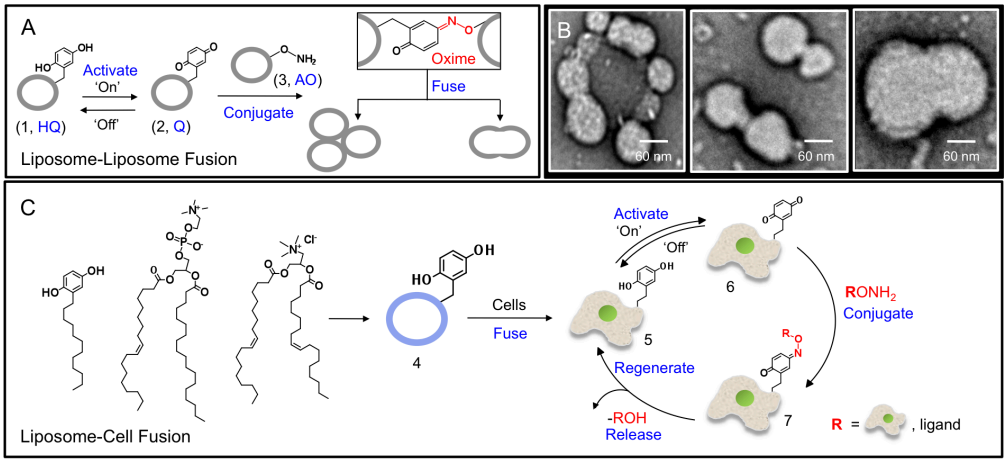

Figure 5.1 Schematic and transmission electron micrographs (TEM) demonstrating dynamic liposome-liposome fusion and liposome-cell fusion for tailoring cell surfaces. (**A**) Hydroquinone (HQ)-containing liposomes (**1**) (3 mM in tris buffer, pH 7.4) are in the 'off state' and are thus, activated to the 'on state' quinone (Q) (**2**) by mild chemical oxidation (20 μL, 5 μM $CuSO_4 \cdot 5H_2O$ in PBS at 10 mol %, 5 min) and mixed with aminooxy (AO)-containing liposomes (**3**). Mixing these two populations (0.2 mM total in PBS, 1:1) over 2 hours results in the formation of (**B**) multi-adherent, partially fused, and completely fused liposomal structures driven by oxime bond formation. Over time, the liposomes grow in size due to fusion. (**C**) General schematic representing the dynamic control of cell surfaces based on liposome-cell fusion for the delivery and tailoring of bio-orthogonal groups. POPC (398 μL, 10 mg/mL in $CHCl_3$ at 88 mol %), DOTAP (10 μL, 10 mg/mL in $CHCl_3$ at 2 mol %), and HQ-functionalized alkane (160 μL, 10 mM in $CHCl_3$ at 10 mol %) are mixed to form liposomes (3 mM in tris buffer, pH 7.4). The HQ-tethered liposomes (**4**) are then added to cells in culture (400 μL to 4 mL, 16 h), resulting in fusion and subsequent presentation of HQ groups from the cell surface (**5**). HQ is then activated to Q (**6**), which reacts chemoselectively with a range of AO (or $RONH_2$)-tethered ligands or cells via a covalent and stable oxime linkage (**7**). Upon a mild change in redox environment, the oxime bond is cleaved (-100 mV, 10 s, pH 7.4) to release the ligand or cell, followed by regeneration of the HQ-presenting cell (**5**) for subsequent rounds of dynamic and controlled conjugation and release.

5.3.2 Biophysical Characterization

To evaluate if liposome-to-liposome fusion can occur via oxime chemistry, we activated HQ- (**1**) to Q-containing liposomes (**2**) and then mixed them with AO-containing liposomes (**3**) (fig. S5). We observed rapid liposome aggregation and fusion (Fig. 1A) as shown by transimission electron microscopy (TEM) image analysis (Fig. 1B). It was demonstrated that over time, an oxime-driven process directed liposomes to first aggregate and then fuse, forming larger assemblies (Fig. 1B). Fluorescence resonance energy transfer (FRET) characterization of liposome fusion displays a clear FRET signal, only when the complimentary oxime pair is present in the liposomes (fig. S6). Furthermore, dynamic light scattering (DLS) analysis shows the spontaneous liposomal growth due to this oxime-driven liposomal fusion (fig. S7). Aggregated or fused liposomal structures were not observed in control experiments where HQ-containing liposomes were not activated or when either oxime pair was missing.

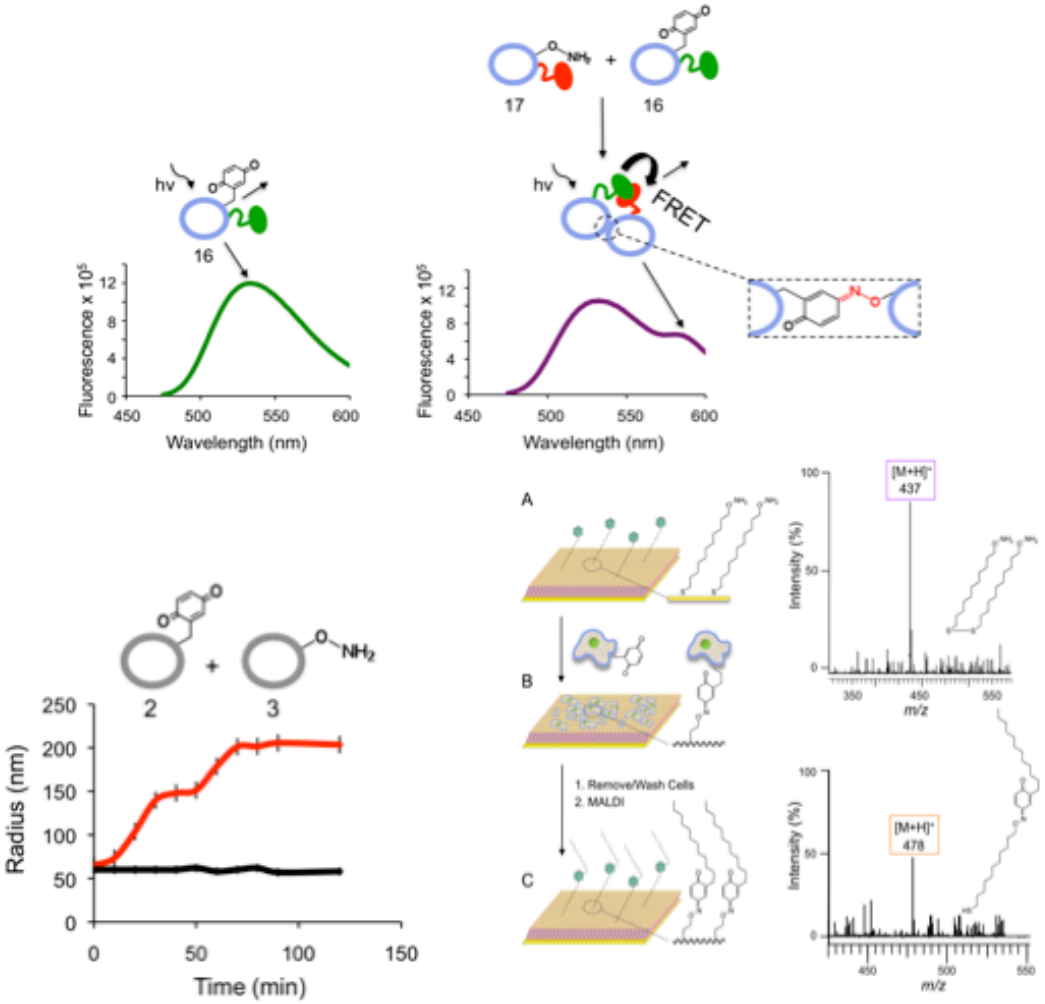

Figure 5.2 Biophysical characterization of liposome adhesion and fusion based on chemoselective oxime formation between Q- and AO-containing liposomes. Top- FRET studies: Q- (160 μL, 10 mM in $CHCl_3$ at 10 mol %) and NBD-PE- (20 μL, 10 mg/mL in $CHCl_3$ at 2 mol %) containing liposomes (**16**) were excited at 471 nm, producing light emission at 531 nm (green trace). When these liposomes (200 μL, 1:1) were mixed with AO- (60 μL, 10 mM in $CHCl_3$ at 5 mol %) and rhodamine-PE/POPG- (28 μL, 10 mM in $CHCl_3$ at 2 mol %) functionalized liposomes (**17**), a FRET emission peak is observed at 578 nm indicating oxime-mediated liposomal adhesion and fusion. No FRET signal is observed with non-activated HQ liposomes or when liposomes without AO groups are mixed. Fluorescence was monitored for 2 h at 2 min intervals, and the temperature was maintained at 25 °C. Bottom left: DLS characterization of liposome adhesion and fusion based on chemoselective oxime formation between Q- and AO-containing liposomes. Q- and AO-containing liposomes (**2** and **3**, respectively) were mixed (0.2 mM in PBS, 100 μL, 1:1) and monitored by DLS to observe the changes in liposome size over reaction time. Over a period of 80 min of mixing, liposomes grew in size due to adhesion, partial, or complete fusion (red trace). As a control, liposome size remained constant when Q-containing liposomes (**2**) were added to liposomes not functionalized with AO groups or un-activated, HQ liposomes (**1**) with AO liposomes (**3**) (black trace). Bottom right: Mass

spectrometry characterization of oxime bond formation at the cell surface. (**A**) Self-assembled monolayers (SAMs) of AO-terminated alkanethiol (1 mM in EtOH, 1 min, backfilled with 1 mM mercaptoundecanol in EtOH, 1 h) were formed on gold-coated (12 nm) MALDI sample plates (123 x 81 mm). MALDI analysis was performed directly on the surface to display mass $[M + H]^+$ of 437 corresponding to the AO-terminated alkanethiol connected by disulfide linkage. (**B**) Q-displaying Fbs (**6**) were seeded (10^7 cells/mL, 3 h in serum-free conditions) on gold-coated MALDI sample plates presenting AO-terminated alkanethiol. The cells were then washed several times (0.1% SDS in PBS, 2 x 3 mL and EtOH, 2 x 3 mL) and dried before testing to result in (**C**) oxime conjugation on the surface. MALDI was again performed, and a mass $[M + H]^+$ of 478 corresponding to the product of Q and AO conjugation was observed.

5.3.3 Dynamic Cell-Surface

After the successful characterization of liposome-to-liposome fusion, we aimed to employ a similar strategy to generate electroactive, dynamic, and switchable cell surfaces. Therefore, we applied our liposome fusion method to deliver the bio-orthogonal HQ (**4**) and AO (**12**) groups for subsequent fusion and presentation from cell membranes. For these studies, HQ alkane was mixed with POPC, and DOTAP (a cationic lipid) in a 10:88:2 ratio, and AO alkane with POPC, and DOTAP (5:93:2) (fig. S5). After addition to cells (swiss 3T3 fibroblasts (Fbs)) in culture, the liposomes first fuse, delivering the chemical groups to cell surfaces (Fig. 1C). HQ can then be activated to generate Q, which will conjugate chemoselectively with AO-tethered ligands or cells to form a stable, interfacial oxime linkage. The oxime bond at the cell membrane can then be selectively cleaved with the simultaneous release of the ligand or cell and regenerate the HQ-presenting cell. This dynamic cycle is non-cytotoxic (fig. S8), redox triggered and switchable (fig. S1), performed *in situ* and under physiological conditions, and provides unprecedented control of cell-cell and cell membrane interactions through the conjugation and release of ligands and cells.

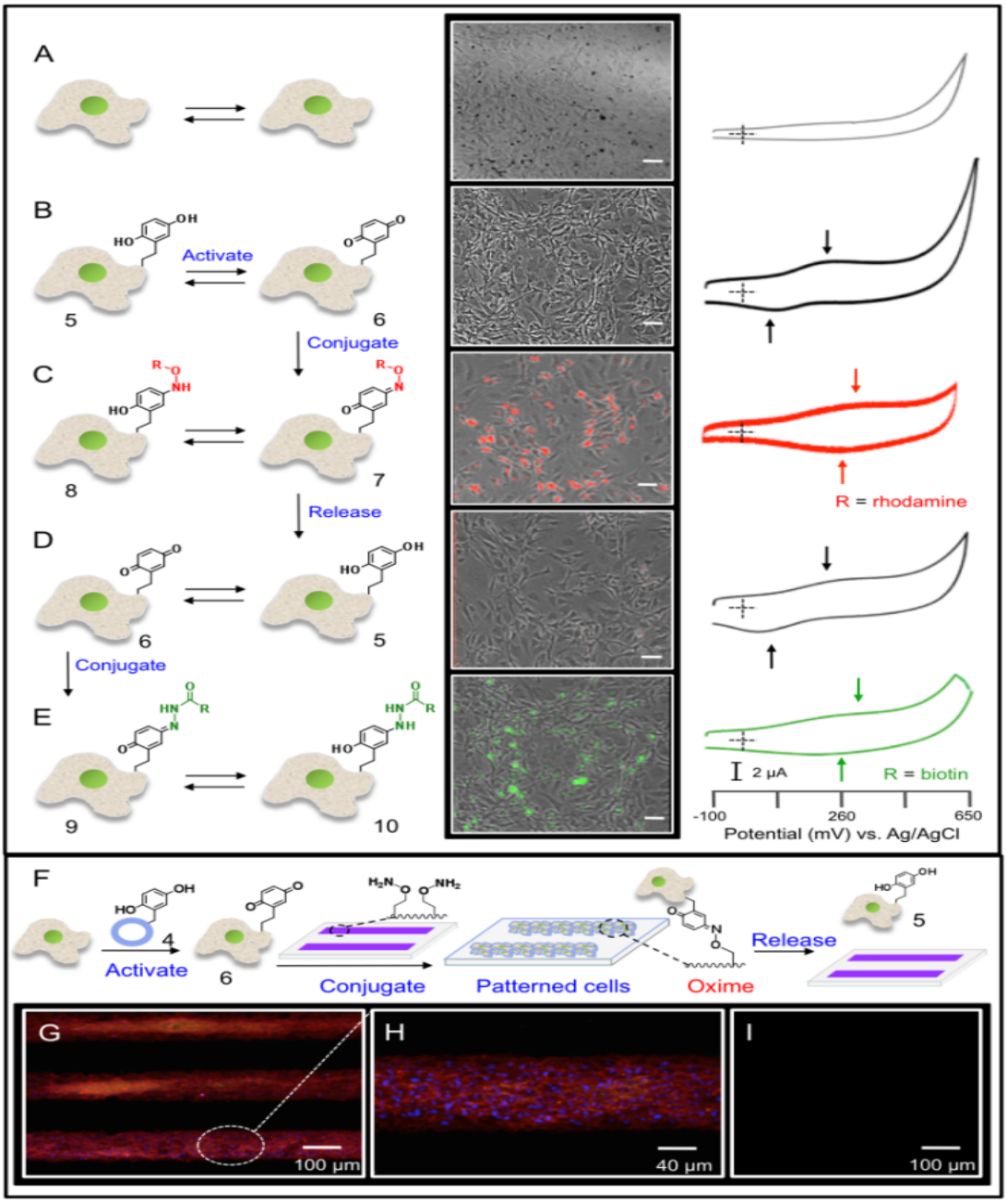

Figure 5.3 (Top) Fluorescent and electrochemical characterization of cyclical cell-surface tailoring and the release of ligands based on redox responsive chemoselective chemistry. (**A**) Fibroblasts (Fb), not fused with liposomes presenting HQ groups show no redox signal or fluorescence. (**B**) HQ-containing liposomes (**4**) are added to Fbs (3 mM in tris buffer, 400 μL to 4 mL, 16 h), resulting in membrane fusion and presentation of HQ from the surface (**5**). The stable HQ (**5**) to Q (**6**) interconversion can be monitored by cyclic voltammetry (CV) (-100 to 650 mV, pH 0, 100 mVs^{-1}) due to its diagnostic redox peaks (black trace, HQ = 130 mV, Q = 258 mV). (**C**) Activated Q-presenting Fbs (**6**) can be chemoselectively reacted with rhodamine-AO (7 mM in H_2O, 100 μL to 4 mL, 30 min) for cell-surface tailoring (**7** and **8**). This results in stable, fluorescently labeled cells

(red) and a diagnostic shift in redox signal (red trace, 252 mv, 284 mV). (**D**) In a reductive environment (-100 mV, 10 s, pH 7.4), the oxime bond is cleaved with the release of rhodamine and the regeneration of HQ-presenting Fbs (**5**) as indicated by a loss in fluorescence and the redox peaks of the HQ to Q cycle (black trace). (**E**) Cell surfaces can once again be conjugated for a second time with hydrazide-tethered biotin (**9** and **10**) and fluorescein-presenting streptavidin (1 mg/mL in PBS, 0.5 mL to 2 mL, 1 h each), resulting in fluorescently labeled cells (green) and a shift in redox peaks (green trace). (Bottom) A general schematic and corresponding fluorescent images demonstrating dynamic control of cell adhesion and release from patterned substrates (**F**). Fbs were cultured with HQ-containing liposomes (**4**), resulting in membrane fusion and subsequent display of HQ from cell surfaces (**5**). Mild chemical oxidation (20 μL, 5 μM $CuSO_4 \cdot 5H_2O$ in PBS at 10 mol %, 5 min) converts the HQ to Q groups on the cell surface (**6**). Q-presenting Fbs (**6**) (10^4 cells/mL, 2 h) were then added to a substrate patterned with AO-terminated ligands (1 mM in EtOH, 1:9 AO/EG_4). Cells adhered to the substrate due to a biospecific interfacial oxime ligation and then proliferated (4 d) within the patterned region as shown in lower (**G**) and higher (**H**) magnified fluorescent micrographs. Upon electrochemical reduction, the interfacial oxime is cleaved and the cells are released from the substrate (**I**). Cells were stained for actin (red, phalloidin), nucleus (blue, DAPI), and anti-vinculin (green, Cy-2).

Figure 3 demonstrates the dynamic and switchable conjugation and release of ligands to and from the cell membrane. After HQ-containing liposomes (**4**) were fused with Fbs (**5**) on a conductive substrate, cyclic voltammetry (CV) was performed, and distinct HQ to Q redox peaks were observed (Fig. 2A) (*27*). Upon activation to Q (**6**) (400 mV, 10 s) and conjugation of AO-tethered rhodamine (**7** and **8**) to cells, a shift in CV peaks, characterisitic of oxime formation (*27*), was observed. The rhodamine-labeled Fbs were also imaged, and red fluorescence was observed (Fig. 2B). After application of a non-cytotoxic, reductive potential (-100 mV, 10 s, fig. S10), rhodamine was released from the cells, and HQ was regenerated on the cell surface as indicated by CV and fluorescence microscopy (Fig. 2C). We then re-activated the HQ-presenting Fbs to Q and conjugated biotin-hydrazide, followed by FITC-streptavidin. It was found that the cells could once again conjugate and release molecules from the cell surface shown by CV and

fluorescence microscopy (Fig. 2D). The oxime linkage is stable, and only upon application of a mild reductive potential does the oxime cleave and release ligands (*27*). In general, this dynamic strategy can be used for controlling the chemical structure of cell surfaces in 3D space and time with micro- or nanoelectrode arrays, where the cell surface ligands can be replaced with any biomolecule of interest, creating a new tool for the modulation of cell interactions.

5.3.4 Cell Viability and Flow Cytometry

Several assays were performed to evaluate cell viability as a function of applied redox potential (fig. 4). As a result, no change in cell viability was observed after applying different electrochemical potentials (-100 to 650 mV, 10 s) on cells cultured with HQ for up to 7 days. Other control experiments concluded that removing either HQ or AO from the fusion liposomes resulted in no ligand conjugation at the cell surface. When AO-alkane or HQ-alkane was added directly to cells in culture but not in liposome form no incorporation of AO or HQ groups in cell surfaces were observed. Additionally, when chemical or electrochemical activation does not occur, conjugation and release of ligands was not observed. Furthermore, we determined the amount of HQ molecules at the cell membrane upon initial liposome fusion by FACS analysis. FACS analysis also demonstrated that HQ remains incorporated in the membrane after several rounds of cell growth and division and that HQ can still be actived for conjugation and release of ligands (fig. 4). These results may lead to new ways to tailor and monitor *in vitro* and *in*

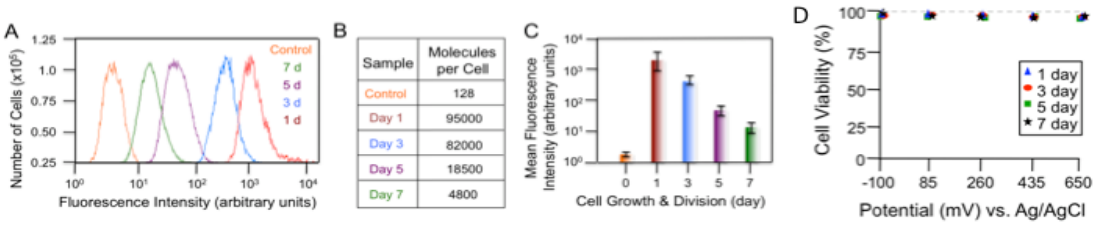

Figure 5.4 Fluorescence activated cell-sorting (FACS) analysis to determine the number of HQ molecules per cell. HQ-containing liposomes (**4**) were added to Fbs in culture (3 mM in tris buffer, 400 μL to 4 mL, 1, 3, 5, and 7 d). The amount of HQ on cell surfaces as delivered by membrane fusion was determined after 1, 3, 5, and 7 days. Before conducting FACs, cells were chemically (20 μL, 5 μM $CuSO_4 \cdot 5H_2O$ in PBS at 10 mol %, 5 min) activated to Q (**6**), followed by conjugation of biotin-hydrazide (**9**) (3 mM in CBS, 1 mL added to 4 mL CBS in cell culture, 37ºC in 5% CO_2, 1 h) and fluorescein-streptavidin (1 mM in CBS, 0.5 mL added to 4 mL CBS in cell culture, 37ºC in 5% CO_2, 1 h). A control population in which Fbs (not functionalized with HQ groups) were reacted with biotin-hydrazide and FITC-streptavidin under the same conditions was also tested. All sample populations were centrifuged (5 min, 1000 rpm), resuspended in RPMI (10^7 cells/mL), centrifuged, and resuspended in RPMI. 1-mL samples were tested against a standard bead (10^7 beads/mL) with known fluorescein molecule density. (**A**) The relationship between the number of cells scanned (~10^5) and fluorescence intensity of control population and cells incubated with HQ-functionalized liposomes for 1, 3, 5, and 7 days as determined by flow cytometry analysis is reported. The fluorescence intensities decrease over time, indicating that cells are able to carry the HQ moiety through division and growth. The control cells show little to no fluorescence. (**B**) The number of fluorescein molecules was calculated by comparing the relative mean intensity to a standard bead with known FITC equivalent molecule density. The numbers of HQ molecules per cell are listed, showing a decrease in density on the cell surface over time. (**C**) The relationship between the mean fluorescence intensity (3 trials per day, error bars) and liposome incubation day is shown as a linear decrease from 1 to 7 days. Cell viability assay of hMSCs and Fbs when subjected to mild redox potentials. HMSCs and Fbs were cultured with HQ-functionalized liposomes (**4**) (3 mM in tris buffer, 400 μL to 4 mL) for 1 (blue triangle), 3 (red circle), 5 (green square), and 7 (black star) days and tested for viability after being subject to varying redox potentials (-100 to 650 mV, 10 s, ~185 mV increments, PBS, pH 7.4). All cell populations (**13** and **15**) maintained viability >95% (trypan blue viability assay, 0.4 % in PBS, 2 min) and were indistinguishable from control populations not exposed to redox potentials.

vivo events that occur at cell membranes and allow for new types of pulse and chase type experiments for cell imaging and for tracking cell movement (*28,29)*.

5.3.5 Dynamic Cell Adhesion

The incorporation and utility of HQ on the cell surface was further investigated by attaching and releasing cells from an OA-patterned substrate (Fig. 2C). HQ-presenting Fbs (**5**) were activated to Q (**6**) and then seeded onto an inert substrate, presenting AO groups (*30*). The Q groups on the cell surface (**6**) reacted biospecifically with the patterned OA ligands to form an interfacial oxime linkage. The cells attached and then proliferated, filling out the patterned regions. An electrochemcial trigger was then applied to cleave the oxime linkage, and cells released from the substrate. Furthermore, a novel MALDI mass spectrometry analysis of cell membrane incorporation shows oxime conjugation between Q presenting cells and OA terminated surfaces (Fig. S11) (*31*). This strategy allows for spatial and temporal control of cell interactions in 2D and may be extended to other materials and nanoparticles for designing new cell-based assays and renewable microarray platforms (*32,33*).

5.3.6 Dynamic 3D Cell Assembly

We extended this methodology to demonstrate the dynamic control over cell-cell interactions by co-culturing HQ-presenting human mesenchymal stem cells (hMSC) (**13**) with AO-displaying Fbs (**15**) to form 3D tissue structures. Upon chemical activation (see Supp. Info.) and mixing in solution, 3D spheroid assemblies were able to be rapidly generated (Fig. 3A). By increasing the mixing duration, control of the spheroid size could be achieved (fig. S12). The interconnected cells that make up the spheroids could then be disassembled, back to individual cells by mild electrochemical reduction (-100 mV, 10 s) (Fig. 3C). Additionally, spheroids were formed when Swiss 3T3 albino mouse Fbs

presenting HQ groups were activated (**6**) and co-cultured with nuclear m-cherry-labeled Rat2 Fbs displaying AO groups (**14**) (Fig. 3B). Figure 3D exhibits a cryo scanning

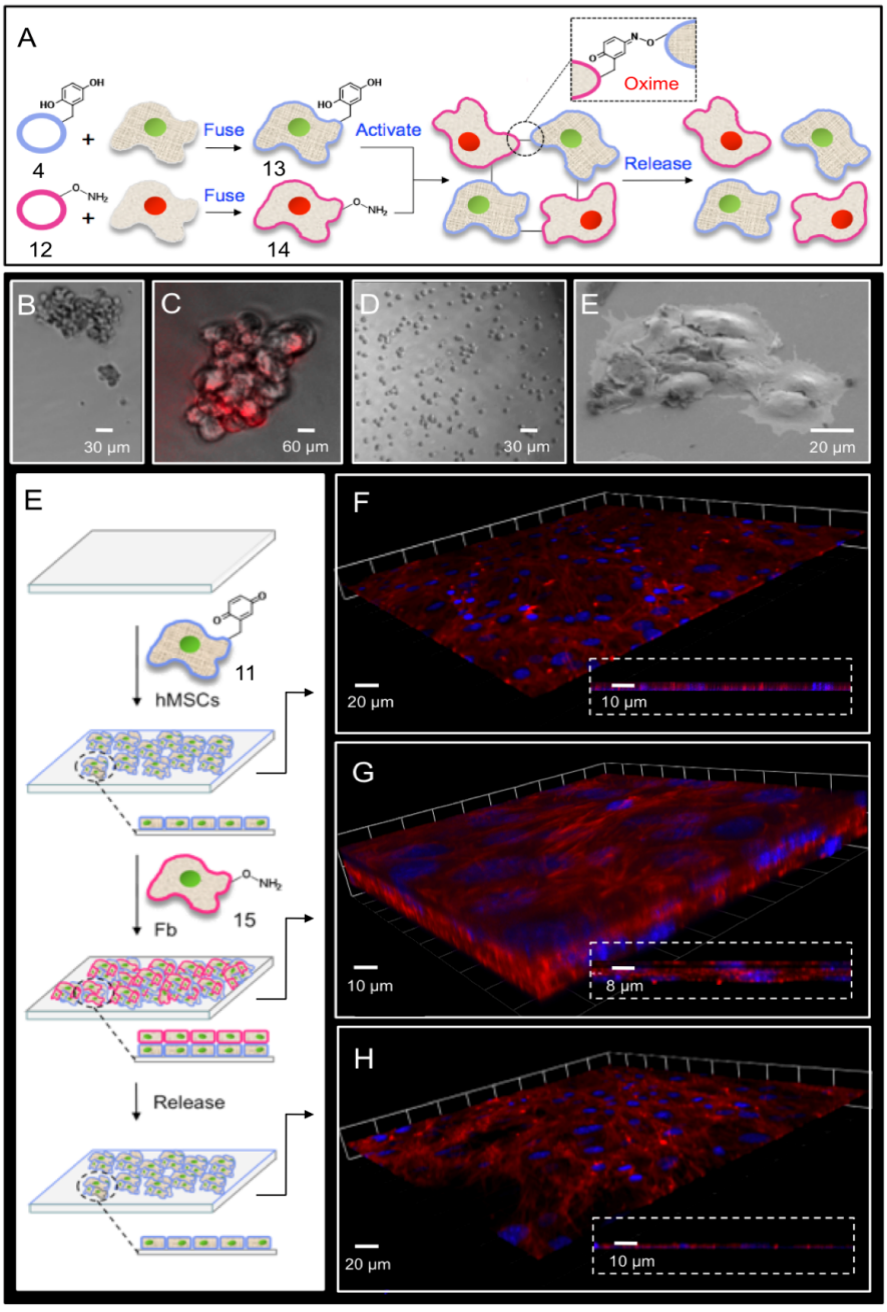

Figure 5.5 Schematic and corresponding images of 3D dynamic spheroid and multi-layered tissue assembly and disassembly via liposome fusion and chemoselective cell-surface tailoring. (**A**) Human mesenchymal stem cells (hMSCs) are functionalized with HQ groups (**13**) (3 mM in tris buffer, 400 µL to 4 mL, 16 h) after liposome fusion and are then activated to Q (**11**). Fbs presenting AO groups (**14**) are then co-cultured (1 mL, 1:1, 3 h) with Q-displaying hMSCs (**11**), producing (**B** and **C**) 3D spheroid assemblies,

interconnected through chemoselective oxime chemistry. Mild electrochemical reduction (-100 mV, 10 s, pH 7.4) causes oxime cleavage and the dynamic disassembly of cells as shown in (**D**). (**E**) Activated, Q-tethered hMSCs (**11**) are cultured on a substrate (10^5 cells/mL, 3 d), resulting in a 2D cell monolayer (**F**). AO-presenting Fbs (**15**) are added (10^5 cells/mL, 2 d) to the hMSCs (**11**), and a 3D interconnected multi-layered structures (**G**). A reductive potential applied to the substrate cleaves the oxime bond and induces the dynamic release of Fbs from the multi-layer, regenerating the 2D monolayer of hMSCs (**H**). The nuclei of OA-tethered Fbs (**14**) shown in C are stained with m-cherry for enhanced visualization. HMSCs (**11**) and Fbs (**15**) displayed in **F**-**H** are stained for actin (red, phalloidin) and nucleus (blue, DAPI).

electron micrograph (SEM) of an oxime ligated, spheroid assembly of hMSC (**15**) and Fbs (**13**) attached to a substrate. Viability for the cells in the spheroids was analyzed over time (1 to 5 hours, trypan blue assay, blue false colored) and found to be > 99%. Control experiments when no activation occurs or when one of the oxime compliments is not present in a cell type showed no spheroid formation. These results indicate that 3D co-culture assemblies in solution can be generated in a straightforward manner with the ability to control both the size, compostion, and the duration of cell-cell interactions. This strategy is general and may be used for numerous studies, including autocrine and paracrine signaling events and when combined with microfabricated scaffolds as a tissue engineering platform.

5.3.7 Dynamic 3D Tissue on Solid Surface

In addition to forming spheroid assemblies, we demonstrate that 3D multi-layered co-culture tissue structures are able to be generated on a solid support. We cultured activated, Q-presenting hMSCs (**11**) on a substrate to form a 2D monolayer (Fig. 5E-F) and then added AO-displaying Fbs (**15**). Chemoselective ligation occurs between the two cell populations followed by 3D multi-layer tissue growth after 3 days (Fig. 5G). When the proper oxime pair is not present, only a single monolayer of hMSC is observed with

no Fbs adhering. We found that cells were viable for many days (> 7 days) and that the HQ and AO could be carried forward on the cell surface (FACS analysis over time, fig. S4) even through cell growth and proliferation. The multi-layers were able to be disassembled by applying a mild reductive potential to the substrate (-100 mV, 10 s, pH = 7.4), which cleaved the oxime linkage and released the interactions between cells. Overall, this dynamic method to generate 3D multi-layer tissue structures may be used to control cell-cell interactions for many co-culture-based cell behavioral and cell tissue applications *(34)*.

5.3.8 Dynamic Platform for Stem Cell Differentiation

We further employed this dynamic strategy to study stem cell differentiation by applying our liposome fusion-based delivery of activatable bio-orthogonal groups to cell surfaces to generate 3D multi-layered cell tissues and induce adipocyte differentiation (Fig. 6). HQ-presenting hMSCs were activated and co-cultured with Fbs as described previously. This tissue was grown in media that induced adipocyte differentiation after 10 days, resulting in 3D multi-layered co-culture tissues of adipocytes and Fbs (Fig. 6D). Application of a mild reductive potential disassembled the 3D tissue, leaving a relatively pure, 2D adipocyte monolayer (Fig. 6E-F). The dynamic and controlled 3D multi-layer cell disassembly indicates that cell-cell interactions, even for complex stem cell differentiation processes over long time periods, can be precisely manipulated. By assembling and disassembling the co-cultures on demand, a time course of cell behavior, due to length of cell-cell interactions, is able to be determined for a range of cell lines and co-culture-based applications (*35,36*).

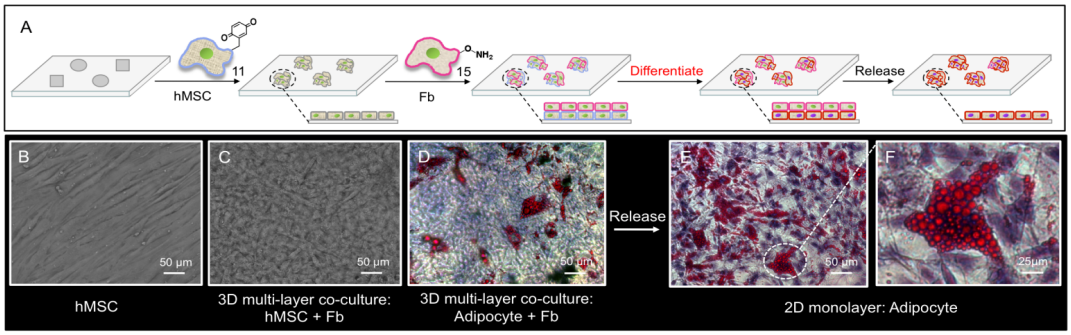

Figure 5.6 Schematic and corresponding phase contrast images displaying the formation, differentiation, and release of 3D dynamic tissues using a Fb/hMSC co-culture. (**A**) Activated, Q-tethered hMSCs (**11**) are cultured on a substrate (10^5 cells/mL, 3 d) and form a 2D monolayer as shown by the image in (**B**). AO-presenting Fbs (**15**) are then added (10^5 cells/mL, 2 d), producing a 3D multi-layered, interconnected co-culture (**C**). When the appropriate induction media is delivered to the co-culture, hMSCs differentiate into adipocytes, resulting in a 3D multi-layered co-culture of Fbs and adipocytes (**D**). A reductive potential (-100 mV, 10 s, pH 7.4) applied to the substrate results in oxime cleavage and the dynamic release of Fbs, leaving only the adhered adipocytes on the surface as a 2D monolayer shown by lower (**E**) and higher (**F**) magnified images. Adipocytes were stained for lipid vacuoles (red, Oil Red O) and nucleus (purple, Harris Hemotoxylin).

5.4 Conclusions

In summary, we have developed a new general and straightforward liposome fusion based methodology to deliver dynamic and switchable bio-orthogonal chemistries to tailor cell membranes and direct the formation of 3D co-culture tissue structures. We demonstrated and extensively characterized the conjugation and release of molecules to and from cell surfaces *in situ*, as well as the triggered assembly and disassembly of 3D spheroid and multi-layered tissues. Additionally, dynamic co-cultures of hMSCs and Fbs were able to be generated and differentiated with this redox oxime strategy.

The dynamic and bio-orthogonal oxime chemistry reported has several key advantages to serve as a cell-surface engineering and cell-tissue generating system. First,

the oxime complimentary pair is synthetically straightforward, and ketone-, hydrazide, and AO-tethered ligands are commericially available. Second, oxime reactivity can be switched 'on' and 'off' with a change in the redox environment and therefore, can be used to monitor cell-surface incorporation of moleucles and cell-surface interactions. Third, the oxime bond forms rapidly and is stable under physiological conditions until subject to a chemical or electrochemical reducing potential. Fourth, the redox manipulation is non-cytotoxic. Fifth, this liposome fusion-based method is general and can be used to deliver the oxime pair to a range of cell lines for a variety of applications. Lastly, this methodology can be used to deliver a variety of other bio-orthogonal 'click' chemistries to cell surfaces.

Future applications of this strategy may be extended to study and manipulate stem cell fate of 3D multi-layered co-culture tissues and for controlling stem cell plasticity. Integration of this approach with 3D polymer scaffolds may lead to the design of new tissue enginering and regenerative medical therapies, devices, and applications. Theranostic applications, where simultaneous delivery of therapies and diagnostic monitoring, may also be possible for a variety of *in vitro* and *in vivo* imaging and cell tracking studies. With the introduction of an electroactive cell surface, it may be possible to track dynamic biophysical events, such as lipid diffusion and endo- and exocytosis. By generating a photo-inducible linker within the bio-orthogonal pair lipids a light sensitive cleavable system may also be generated for spatial and temporal control of cell-cell interactions (*11,37*). By altering the lipid composition and mix of bio-orthogonal groups in cell membranes via liposome fusion and delivery, potential cell to cell fusion experiments and the generation of tailored giant unilamellar vesicles may be possible.

Finally, by tailoring and controlling cell surfaces and cell-cell interactions, new types of autocrine and paracrine signaling studies for fundamental cell behavior and tissue regeneration applications may be explored (*38,39*).

5.5 Acknowledgements

The authors thank Prof. Joe DeSimone for cell culture and microfabrication assistance, Prof. Nancy Thompson for expertise in liposome formation and characterization, Prof. Rudy Juliano for liposome fusion expertise, Prof. James Bear for supplying the m-cherry labeled fibroblasts, Dr. Michael Chua for expertise in confocal microscopy, and Lisa Bixby for help with FACS analysis. This work was supported by the National Cancer Institute (Carolina Center for Cancer Nanotechnology Excellence), the Burroughs Wellcome Foundation (Interface Career Award) and the National Science Foundation (Career Award).

5.6 References:

1. Nelson, C. M.; Bissel, M. J. *Annu. Rev. Cell and Dev. Biol.* **2006**, **22**, 287.

2. L. Li, T. Xie *Annu. Rev. Cell and Dev. Biol.* **21**, 605 (2005).

3. Meshel, A. S.; Wei, Q.; Adelstein, R. S.; Sheetz, M. P. *Nat. Cell Biol.* **2005**, **7**, 157 (2005).

4. Engler, .A; Sen, S.; Sweeney, H. L.; Discher, D. E. *Cell 2006,* **126**, 677.

5. Badylak, S. F.; Nareem, R. M. *Proc. Nat. Acad. Sci. U.S.A.* **2010**, **107**, 3285.

6. Ibold, Y.; Frauenschuh, S.; Kaps, C.; Sittinger, M.; Ringe, J.; Goetz, P. M. *J. Biomol. Screen.* **2007**, *12*, 956.

7. Y. Geng, P. Dalhaimer, S. Cai, R. Tsai, M. Tewari, D. E. Discher, *Nat. Nanotech.* **2007**, *2*, 249.

8. Albrecht, D. R.; Underhill, G. H.; Wassermann, T. B.; Sah, R. L.; Bhatia, S. N. *Nat. Methods* **2006**, *3*, 369.

9. Legant, W. R.; Pathak, A.; Yang, M. T.; Deshpande, V. S.; MacMeeking, R. M.; Chen, C. S. *Proc. Nat. Acad. Sci. U.S.A.* **2009**, *106*, 10097.

10. Raghavan, S.; Nelson, C. M.; Baranski, J. D.; Lim, E.; Chen, C. S. *Tissue Eng. Part A* **2010**, *16*, 2255.

11. Kloxin, A. M.; Kasko, A. M.; Salinas, C. N.; Anseth, K. S. *Science* **2009**, *324*, 59.

12. Lutolf, M. P.;

13. Hubbell, J. A.; *Nat. Biotechnol.* **2005**, *23*, 47.

14. Falconnet, D.; Csues, G.; Grandin, H. M.; Textor, M. *Biomaterials* **2006**, *27*, 3044.

15. Khademhosseini, A.; Langer, R.; Borenstein, J.; Vacanti, J. P. *Proc. Nat. Acad. Sci. U.S.A.* **2006**, *103*, 2480.

16. Gartner, Z. J.; Bertozzi, C. R. *Proc. Nat. Acad. Sci. U.S.A.* **2009**, *106*, 4606.

17. Mahal, L. K.; Yarema, K. J.; Bertozzi, C. R. *Science* **1997**, *276*, 1125.

18. Yoder, N. C.; Yuksel, D.; Dafik, L.; Kumar, K.; *Curr. Opin. Chem. Biol.* **2006**, *10*, 576.

19. Raghavan, A. S.; Hang, H. C. *Drug Discov. Today* **2009**, *14*, 178

20. Best, M. D. *Biochemistry* **2009**, *48*, 6571.

21. Saxon, E.; Bertozzi, C. R. *Science* **2000**, *287*, 2007

22. Gong, Y.; Luo, Y.; Bong, D. *J. Am. Chem. Soc.* **2006**, *128*, 14430

23. Lee, J.; Jun, H.; Kim, J.; *Adv. Mater.* **2009**, *21*, 3674

24. Sarkar, D.; Vemula, P. K.; Zhao, W.; Gupta, A.; Karnik, R.; Karp, J. M. *Biomaterials*, **2010**, *31*, 5266

25. Yousaf, M. N.; Houseman, B. T.; Mrksich, M. *Proc. Nat. Acad. Sci. U.S.A.* **2001**, *98*, 5992

26. Chan, E. W.; Park, P.; Yousaf, M. N. *Angew. Chem. Int. Ed.* **2008**, *47*, 6267

27. Chan, E. W. L.; Yousaf, M. N. *J. Am. Chem. Soc.* **2006**, *128*, 15542

28. Fuchs J.; Bohme, S.; Oswald, F.; Hedde, P. N.; Krause, M.; Wiedenmann, J.; Nienhaus, G. U. *Nat. Methods* **2010**, *7*, 627

29. Larsen, M.; Wei, C.; Yamada, K. M. *J. Cell. Sci.* **2006**, *119*, 3376

30. Park, S.; Yousaf, M. N. *Langmuir* **2008**, *24*, 6201

31. Mrksich, M. *ACS Nano* **2008**, *2*, 7

32. Karnik, R.; Hong, S.; Zhang, H.; Mei, Y.; Anderson, D.; Karp, J.; Langer, R. *Nano Letters* **2008**, *8*, 1153

33. Khetani, S. R.; Bhatia, S. N. *Nat. Biotech.* **2008**, *26*, 120 (2008).

34. Inaba, R.; Khademhosseini, A.; Suzuki, H.; Fukuda, J. *Biomaterials* **2009**, *30*, 3573

35. Gan, L.; Kandel, R. A. *Tissue Eng.* **2007**, *13*, 831

36. Kidambi, S.; Sheng, L.; Yarmush, M. L.; Toner, M.; Lee, I.; Chan, C. *Macromolecular Biosciences* **2007**, *7*, 344

37. Chan, E. W. L.; Yousaf, M. N. *Mol. BioSyst.* **2008**, *4*, 746

38. Langer, R. *Adv. Mater.* **2009**, *21*, 3235

39. Discher, D. E.; Janmey, P.; Wang, Y. L. *Science* **2005**, *310*, 1139

CHAPTER 6

A Dual Receptor and Reporter for Multi-Modal Cell-Surface Engineering

6.1 Introduction

Proper understanding of biological system is the key for any therapeutic and medical based research and technology. Visualizing and quantifying the signaling molecules and events with spatial and temporal control in cellular processes goes a long way in serving the purpose. Advances on genetic engineering producing new variants in green fluorescent proteins coupled with development in fluorescence microscopy has provided the basic tools to investigate the complex processes in cell biology.[1] The fluorescent protein based indicators can be designed to target sub-cellular compartments, whole organisms and tissues and can respond to a variety of biological signals and events. Although GFP and its variants[2-6] are extremely useful for tracking the localization and expression of proteins and investigate important cellular processes, small-molecule probes like organic dyes[7], quantum dots[8] and different class of nanoparticles[9] with less steric bulk, faster rates of labeling and the ability to provide readouts in addition to, or other than fluorescence is desired.

Cell-surface modification can facilitate the characterization of a number of cellular processes and signal transduction pathways in terms of identifying key proteins and signaling molecules.[10] One major application of engineering cell surfaces can be in modifying the cell membrane with molecular and detection probes for subsequent

tracking and chasing in cell based therapy.[11] Cell based therapy has been widely used as a therapeutic approach towards regenerative medicine. In particular, stem cells can be used to restore tissue functions either as integrated participants in the target tissue or as vehicles that deliver complex signals to a target tissue without actually participating into the tissue itself.[12] So any fluorescence based reporter system that can provide us with a spatial and temporal control in tracking the delivered cell from its injection through transport inside the body will be highly beneficial to the field of tissue engineering and drug delivery.

Calcein dye is a polyanionic derivative of fluorescein that exhibits fluorescence that is essentially independent of pH between 6.5 and 12. It is well retained in cells. These features have made it a popular and versatile dye for various applications, including cell volume changes in neurons and other cells, endocytosis, gap junctional communication, membrane integrity and permeability, angiography, etc. [13-17] Dabcyl has been routinely used as a general-purpose dark quencher for many commonly used fluorophores including calcein. It quenches the fluorphores by FRET (Fluorescence Resonance Energy Transfer) which is a dynamic quenching mechanism that does not affect the probe's absorption spectrum.[18] FRET is a highly distance dependent interaction between a reporter dye in an excited state and a quencher in its ground state. Energy is transferred from one molecule (fluorophore) to the other (the quencher) without the emission of a photon. In order for efficient FRET quenching to take place the fluorophore and the quencher molecules must be closer to each other (10 – 100 A°). In this study we have developed a liposome fusion based dual receptor-reporter system where cell surfaces were tailored and made fluorescent with a lipid tail conjugated calcein dye. Spatial and

temporal control on the cell-surface fluorescence was achieved by coupling the dye with its FRET quenching partner dabcyl using oxyamine exchange chemistry. We also applied the methodology to make three dimensional fluorescent tissue spheroids. Delivering the fluorescent tissue patches can not only have potential uses in surgery and regenerative medicine, particularly in wound healing applications but might also enable us to answer many fundamental questions in cell and molecular biology.

6.2 Materials and Methods

6.2.1 Materials

All chemical reagents were of analytical grade and used without further purification. Lipids egg palmitoyl-oleoyl phosphatidylcholine (POPC) and 1,2-dioleoyl-3-trimethylammonium-propane (DOTAP) were purchased from Avanti Polar Lipids (Alabaster, AL). Antibodies and fluorescent dyes were obtained from Invitrogen (Carlsbad, CA). FITC labeled beads were purchased from Spherotech, Inc. (Forest Lake, IL) and all other chemicals were obtained from Sigma-Aldrich or Fisher. Swiss 3T3 albino mouse fibroblasts (fbs) were obtained from the Tissue Culture Facility at the University of North Carolina (UNC).

6.2.2 Formation of Lipid Vesicles

To generate ketocalcein-containing liposomes for cell fusion studies, ketocalcein (46 μL, 10 mM solution in $CHCl_3$ at 10 mol %) was dissolved with egg-POPC (424 μL, 10 mg/mL in $CHCl_3$ at 93 mol %) and 1,2-dioleoyl-3-trimethylammonium-propane (DOTAP, 10 μL, 10 mg/mL in $CHCl_3$ at 2 mol %) in chloroform followed by concentration under high vacuum for 4 h. The dried lipid samples were then reconstituted

and brought to a final volume of 3 mL in PBS buffer, pH 7.4. The contents of the vial were warmed to 50 ˚C and sonicated for 20 min, in a tip sonicator, until the solution became clear, and LUVs containing ketocalcein groups were formed.

6.2.3 Fluorimetry

Liposomes were made starting with 2.7 mM of DOTAP and POPC and 0.3 mM of **1** dissolved in chloroform. Following literature procedure, the liposomes were synthesized and size selected for a distribution of 60-100 nm, which was verified by TEM. After the liposomes were made, they were diluted 1:10 into 2 mL of pH 7 phosphate buffer, and a fluorescent scan from 500 – 600 nm with excitation at 495 nm was made. To monitor the quenching reaction, dabcyl hydrazide was saturated into the solution and the fluorescence was monitored at 520 nm with 495 nm excitation over 12h. To measure recovery, liposomes were synthesized using 2.7 mM of DOTAP and POPC and 0.3 mM of **5.** To measure recovery, liposomes were synthesized using 2.7 mM of DOTAP and POPC and 0.3 mM of **5.** These quenched liposomes were then diluted 1:10 into 2 mL of pH 7 phosphate buffer and 50 mg of methyloxyamine was added. To monitor the exchange reaction, the fluorescence was measured at 525 nm with 495 nm excitation over 12h.

6.2.4 Flow Cytometry

Fluorescence activated cell sorting (FACS) analysis was performed in order to quantify the approximate number of ketone and oxyamine groups at the cell surface after membrane fusion. Liposomes (**5**) were prepared as described above and were delivered to Swiss 3T3 albino mouse fbs in culture (3 mM in tris buffer, 400 μL added to 4 mL, 16 h).

A time course assay was also conducted using FACS to determine whether the chemistry was being carried on after cell growth and division. Fbs were cultured with ketocalcein-containing liposome for 2, 4, and 6 d followed by fluorescein-conjugated streptavidin (1 mM in CBS, 0.5 mL added to 4 mL CBS in cell culture, 1 h). A control cell population (not displaying ketone groups) was only incubated with biotin-hydrazide and streptavidin-fluorescein for 1 h each, under the same conditions. Cells were then centrifuged (5 min, 1000 rpm), resuspended in RPMI (without phenol red), centrifuged (5 min, 1000 rpm), and resuspended in RPMI (~10^7 cells/2 mL). Fluorescence measurements were calibrated using RCP-5-30 beads (~10^7 beads/mL, Spherotech, Inc., Lake Forest, IL) of known fluorescein equivalent molecule density. Fluorescent intensities based on number of cells counted were compared to the standard bead and control cells lacking fluorescent molecule conjugation and approximate numbers of fluorescent compound bound to the surface was calculated. Flow cytometry was carried out using a Dako CyAn ADP (Beckman-Coulter, Brea, CA), and data was analyzed with Summit 4.3 software.

6.2.5 Fibroblast (Fb) Culture

Swiss 3T3 albino mouse fbs and Rat2 fbs were cultured in Dulbecco's Modified Eagle Medium (Gibco) containing 10 % calf bovine serum (CBS) and 1 % penicillin/streptomycin at 37 °C in 5 % CO_2. **Delivery of functionalized liposomes to cells.** Cells were seeded onto a tissue culture plate and allowed to grow for 48 h at 37 °C in 5 % CO_2 in CBS media. Solutions of ketocalcein-LUV (**5**) were added to cells for 4 h. The cells were then washed with PBS (4 x 4 mL) and imaged under a fluorescence

microscope with an exposure time of 1/1200 s. **Cell-surface reaction to ketoncalcein-presenting cells.** Solutions of ketocalcein-LUV were reacted with dabcyl hydrazide (1 mg/mL) for 3 h and then added to the culture to give the desired final ketocalcein concentration of 100 μg/mL in a total volume of 2 mL. The cells were incubated with the keto-LUVs for 4 h and washed with PBS (4 x 25 mL. The cells were then removed with a solution of 0.05 % trypsin 0.53 mM EDTA and re-suspended in serum-free medium (~10^4 cells/mL). The cells were then seeded to a fibronectin-coated surface for 2 h. After 2 h, serum-containing media was added for cell growth and imaged after 3 days. **Fluorescence recovery of quenched cells.** Cells treated with quenched ketocalcein-LUVs were treated with biotin hydrazide (3mg/mL, 1:20 v/v) for 16 h. The conjugated dabcyl hydrazide was exchanged by biotin over time and the green fluorescence was recovered. The presence of biotin on cell-surface was confirmed by adding rhodamine conjugated streptavidin (1 mg/mL) which has high affinity towards biotin and turns the cells fluorescent red.

6.2.6 3D Co-Culture Spheroid Generation

Ketocalcein-LUVs were generated as previously reported and added to Swiss 3T3 albino mouse fb (3 mM in tris buffer, 400 μL added to 4 mL, 16 h) and were cultured, resulting in fusion and display of ketones from the cell surface and also making the cells fluorescent green. 200 μL of 10 mM RGD-oxyamine was added to 4 mL of the fluorescent cell. After 3 h the cells were trypsinized and added to a Swiss 3T3 albino mouse fb solution. These two cell populations were then trypsinized and mixed together in serum containing (10 % FCS, pH of 7.4) media in a 10 mL flask and incubated at 37

°C and 5 % CO_2 for 1, 2, 3, and 5 h. After mixing for the allotted time, cells were seeded onto a glass surface and visualized under a Nikon TE2000-E inverted microscope under the brightfield setting (75 ms exposure time). Controls were also performed where fbs displaying ketone groups were reacted with RGD with no oxyamines and scrambled RGD with oxyamines and co-cultured with fbs (not displaying ketones groups) for each of the corresponding time points, 1, 2, 3, and 4 h, seeded onto glass, and imaged under the brightfield setting (75 ms). Image acquisition and processing was performed using Metamorph software.

6.3 Results & Discussion

6.3.1 Motivation of Work

In order to create our cell surface receptor/reporter system, we pooled many different features from divergent fields. For our studies, we sought the simplest molecule that was both fluorescent, had a handle for cell surface immobilization, and could be act as a lipid. To combine these functionalities into one molecule, we used a calcein derivative **1**. Calcein is a cell impermeable fluorescent dye used for live/dead cell assays and is highly charged, and when coupled with a 12 carbon chain, it acts like a lipid where the calcein serves as the charged head and the dodecyl chain serves as the greasy tail. This feature makes **1** prefer the surface of the lipid instead of its hydrophobic core and stay on membrane surfaces. At pH 7, calcein forms a tautomer that contains a ketone, which provides a handle for functionalization. Despite previous studies that have synthesized both the ketone and oxyamine derivatives of fluorescein, we reasoned we could directly couple hydrazines and oxyamines to this ketone. Additionally, this molecule is simple to synthesize requiring only one step to generate **1** from inexpensive starting materials. In

order to functionalize the cell surface with a cell surface receptor, we wanted to combine a cell labeling methodology with oxyamine/ketone chemistry to gain access to a chemoselective bio-orthogonal reaction strategy, thereby creating a fluorescent cell surface receptor. To functionalize the cell surface and introduce the fluorescent cell surface receptor, liposome fusion was used. Positively charge liposomes have been shown to fuse non-specifically to cells surfaces. In previous studies, these liposomes were doped to contain synthetic fluorescent lipids to label cell surfaces and mark certain populations in cell culture.[19] For our studies, POPC **2** served as the background lipid, DOTAP **3** served as the cationic lipid used to initiate cell surface fusion, and we mixed in a fluorescent lipid containing a ketone. For the immobilization strategy, oxime and hydrazone formation from a ketone was chosen. These chemistries offer several significant advantages as an immobilization strategy. They are bio-orthoganol, take place in the presence of cells, they do not require catalyst, they can be exchanged in the precence of other oxyamines and hydrazines, and synthesizing oxyamines and hydrazides is relatively simple.[20] To create the cell surface reporter/receptor, we leveraged oxyamine/hydrazine exchange reaction. Many groups have harnessed the ability for an oxyamine to exchange for another for enzymatic labeling and small molecule library synthesis. For our studies, the initial ligand was dabcyl hydrazide, **4**, a broad-spectrum fluorescent quencher. Here, we coupled the hydrazide derivative to the calcein dye to synthesize calcein derivative **5**. With the dabcyl coupled to the calcein, the fluorescence was effectively quenched. However, when another oxyamine or hydrazide ligand was exchanged for the dabcyl hydrazide on the cell surface, the fluorescence was recovered, thereby providing signal that the ligand of interest had bound the receptor on the cell

surface. Before undertaking liposome studies, we synthesized both **1** and **5** in solution and were able to exchange the dabcyl hydrazide from **5**. We verified this with NMR and mass spectrometry.

6.3.2 Fluorimetry Studies

After the solution studies, flouremetry was used to monitor both the quenching and exchange reactions on the liposomes. Liposomes were made starting with 2.7 mM of DOTAP and POPC and 0.3 mM of **1** dissolved in chloroform. Following literature procedure, the liposomes were synthesized and size selected for a distribution of 60-100 nm, which was verified by TEM. After the liposomes were made, they were diluted 1:10 into 2 mL of pH 7 phosphate buffer, and a fluorescent scan from 500 – 600 nm with excitation at 495 nm was made. The scan showed the presence of the calcein derivative in the liposome. To monitor the quenching reaction, dabcyl hydrazide was saturated into the solution and the fluorescence was monitored at 520 nm with 495 nm excitation over 12h. Before the addition of dabcyl hydrazide, the liposomes were highly fluorescent with a peak at 525 nm. However, as **4** reacted with the calcein on the liposome surface, the fluorescence decreased and was fully quenched after 10h. After the quenching reaction, a scan was made from 500-600 nm with an excitation at 495 nm, and it was observed the fluorescence was reduced by a factor of 5. To measure recovery, liposomes were synthesized using 2.7 mM of DOTAP and POPC and 0.3 mM of **5**. A scan of these liposomes showed they were similar in fluorescence to the liposomes quenched by reaction. These quenched liposomes were then diluted 1:10 into 2 mL of pH 7 phosphate buffer and 50 mg of methyloxyamine was added. To monitor the exchange reaction, the fluorescence was measured at 525 nm with 495 nm excitation over 12h. As the exchange

took place and the dabcyl hydrazide was removed from the molecule, fluorescence was recovered leading to an increase in signal. The exchange reaction took 12h to fully recover and after the exchange reaction had gone to completion, another scan with the same parameters as before showed the fluorescence had fully recovered and was comparable to the fluorescence before the quenched reaction.

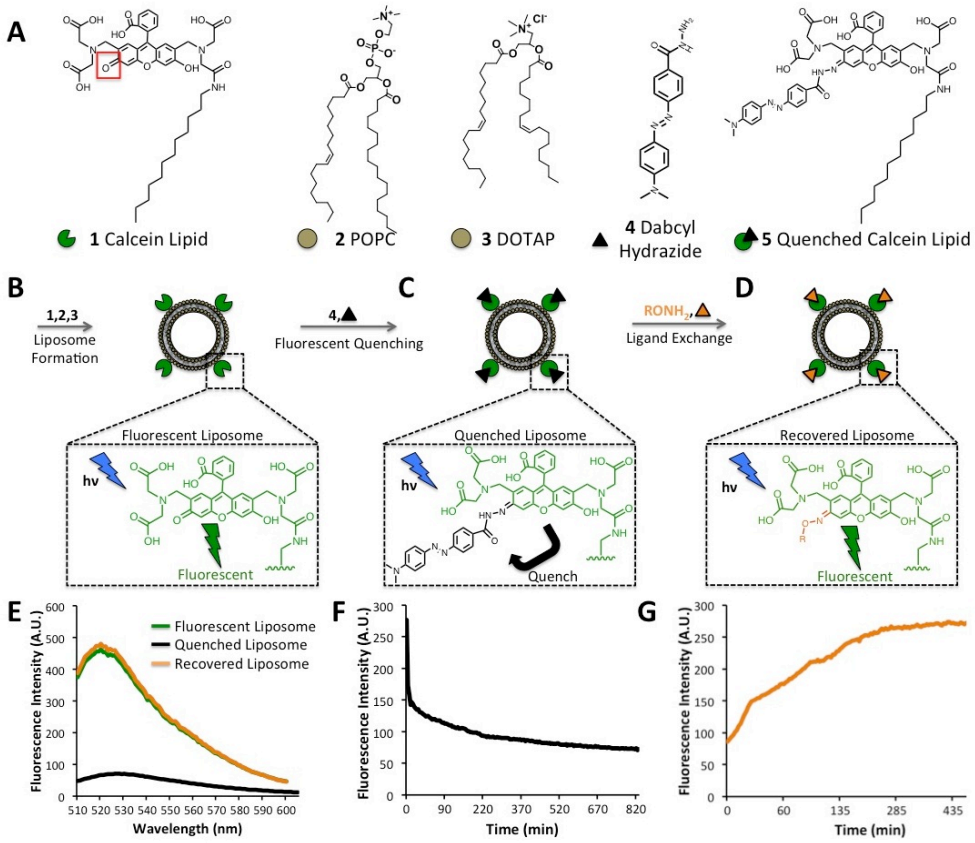

Figure 6.1 Design and Characterization of Cell Surface Fluorescent Receptor/Reportor system. A) List of molecules used in this study. B) Fluorescent liposomes were synthesized by sonication containing **1**. C) These fluorescent liposomes were quenched via a chemoselective and bio-orthogonal reaction with dabcyl hydrazide. D) The fluorescence was recovered by oxyamine exchange in the cell dye. E) Graph of fluorescent intensity vs. wavelength. Both the recovered and initial fluorescent liposomes were highly fluorescent. However, once reacted with the dabcyl hydrazide, a efficient quencher, the fluorescence from the liposomes was significantly reduced. F) Graph of fluorescent intensity vs. time for the liposome quenching reaction measured at 525 nm with 495 nm excitation. G) Graph of fluorescent intensity vs. time for the fluorescent recovery reaction measured at 525 nm with 495 nm excitation.

6.3.3 Flow Cytometry and Cell Viability

Once the solution and liposome studies were successful, we moved onto integrating this methodology with cells. Liposomes containing **1,2,3** were synthesized and fused with fibroblasts for 4h. The cells were allowed to culture for 1, 4, and 6d and their fluorescence was measured by FACS analysis. FACS analysis allowed for the cell fluorescence to be measured. As a control, liposomes were not fused to a certain cell population. Compared to the control, there was a large increase in fluorescence after fluorescent liposome fusion. As the cells were allowed to grow in the cell culture, the fluorescence decreased over time, most likely due to the dilution and degradation of the lipids. These results verified the introduction of fluorescence to the cells. Next, the quench and recover was verified on the cell surface. Liposomes were synthesized using **5,3,2** and then fused to cell surfaces as before. Once the liposomes were fused to the surface, FACS analysis demonstrated similar fluorescence to the control. To verify the fluorescence recovery on the cell surface, the cell media was exchanged for media that had 1 mg/mL of methyloxyamine. The cells were allowed to culture for 12h and then the media was exchanged again. These cells were allowed to grow for 1, 4, and 6d and then analyzed by FACS. The fluorescence intensity matches that of the cells containing **1** demonstrating recovery of the fluorescence after the oxyamine exchange reaction on the cell surface. Next, the viability of fibroblasts was verified with the trypan blue assay. Cells were fused with both fluorescent and quenched liposomes and their viability was measured after 1, 3 and 5 d. The cells were found to be >90% viable and were comparable to control cell populations not fused with the liposomes.

6.3.4 Fluorescence Recovery by Cell Surface Exchange Reaction

After the cell fluorescence and viability were verified, the fluorescent recovery on the cell surface was verified with fluorescence microscopy. Fibroblasts were fused with quenched lipids. Fluorescent microscopy revealed the cells had no appreciable fluorescence. After this, 1 mg/mL of methyl oxyamine was added to the media. The cells were imaged after 6h and cells were becoming fluorescent. After 12h, the cells were fully fluorescent and were comparable with cells fused with non-quenched lipids. This data demonstrates the ability of the exchange reaction to take place on the cell surface even in the presence of other cells without harming cell viability. No recovery was observed without an oxyamine-terminated ligand or in the presence of an amine one.

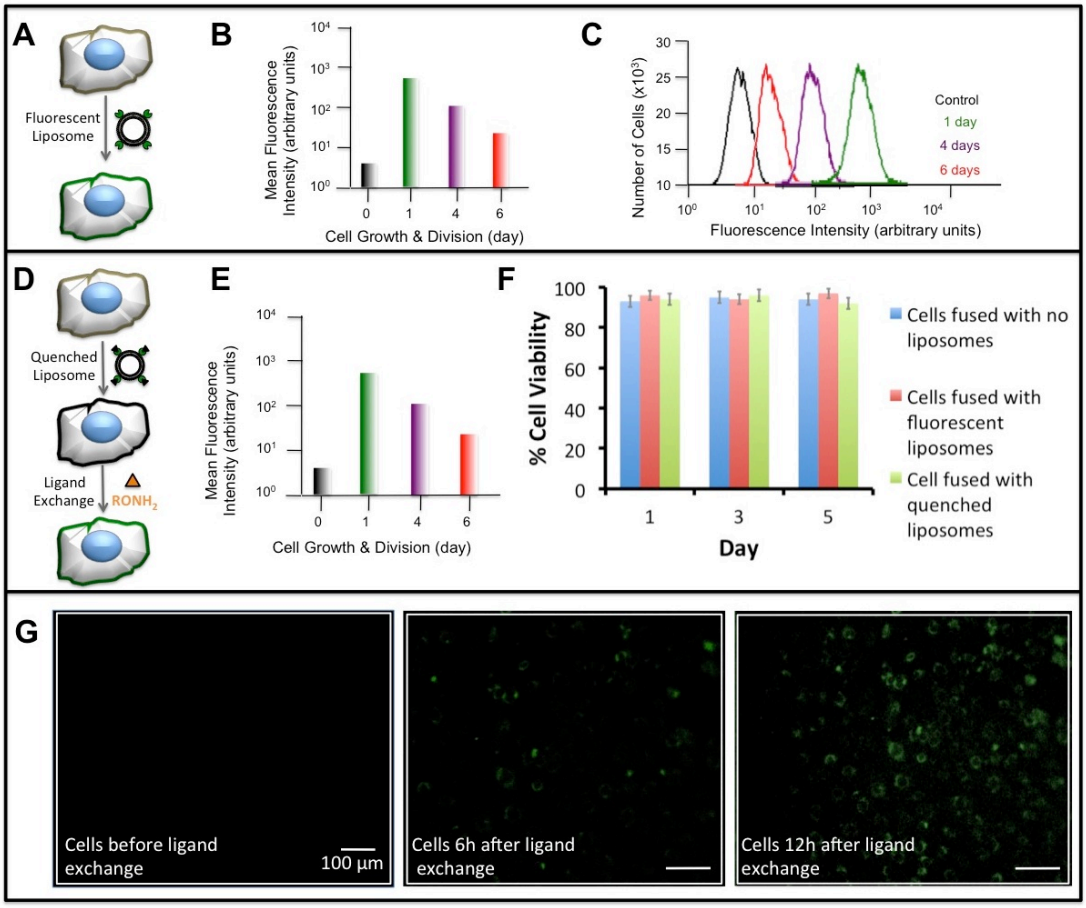

Figure 6.2. Cell viability and fluorescent recovery. A) Lipsomes containing **1** were fused to fibroblast surfaces resulting in fluorescent labeling of the cell surface. B) Bar graph of the fluorescence intensity of the cells vs. time determine by FACS. No liposomes were fused to the control. C) FACS analysis of the cells showed an increase in fluorescence vs. the control, which decreased over time as the lipids were diluted by cell division. No liposomes were fused to the control D) Quenched Liposomes were fused to fibroblast surfaces to study fluorescent recovery by oxyamine exchange. After the quenched liposomes were fused to the cell surface, an oxyamine was added to the cell media and as the oxyamine exchanged the dabcyl , the fuorescence was recovered. E) Cell viability studies of cell fused with liposomes, both fluorescent and quenched. Cells were found to be >90% viable using the trypan blue assay. F) FACS analysis after the cells had recovered their fluorescence after 1,4, and 6d. As control, cells were fused with liposomes and cells were fed quenched liposomes, but no oxyamine exchange reaction took place. G) A series of fluorescent images taken after methyloxymine was added to the cell media. After 12h of oxyamine exchange, the cells were fluorescent.

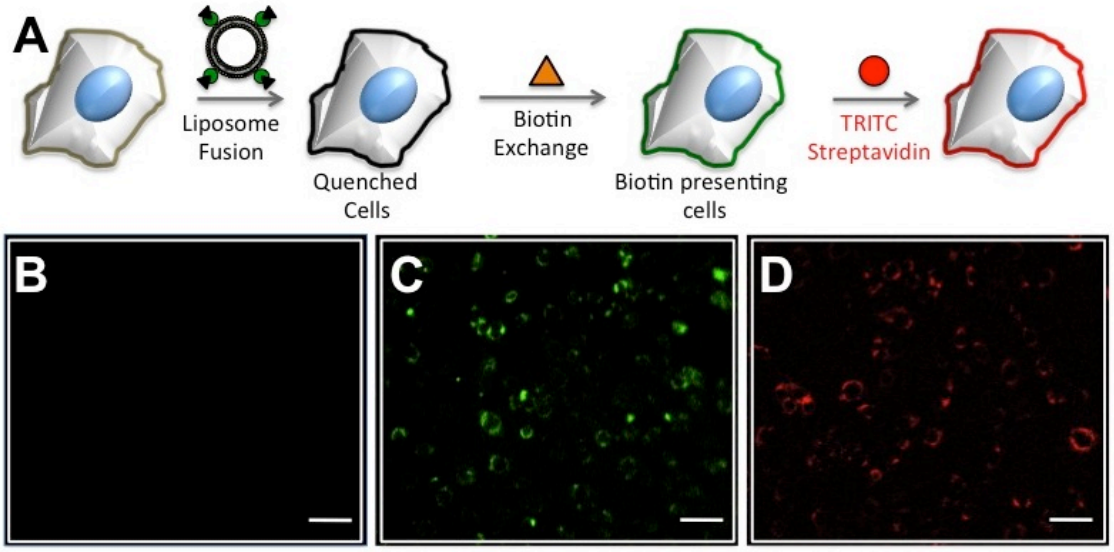

Figure 6.3 Cell surface ligand immobilization and protein surface functionalization. A) Cells were fused with quenched liposomes and biotin hydrazide was added to the media to exchange the dabcyl and functionalize the cell surface with biotin. Then, TRITC labeled streptavidin was immobilized to the biotin on the cell surface. B) Fluorescent Micrograph of the cells fused with the quenched liposomes. C) Fluorescence recovery 12h after media containing 1 mg/mL of biotin hydrazide was added to the cells to label cell surfaces with biotin. D) Biotin presenting cells after 4h of exposure to media containing 1 mg/mL of TRITC labeled streptavidin. The streptavidin had bound the cell surface and made them fluoresce red.

6.3.5 Cell-Surface Receptor

Once the cell compatibility and cell surface exchange reaction were verified, we wanted to demonstrate the ability to modify the cell surface with proteins using the ligands introduced to the cell surface. For these experiments, we chose the biotin streptavidin complex. Biotin-streptavidin has one of the highest affinities in nature and has been used to modify a variety of materials. After quenched liposomes containing **5** were fused to cells, the cell media was exchanged to contain 1 mg/mL of biotin hydrazide. After 12h, the cells were imaged and observed to be fluorescent, signifying the exchange reaction has taken place on the surface. Next, the media was changed to 1 mg/mL of TRITC streptavidin and allowed to react with the surface for 4h. The TRITC streptavidin recognized and bound the biotin on the cell surface and the cells became fluorescently red, demonstrating streptavidin binding to the cell surface. As controls, the cells did not become fluorescent when biotin was added to the media instead of biotin hydrazide and TRITC streptavidin did not bind the cells when methyloxyamine was present instead of biotin hydrazide.

6.3.6 3D Cellular Assembly

For the final experiment, the cell surface receptors were used to create cell assemblies. Quenched liposomes containing **5** were fused to the cell surface using the same procedure as above. Then, the tripeptide RGD was reacted to the cell surface. RGD is a tripeptide that has been shown to act as an epitope for fibronectin. It activates the integrin receptors on the cell surface that mediate cell adhesion to the extracellular matrix. A second cell population was added to the first and recognized the RGD ligand on the cell surface and bound to it, leading to the formation of cell assemblies. As a

control, the cell surfaces were reacted with the scrambled peptide DRG instead of RGD and the cell became fluorescent, but did not form cell assemblies. Once fed RGD, the cells became fluorescent and formed tissue-like structures demonstrating the ability of these cell receptors to occur in the presence of cells. A timecourse showed an increase in the diameter of the assemblies. Additionally, it was observed not all the cell are fluorescent demonstrating the ability of the methodology to not only modify the cell surface, but mark which cells have been modified with a cell ligand. The largest structure formed was several hundred microns wide and contained multiple layers of cells demonstrating the ability of this methodology to generate large 3D structure from simple materials.

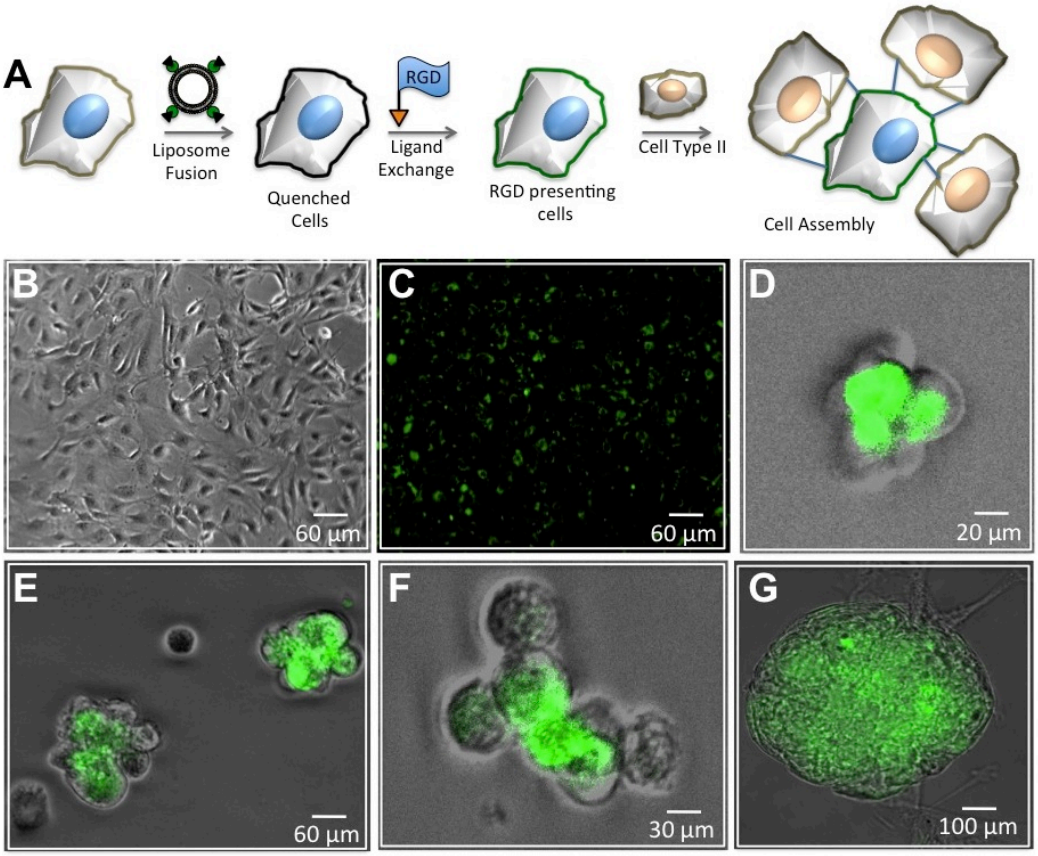

Figure 6.4 Formation of cell assemblies by cell surface engineering. A) Cells were fed quenched liposomes. These cells were reacted with RGD oxyamine to both recover the fluorescence and generate RGD presenting cells. These cells were mixed with another population of cells bound and recognized these RGD presenting cells forming cell assemblies. B) Brightfield image of fibroblasts fed quenched liposomes then reacted with a scrambled oxyamine peptide. C) Fluorescent micrograph of the same cells demonstrating the fluorescence had been recovered, but no assemblies formed due to the lack of a bio specific interaction. D) Overlay of both brightfield and fluorescent images of cells fed quenched liposomes then reacted with RGD and mixed with another population of non-labeled cells. Cells were allowed 1h to form in solution. The same experiment repeated for E) 2h, F) 4h, and G) 8h. The cell clusters grew in size and the RGD cells are marked by their fluorescence.

6.4 Conclusions

In conclusion, we have developed a general methodology based on simple chemistry to modify cell surfaces with a fluorescent molecule capable of not only marking cells, but fluoresces when a molecule binds the surface. The cell surfaces were modified with

liposomes driven by positively charged lipids. Both the quenching and exchange reactions were studied on the liposomes using fluoremetry and took place in about 12h. The liposomes were then characterized on the cells. Cell viability and FACS demonstrated the cells remained viable after fusion and were fluorescent. Additionally, the dabcyl could be exchanged on the cell surface to recover the fluorescence. Next, the availability of the ligand was verified using biotin hydrazide-TRITC-streptavidin. Finally, cell assemblies were synthesized using RGD ligand. However, the method is general. These quenched fluorescent pairs are simple to synthesize in solution and there are more than 20 dyes with similar structures that could be applied to. In future, we hope to study other quenched and two color FRET pairs.

6.5 Acknowledgements

This work was supported by the Carolina Center for Cancer Nanotechnology Excellence (NCI) and grants from the Burroughs Wellcome Foundation (Interface Career Award) and the National Science Foundation (Career Award). We thank Prof. Nancy Thompson and her group (UNC-Chapel Hill) for expertise in bilayer formation and fluorescence microscopy advice.

6.6 References

1. Zhang, J.; Campbell, R. E.; Ting, A. Y.; Tsien, R. Y. *Nature* **2002**, 3, 906-918.

2. Tsien, R. Y. *Annu. Rev. Biochem.* **1998**, 67, 509-544.

3. Sawano, A.; Miyawaki, A. *Nucleic Acids Res.* **2000**, 28, E78

4. Griesbeck, O.; Baird, G. S.; Campbell, R. E.; Zacharias, D. A.; Tsien, R. Y. *J. Biol. Chem.* **2001**, 276, 29188-29194.

5. Nagai, T.; Ibata, K.; Park, E. S.; Kubota, M.; Mikoshiba, K.; Miyawaki, A. *Nature Biotechnol.* **2002**, 20, 87-90

6. Scholz, O.; Thiel, A.; Hillen, W.; Niederweis, M. *Eur. J. Biochem.* **2000**, 287, 1565-1570.

7. Sugden, J. K. *Biotech. Histochem.* **2004**, 9, 71-90.

8. Warnement, M. R.; Faley, S. L.; Wikswo, J. P.; Rosenthal, S. J. *IEEE Trans Nanobioscience*, **2006**, 4, 268-272

9. Shenoy, D.; Fu, W.; Li, J.; Crasto, C.; Jones, G.; DiMarzio, C.; Sridhar, S.; Amiji, M. *Int. J. Nanomedicine*, **2006**, 1, 51-57.

10. Stevens, M. M.; George, J. H. *Science*, **2005**, 310, 1135-1138.

11. Daley, G. Q.; Scadden, D. T. *Cell*, **2008**, 132, 544-548.

12. Mirotsou, M.; Zhang, Z.; Deb, A.; Zhang, L.; Gnechhi, M.; Noiseux, N.; Mu, H.; Pachori, A.; Dzau, V. *Proc. Natl. Acad. Sci. U.S.A.* **2007**, 104, 1643-1648.

13. Beghetto, C.; Renken, C.; Eriksson, O.; Jori, G.; Bernardi, P.; Ricchelli, P. *Eur. J. Biochem.* **2000**, 267, 5585-5592.

14. Benard, N.; Gonzalez, B. J.; Schouft, M-T.; Morel A.; Vaudry, D.; Chan, P.; Vaudry, H. *J. Biol. Chem.* **2004**, 42, 43487-43496.

15. Nataf, S.; Anginot, A.; Vuaillat, C.; Malaval, L.; Fodil, N.; Chereul, E.; Langlois, J-B.; Dumontel, C.; Cavillon, G.; Confavreux, C.; Mazzorana, M.; Vico, L.; Belin, M-F.; Vivier, E.; Tomasello, E.; Jurdic, P. *American J. Pathol.* **2005**, 166, 275-286.

16. Petronilli, V.; Miotto, G.; Canton, M.; Brini, M.; Colonna, R.; Bernardi, P.; Di Lisa, F. *Biophy J*. **1999**, 76, 725-734.

17. Thomas, F.; Serratrice, G.; Beguin, C.; Aman, E. S.; Pierre, J. L.; Fontecave, M.; Laulhere, J. P.; *J. Biol. Chem*. **1999**, 274, 13375-13383.

18. A-C. Syvannen, *Nat. Reviews Genetics*, **2001**, 2, 930

19. Csiszar, A.; Hersch, N.; Dieluweit, S.; Biehl, R.; Merkel, R.; Hoffmann, B. *Bioconjugate Chem*. **2010**, *21*, 537-543.

20. Dutta, D.; Pulsipher, A.; Luo, W.; Yousaf, M. N. *J. Am. Chem. Soc*. **2011**, 133, 8704-8713.

CHAPETER 7

General Conclusions and Future Directions

7.1 General Conclusions

This dissertation focused on the use of chemoselective liposome fusion as a tool for engineering cell-surface and it's further application in tissue engineering. Chapter II discussed the development of a general method to pattern electroactive and chemoselective fluid lipid bilayers on gold surfaces for a range of biospecific ligand-receptor interaction studies on model membranes. In this study, a variety of oxyamine-tethered ligands (fluorescent dye, sugar) were successfully immobilized in arrays using microfluidic lithography. This platform is rapid and flexible and can be extended to many areas in biochemistry, cell biology and material science to study fundamental membrane activity and enzymology.

Chapter III described the development of a chemoselective synthetic cell receptor system based on liposome delivery and fusion strategy. Ketone and oxyamine groups were introduced to a liposomal system and chemoselective vesicle fusion was achieved using molecular recognition and interfacial oxime bond formation. Subsequent delivery of the decorated liposomes to cells lead to fusion and modification of a cell surface by bio-orthogonal reactive groups that serve as synthetic chemoselective cell receptors. Ketone and oxyamine modified cells were patterned on solid surfaces, displaying oxyamine and ketone groups respectively.

Chapter IV focused on the application of the liposome delivery and fusion strategy to generate 3D spheroid cellular assembly with controlled interconnectivity and patterned multi-layered tissue like structures. Furthermore, 3D multi-layered stem cell and fibroblast (fb) co-cultures were generated, and differentiation was induced to form tissue-like structures of adipocytes and fbs.

Chapter V described the development of a new general and straightforward liposome fusion based methodology to deliver dynamic and switchable bio-orthogonal chemistries to tailor cell membranes and direct the formation of 3D co-culture tissue structures. We demonstrated and extensively characterized the conjugation and release of molecules to and from cell surfaces *in situ*, as well as the triggered assembly and disassembly of 3D spheroid and multi-layered tissues. Additionally, dynamic co-cultures of hMSCs and Fbs were able to be generated and differentiated with this redox oxime strategy.

Chapetr VI described the development of a general methodology based on simple chemistry to modify cell surfaces with a fluorescent molecule capable of not only marking cells, but fluoresces when a molecule binds the surface. The cell surfaces were modified with liposomes driven by positively charged lipids. Both the quenching and exchange reactions were studied on the liposomes using fluoremetry and took place in about 12h. The liposomes were then characterized on the cells. Cell viability and FACS demonstrated the cells remained viable after fusion and were fluorescent. Additionally, the dabcyl could be exchanged on the cell surface to recover the fluorescence. Next, the availability of the ligand was verified using biotin hydrazide-TRITC-streptavidin. Finally, cell assemblies were synthesized using RGD ligand.

7.2 Future Directions

As discussed in the dissertation cell-surface engineering has a prominent role to play in the field of tissue engineering and other biomedical applications. In future I plan to extend the liposome fusion strategy to deliver bioorthogonal chemoslective functional groups to other biologically and medically important cell lines. Specifically I want to couple microfabrication and other surface chemistry tool with the liposome delivery method with study the spatial aspects of T cell costimulation in a three dimensional environment[1]. It is increasingly clear that the spatial organization of CD28 and TCR signaling influences the activation of CD4 T cell activation[2]. Efforts have been there to develop patterning techniques to identify the molecular mechanisms that allow T cells to read these patterns. My future goals will be to make these surfaces dynamic and chemically active which will lead to the better understanding of the kinetics of T cell signaling.

7.3 References

1. Shen, K.; Thomas, V. K.; Dustin, M. L.; Kam, L. C. *Proc. Nat. Acad. Sci. U.S.A.* **2008**, 15, 7791-7796.

2. Friedel, P.; den Boer, A. T.; Gunzer, M. *Nat. Rev. Immunol.* **2005**, 5, 532-545.